Physical Oceanography of Northern Estuaries

by

Lorraine Veilleux

Department of Meteorology

McGill University, Montréal

June 1990

A Thesis submitted to the Faculty of Graduate Studies and Research in partial fulfilment of the requirements for the degree of Master of Sciences

ABSTRACT

Within the context of oceanographic research on northern estuaries in James Bay and Hudson Bay, and in relation with hydroelectric developments and their impact on the physical environment, two studies were undertaken. Both concern the importance of bottom topography, tidal motion and fresh water input on the estuarine processes in these areas.

The first one, in Rupert Bay (south-eastern corner of James Bay), describes tidal and local wind effects on circulation and mixing patterns for summer conditions. An estimate of terms in the lateral momentum equation shows that the centrifugal acceleration, the Coriolis force and the baroclinic pressure gradient are the most important forces at a mid-bay cross section transect.

The second study is concerned with the freshwater plume of Great Whale River (south-eastern Hudson Bay). CTD measurements were used to examine the lift-off point of the plume for under-ice and increasing discharge conditions. Comparison with existing models shows them to be inappropriate for under-ice conditions. Finally, the presence of supercooled water masses in the region of the study is reported.

RÉSUMÉ

Dans le cadre des recherches océanographiques sur les estuaires nordiques des baies de James et d'Hudson, en relation avec les développements hydroélectriques et leurs impacts sur le milieu physique, deux études ont été entreprises. Elles tentent toutes deux d'évaluer l'importance de la topographie du fond, de la marée et du débit d'eau douce sur les mouvements estuariens dans ces régions.

La première, portant sur la Baie de Rupert (coin sud-est de la Baie de James), décrit principalement l'effet des marées et des vents locaux sur les patrons de circulation et de mélange en condition d'été. Une évaluation des termes de l'équation latérale de quantité du mouvement démontre que l'accélération centrifuge, la force de Coriolis et le gradient de pression barocline sont des forces dominantes sur une section transversale, au milieu de la baie.

La seconde étude, quant à elle, porte sur le panache d'eau douce de la Rivière Grande Baleine (sud-ouest de la Baie d'Hudson). Le point de décollage du panache (lift-off point) y est inspecté à l'aide de mesures CTD, et ce pour des conditions sous la glace et en débit croissant. Une comparaison avec des modèles déjà existants démontre qu'ils ne sont pas appropriés en présence d'un couvert de glace.

Finalement, la présence de masses d'eau surgelée dans la région étudiée est signalée.

ACKNOWLEDGEMENTS

The author wishes to thank all those people who helped in the realization of this thesis : Dr.R.Grant Ingram , her thesis supervisor, for his suggestions and help in revising this work, and also for financial support ; to Serge Lepage and Jean-Claude Deguise for their support and guidance ; to Paul Peltola for technical assistance and to the Groupe Interuniversitaire de Recherches Océanographiques du Québec for additional financial support.

She is also grateful for the support and encouragement offered by her parents, François Dallaire and all the members of the Coffee Club.

TABLE OF CONTENTS

APPENDICES

LIST OF FIGURES

page

CHAPTER 2

CHAPTER 3

APPENDICES

LIST OF TABLES

page

CHAPTER 2

CHAPTER 3

APPENDICES

LIST OF SYMBOLS

A - cross-sectional area of the estuary

b - estuary breadth or discharge half-width

C_D - bottom friction coefficient

D - mean depth

f - frequency or Coriolis parameter = $2\omega\sin\varphi$

F - frictional force or Froude number

F_B - surface shear stress

F_C - tidal currents form number

Fr - densimetric Froude number

F_S - sea bed shear stress

F_W - water level form number

g - acceleration due to gravity

g' - reduced gravity

h - depth of water

H - high tide

L - total length of basin or low tide

p - pressure

Q - discharge

r - cross correlation coefficient

R - radius of curvature of streamlines

Ri - bulk Richardson number

S - salinity

T - period and also temperature

t - time

U - tidal variation of longitudinal velocity

u - longitudinal velocity

u' - turbulent longitudinal velocity fluctuations

$\bar{u}$ - mean longitudinal velocity

V - tidal variation of lateral velocity

v - lateral velocity

$\bar{v}$ - mean lateral velocity

x - longitudinal axis

y - lateral axis

z - vertical axis or instrument depth

α - entrainment rate

ρ - density

φ - angle of latitude

ω - angular velocity of earth's rotation

ζ - elevation of water surface relative to Mean Sea Level

Σ - ratio of tidal range to mean water depth

Abbreviations for frequently used units (SI) :

m : metre kg : kilogram km : kilometre

s : second hr : hour

PREFACE

STATEMENT OF ORIGINALITY

This thesis presents two comprehensive physical oceanographic studies dealing with northern estuaries. The first study is based on a data set which was collected by Dr.Grant Ingram's team in Rupert Bay during the summer of 1976. Preliminary analysis had already been done on the observations and, for the purpose of the present study, a complete data analysis of the survey results was undertaken. These included variance analysis, spectral analysis, tidal height and tidal current analyses and an analytical method which provided new insight on the possible dynamical balance of the Rupert Bay estuary. The second study presents a complete and original research project dealing with a subject that had never been investigated in an ice covered estuary; it includes a literature review, the design of the fieldwork, data analysis and interpretation. Finally, three appendices provide information on the standard data procedures applied in this study, a description of the equipment and some time series obtained from data analysis.

LITERATURE REVIEW

A complete review of previous relevant work can be found in the GENERAL INTRODUCTION, and in the INTRODUCTION and text of each manuscript (chapters 2 and 3).

DECLARATION OF ASSISTANCE

The candidate acknowledges the contribution of the co-author, Dr.Grant Ingram, for his supervision, guidance and advice rendered during both projects, and his critical review of the whole thesis. In accordance with section 7 of the Thesis Guidelines, the candidate declares that the data handling and writing of the first manuscript, and the study design, field work, data analysis, data interpretation, and writing of the second manuscript were done by the candidate alone.

THESIS FORMAT

In accordance with section 7 of the Thesis Guidelines, this thesis has been prepared as two manuscripts suitable for submission to scientific journals for publication. For this reason, each chapter contains its own Abstract, Introduction, Methodology, Results and Discussion, Conclusion and References sections. Additional material (description of equipment and data handling) is provided in appendices. The present thesis format has been approved by the thesis committee and is in accordance with the Institute of Oceanography procedures. This thesis was started before the closing and is therefore under the aegis of the Institute of Oceanography.

CHAPTER 1. GENERAL INTRODUCTION

ESTUARIES

An estuary may be defined as a partially enclosed body of water which receives an inflow of fresh water from land drainage and which has a free connection with the open sea (Bowden, 1967). The water within an estuary then consists of a mixture of fresh water and sea water in proportions which vary with time and space and, for this reason, an estuary can be categorized as a complex physical system and a particularly vulnerable environment.

Bays and river mouths have always been attractive areas for human development. They have unique advantages : most are semi-enclosed and therefore provide natural harbours; many are effective nutrient traps and therefore rich in marine resources; as a thoroughfare between the ocean (or sea) and inland rivers many became hubs of transportation; and their high rates of flux and dilution permit disposal of great quantities of waste materials (e.g. Saint-Lawrence Estuary, Long Island Sound, etc).

For the northern estuaries of Hudson Bay and James Bay, the human impact comes from hydroelectric development of the rivers, and associated modification of their natural discharge cycles and adjacent marine ecosystems.

CONTEXT OF STUDY

Recent and projected developments on the rivers flowing into Hudson and James Bays will surely have an impact on the overall dynamics of these large inland seas and on the fragile estuarine systems that border them. Existing developments include the Nelson-Churchill and The La Grande-Eastmain systems; the Grande Baleine project is in the advanced planning stages, while the Nottaway-Broadback-Rupert Complex will be developed soon after the year 2000.

The most obvious and direct effect of such developments is their impact on the annual cycle of freshwater discharge, giving significant reduction of the normally high spring freshet and, in the cold months of winter when the electrical demand is maximum, flows five to ten times higher than the natural low discharge rates (Freeman et al., 1982).

The effect of such modifications on the freshwater input will be felt on two levels. At the estuarine system scale, direct changes in the salinity distribution will affect the fauna and flora at the mouth of the river and within the freshwater plume. At the larger scale, changes in the annual ice-cover, currents and salinity structure (Prinsenberg, 1986) may induce slow climatic modification (Rouse and Bello, 1985 and Prinsenberg, 1984) in the receiving basins.

In order to predict potential impacts on the sedimentological regime, the geochemical and biological cycles, the migratory fauna and local population, one needs to understand the physical oceanographic regime for these estuaries prior to disturbance. Two estuaries of particular interest are Rupert Bay and the Great Whale River. Both will be drastically altered in the hydroelectric projects planned over the next decade.

GENERAL OBJECTIVE

The general purpose of this study is to help in our understanding of the physical regime in northern estuaries subject to future modification. To achieve this, two projects were undertaken. The first one involved the analysis and interpretation of oceanographic field data which had been collected in the Rupert Bay area (south-eastern James Bay) during the summer of 1976. The aim of the study was to describe the summer circulation and mixing patterns of this particularly large and shallow estuary. This was done by assessing the contribution of the driving forces (e.g. tides, wind stress, river runoff) and secondary forces (e.g. Coriolis, pressure gradient, friction and centrifugal forces). The motivation behind this study is the forthcoming development of the Nottaway-Broadback-Rupert Complex.

The second one, a smaller scale study, required fieldwork in the spring of 1988 and was part of a much larger research program conducted by GIROQ (*) in the Great Whale River area (south-eastern Hudson Bay). While one objective of the physical oceanographic part of this study was to understand the dynamics of the freshwater plume under sea ice cover, the object of the study presented here is the lift-off characteristics of the plume. The lift-off point, located in the vicinity of the river sill and controlled mainly by the river discharge (buoyancy flux), is the region where the river waters detach from the bottom and become a surface buoyant plume. Learning more about what variables control the location of this point for different discharge rates and tidal phases is expected to give some insights into the behaviour of freshwater plumes under sea ice cover. One incentive for this study is the imminent start of construction for the Great Whale River Complex and the proposed alterations of discharge in the river and adjacent Manitounuk Sound. In selecting a common thread between both studies, the importance of bathymetry on the processes examined is found to be dominant.

* GIROQ : Groupe Interuniversitaire de Recherches Océanographiques du Québec

CHAPTER 2. PHYSICAL OCEANOGRAPHY OF A LARGE SHALLOW NORTHERN ESTUARY : RUPERT BAY

ABSTRACT

Measurements of current velocity, temperature, salinity and water level were made over a period of two months in Rupert Bay, a large shallow estuary located on the south-eastern corner of James Bay (Canada). From an analysis of current meter time series, the main features of the circulation and mixing patterns were obtained. Because of the large tidal amplitude/depth ratio, mixing was sufficiently intense to create vertically homogeneous conditions in many areas. Wind effects were found to be an important factor in understanding the variability of some physical processes. Secondary flows, associated with lateral gradients of temperature and salinity, were also significant. Estimates of the terms in the lateral momentum balance equation showed that the centrifugal acceleration, the Coriolis force and the baroclinic pressure gradient were dominant terms at a mid-bay cross section transect.

INTRODUCTION

Since the early 1970's, extensive oceanographic field studies have been undertaken in the coastal areas of south-eastern Hudson Bay and eastern James Bay. The renewed interest in a region that had been neglected for so many years (Dunbar, 1982) arose because of plans to develop major hydroelectric schemes on many rivers in northern Québec. At that time, three main projects were under consideration : the La Grande Complex, the Nottaway-Broadback-Rupert (NBR) and the Grande Baleine (Figure 1).

For economic reasons, the Québec government initially opted for the La Grande scheme, while the other two projects were delayed for future development. However, oceanographic observations that had been taken at the time in the Rupert Bay area are of interest in helping to understand estuarine processes in large shallow northern bays.

The data analysed in the present study were collected during the summer of 1976 by GIROQ (Groupe Interuniversitaire de Recherches Océanographiques du Québec) under contract with the SEBJ (Société d'Énergie de la Baie James). The goal was to gather information on the physical oceanography, the sedimentological regime and the biological oceanography (including benthos and fish, as well as the ecology of the

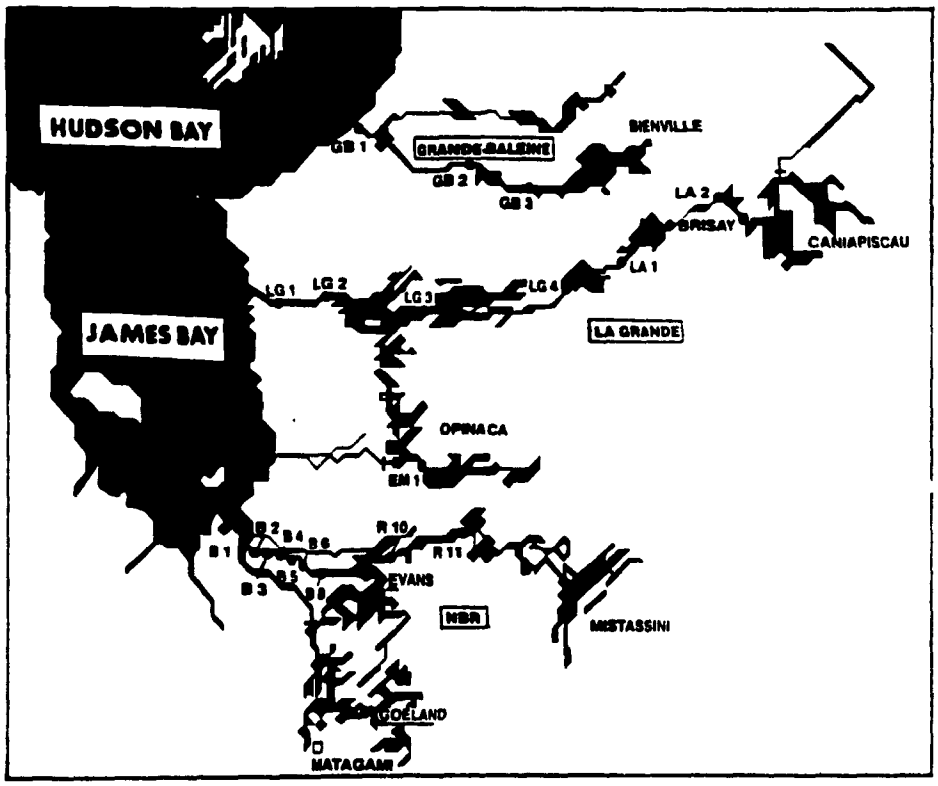

Figure 1. Québec's proposed hydroelectric development on northern rivers : the La Grande Complex, the Nottaway-Broadback-Rupert (NBR) and the Grande Baleine projects.

coastal marshes) of Rupert Bay. The results of those observations were reported in technical reports (d'Anglejan, 1977; Ingram, 1977; Ouellet, 1977; Simard & Legendre, 1977) and a few articles (d'Anglejan, 1980; Ingram and Chu, 1987;). Of particular interest for the present study is the report by Ingram (1977). He described the general characteristics of the water masses, the mean and tidal circulation and assessed in a preliminary manner the impact of the NBR diversion plan on physical processes within the estuary.

The objectives of the present study are two-fold. Firstly, to exam the physical oceanographic observations of Rupert Bay and to understand some of the variability on the basis of tidal, meteorological and freshwater forcing. Secondly, to determine the relative importance of the various acceleration terms in the lateral momentum equation along a mid-estuary cross-section. The results obtained are expected to be important in studies assessing the impact of future hydro-electric developments in this area and similar estuaries elsewhere.

THE STUDY AREA - RUPERT BAY

Rupert Bay is a very large shallow estuary located off the south-east corner of James Bay (Figure 2) in the physiographic region of the Eastmain Lowland. Its dimensions

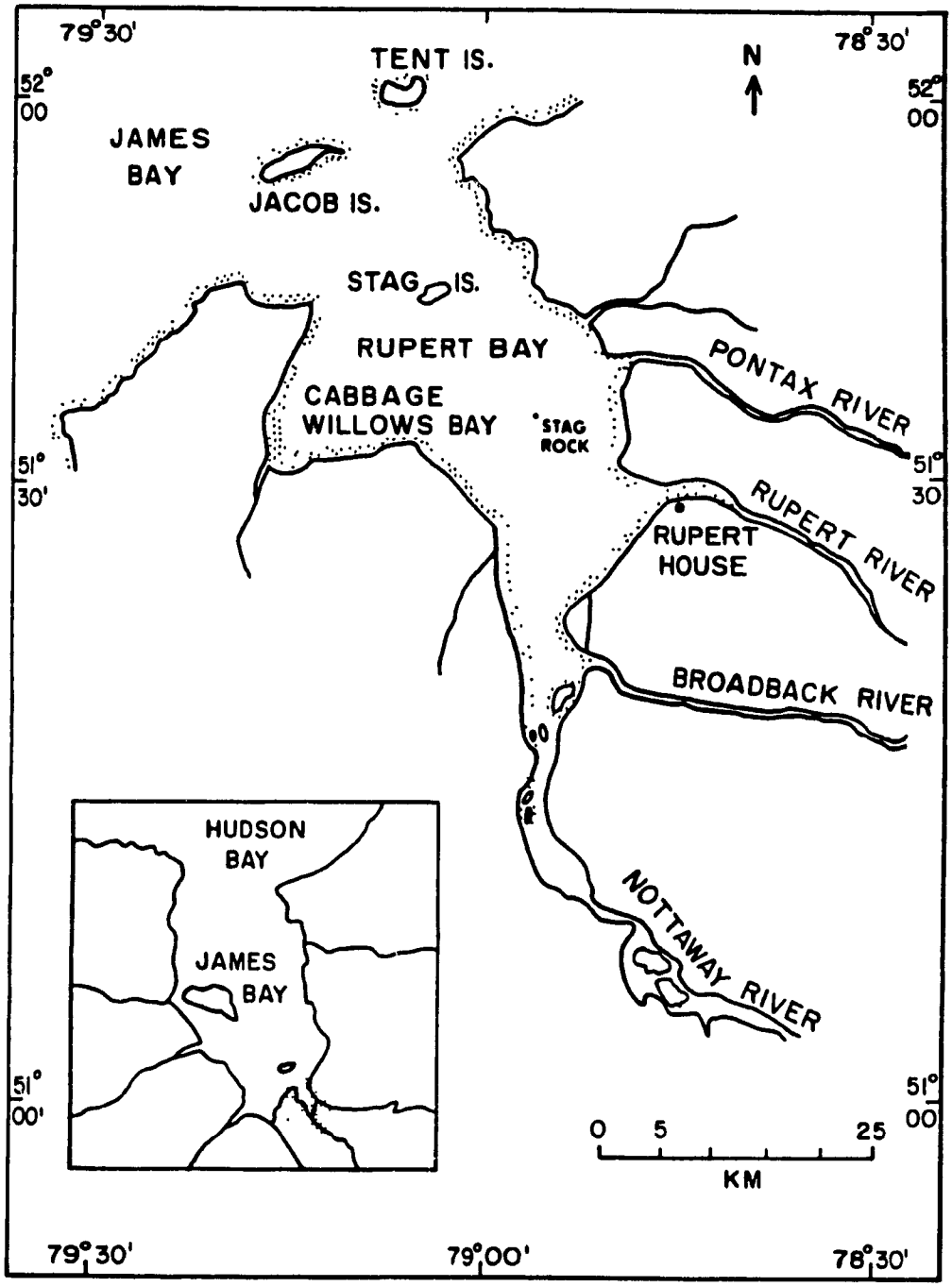

Figure 2. Rupert Bay : location map.

are approximately 60 km long by 20 km wide and it covers an area of about 875 km² in a NW-SE orientation. The estuary receives a mean annual fresh water discharge of 2340 m³/s from four rivers : the Nottaway (1020 m³/s), Broadback (320 m³/s), Rupert (870 m³/s) and the Pontax (130 m³/s). Together, they drain a 136,000 km² watershed and are regulated by large lakes and swampy depressions developed by ice erosion and glacial deposit during the Tyrrell Sea transgression (retreat of the Laurentian ice cap) (d'Anglejan, 1980).

The largest settlement in this area is Waskagheganish (Rupert House), which was established many centuries ago at the mouth of Rupert River.

Its geographical situation, between 78°30' and 79°00' W of longitude and 51°00' and 51°30' N of latitude , places Rupert Bay in the subarctic estuary category. This type is characterized by large seasonal fluctuations in river run-off (peak annual discharge in May) and by the alternation between an ice-covered and an open-water period, both approximately six months in duration.

The estuary is very shallow, with low water depths of 3 to 5 m characterizing most of the region (Figure 3). Downstream of Stag Rock, three deeper channels extending inland from James Bay can be found : the Inenew, Emelia and

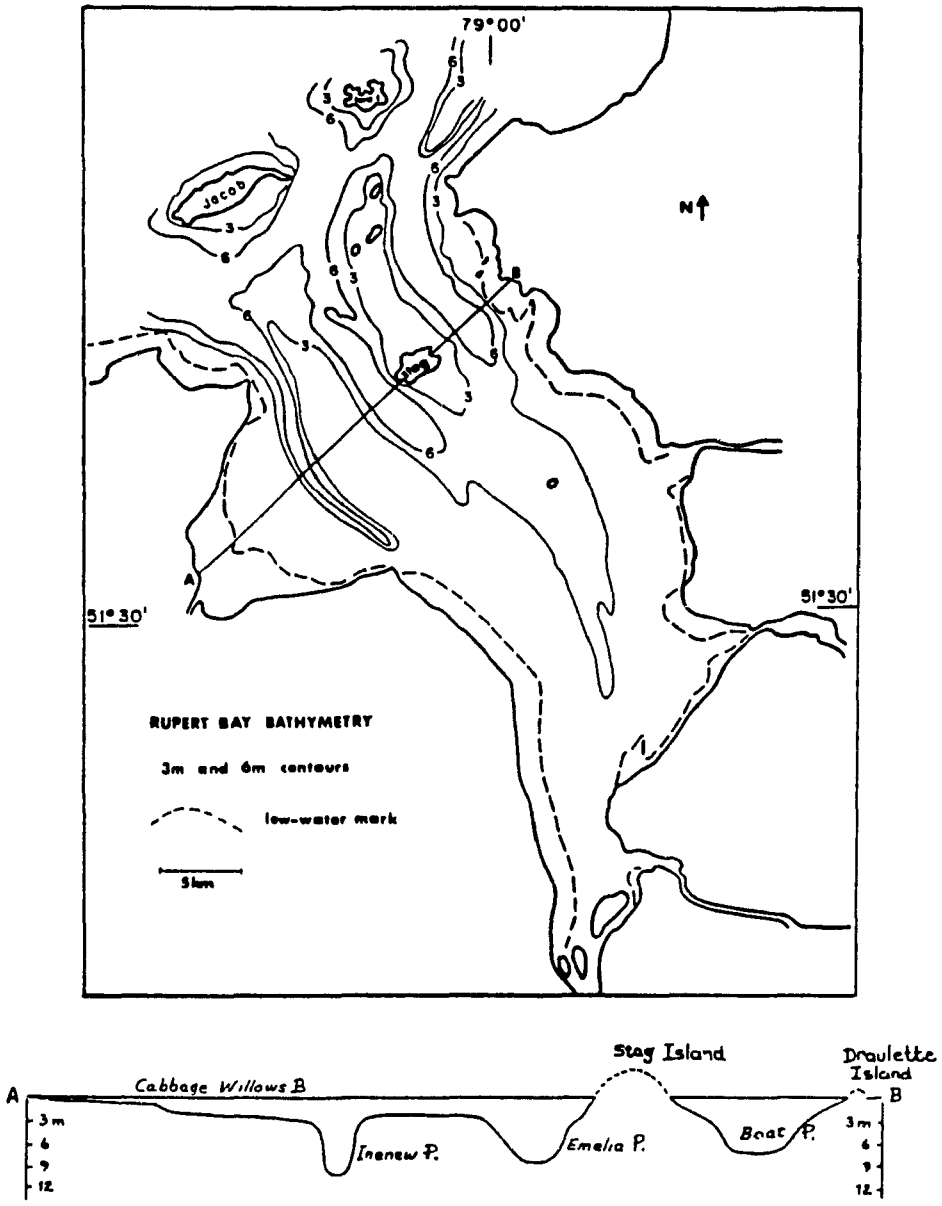

Figure 3. Rupert Bay bathymetry and cross channel profile showing the main passages.

Boat Passages. Maximum channel depth is less than 15 m. Many islands can be found in the downstream portion of the bay, the most important being Jacob Island and Tent Island at the boundary (not well defined) of James and Rupert bays, and Stag Island.

The bottom of Rupert Bay is covered by silts and clays of the Tyrrell Sea deposits which provide an abundant source of fine sediments and make the waters very turbid. The shoreline is marked by large marshes and muddy foreshores, particularly in Cabbage Willows Bay and between the mouths of the Broadback and Rupert Rivers. Similar to much of the adjoining areas, the well developed vegetation is highly favoured by waterfowl. The east coast of James Bay is a stopping place for millions of migratory birds each year. Rupert Bay is one of the principal sites, attracting more than half of the migratory fauna.

The estuary has an important phytoplanktonic production in the downstream region, while the relative abundance and diversity of fish species are quite high. The main species are : white- fish, longnose sucker, walleye, cisco and capelin (Simard and Legendre, 1977).

METHODOLOGY

During the 45-day program, in July and August 1976, Aanderaa RCM-4 current meters were moored at different locations within the bay to monitor (5-min sampling) current speed and direction, temperature, conductivity and pressure. An Aanderaa water level recorder was installed on a mooring line at the entrance of the bay for a 33-day period and a meteorological station (air temperature, wind speed and direction) was positioned on a small island in the upstream portion of the bay (Figure 4). Other meteorological data (sea level barometric pressure at Moosonee, 100 km west of Rupert Bay) were obtained from the Atmospheric Environment Service. Bathymetric features of the estuary were taken from the Canadian Hydrographic Service map, number 5414 and daily freshwater runoff values, for the three main tributaries, were provided by the Ministère de l'Environnement du Québec. Finally, some qualitative information was extracted from aerial pictures produced by the Canadian Centre for Remote Sensing in 1976 (Figure 5).

All current and wind vectors have been decomposed into along-channel components (u), positive into the bay (135°true), and cross-channel components (v), positive along 45°true. It is anticipated that some contamination of the velocity data will occur because of wave induced motions in

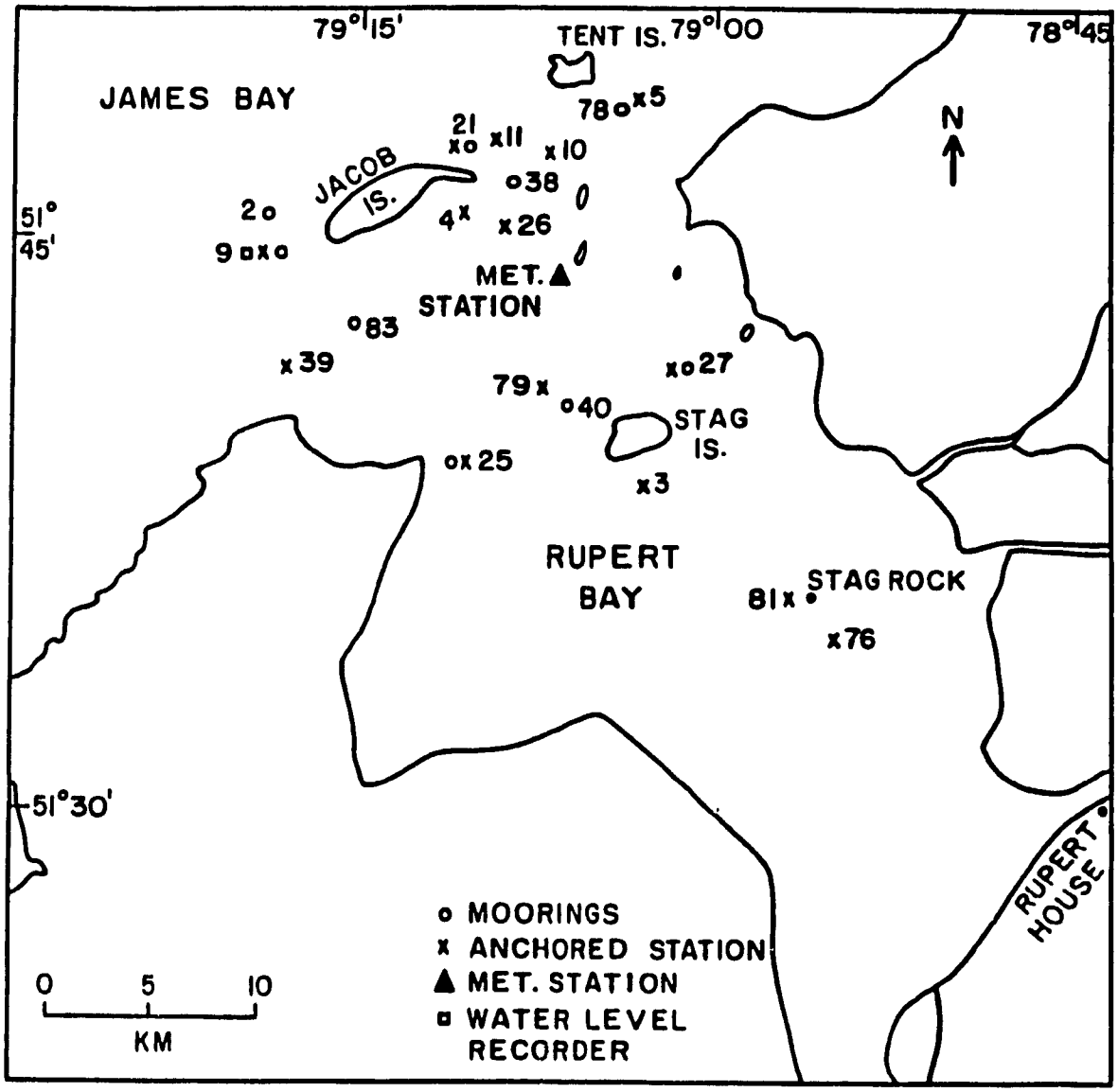

Figure 4. Sampling scheme.

Figure 5. Satellite image of Rupert Bay (Canada). Water masses from the four rivers of different sediment concentrations remain distinct over a major portion of the bay.

these near surface moorings. Current meter data were filtered using an $a_6a_6a_7/6*6*7$ type moving mean to reduce the relative frequency of observations to hourly values. Smoothed hourly values were also filtered with an $a_{24}a_{24}a_{25}/24*24*25$ filter to eliminate diurnal and higher frequencies, according to the methods discussed in Godin (1972). A complete description of the equipment and methods is given in Appendix 1, for the recording current meter, and in Appendix 2, for the water level recorder.

RESULTS

Time series obtained from the moored current meters and from the water level recorder are displayed in Appendix 3, while results of the data analysis are presented in the following pages. Table 1 gives a summary of the mean temperatures, salinities, M2 tidal component amplitudes, mean and tidal current velocities for the sampling period.

In order to discriminate the different mixing processes and driving forces, a variance analysis was first performed on all salinity time series. The unfiltered, smoothed and low-pass filtered data were analysed with the procedure described in Appendix 1 (variance analysis). The results, given in Table 2, reveal which portion of the salinity variance corresponds to high frequencies events (f > 1/hr), to semidiurnal and

Table 1. RCM moorings - depth of instrument, mean and tidal current velocities, M2 component amplitude, mean salinity and temperature for the sampling period.

STATION	DEPTH (m)	$\bar{u}$	$\bar{v}$	U (cm/s)	M2	$\bar{S}$ (°/$_{oo}$)	$\bar{T}$ (°C)
9 (13)	4	-6.5	-3.9	51	70	11.0	11.9
21 (25)	10	5.3	9.3	63	77	15.0	9.9
25 (9)	3	-5.5	-12.3	78	104	6.7	14.1
27 (10)	3	-5.4	-11.1	56	80	8.8	13.4
38 (31)	5	-4.1	15.5	42	62	13.2	11.8
40 (11)	3	-6.7	-3.0	46	66	9.7	12.9
40 (11)	5	-0.1	-10.0	28	32	9.8	12.9
78 (27)	11	3.2	-12.0	25	65	14.9	11.1
83 (25)	4	-7.8	-0.7	41	30	13.3	11.5

NOTES :

* u-direction is 135°(T),inshore, and v-direction is 45°(T).
* digits in ( ) are the number of days of recorded data.
* U is the RMS value of U-velocity observations.
* M2 is the value of the semi-diurnal component from the TCA analysis (Foreman, 1978).
* station 83 : mooring moved during sampling period.

Table 2. Variance analysis of salinities recorded at the moorings. Digits in () are percentages of total variance.

STATION	ABSOLUTE VARIANCE (‰)²			
	TOTAL	HIGH FREQ.	TIDAL	LOW FREQ.
9	2,79 (100)	0,45 (16,1)	2,17 (77,8)	0,17 (6,1)
21	1,74 (100)	0,34 (19,5)	1,21 (69,5)	0.19 (11,0)
27	13,41 (100)	0,91 (6,8)	10,95 (81,7)	1,55 (11,6)
40 surf	10,28 (100)	0,82 (7,9)	9,35 (91,0)	0,11 (1,1)
40	9,78 (100)	0,92 (9,4)	8,78 (89,8)	0,08 (0,8)
25	12,85 (100)	1,12 (8,7)	10,96 (85,3)	0,77 (6,0)
38	5,10 (100)	0,67 (13,1)	3,14 (61,6)	1,29 (25,3)
83 *	10,67 (100)	2,05 (19,2)	7,58 (71,0)	1,04 (9,8)
78	2,50 (100)	0,20 (8,0)	1,64 (65,6)	0,66 (26,4)

MEAN - TIDAL FREQUENCIES : 77.0 %

HIGH FREQUENCIES : 12.1 %

LOW FREQUENCIES : 10.9 %

* mooring moved during sampling period

diurnal tidal frequencies (1/hr > f > 1/25 hr) and to low frequencies (f < 1/25 hr). Basically, 77 % of the salinity variations in Rupert Bay are related to tidal phenomena (semi-diurnal and diurnal components), 12.1 % to high frequencies events (assumed to be mostly related to winds) and 10.9 % to low frequencies (atmospheric systems, long period tidal components, river runoff, etc).

SALINITY DISTRIBUTION

The upper limit of the salt intrusion during the flood tide is located near Stag Rock, while during the ebb, fresh water can be found as far downstream as Stag Island (Figure 6). The location of the boundary between salt and fresh water depends both on the river discharge and on the strength of the tidal flow from James Bay. The decrease of river runoff in August (ref. Appendix 3,p.147) can be correlated with the trend toward higher salinities at stations 27 and 78 (ref. Appendix 3, p.133 and 141). Both stations are on the north side of the bay, in the main freshwater stream (ref.Figures 4 and 5). Winds may also have an effect on the location of the transition zone.

Figure 6 illustrates the isohaline distribution at the surface and at 5 m, for both the ebb tide (L+1) and the flood

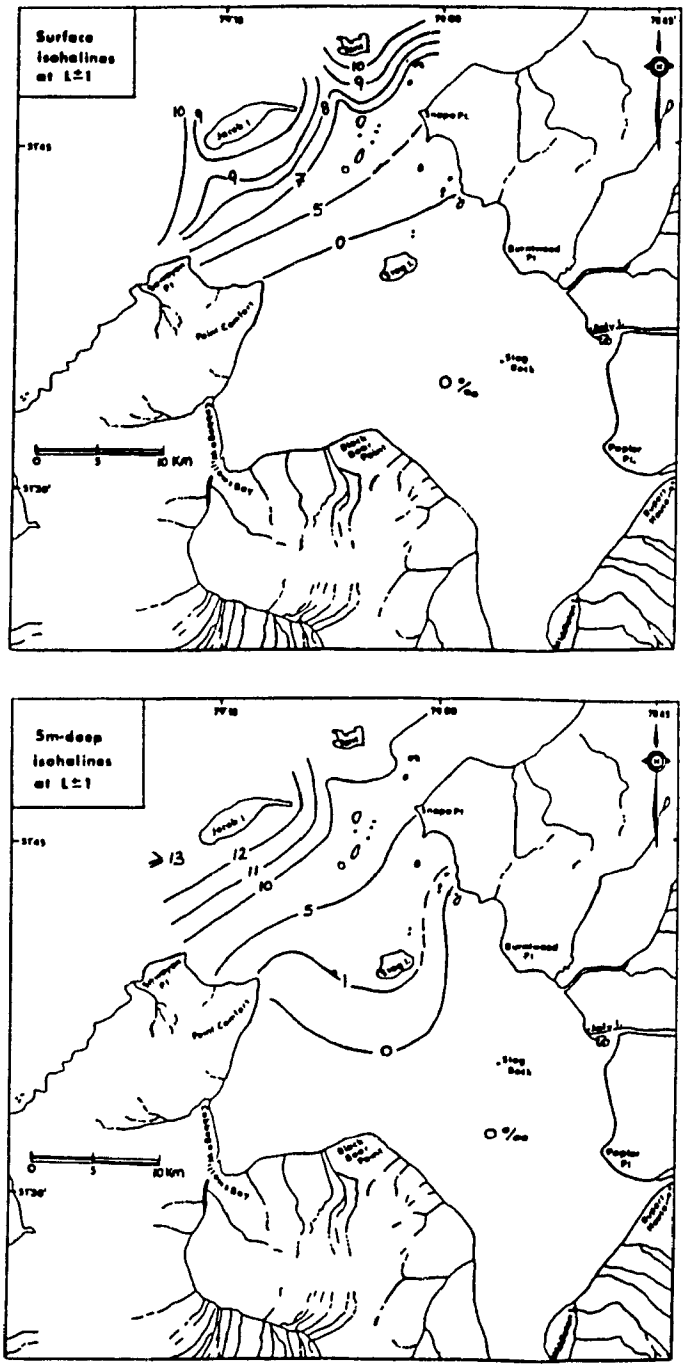

Figure 6. Isohalines at surface and at 5 m, for ebb tide (L+1) and for flood tide (H+1).

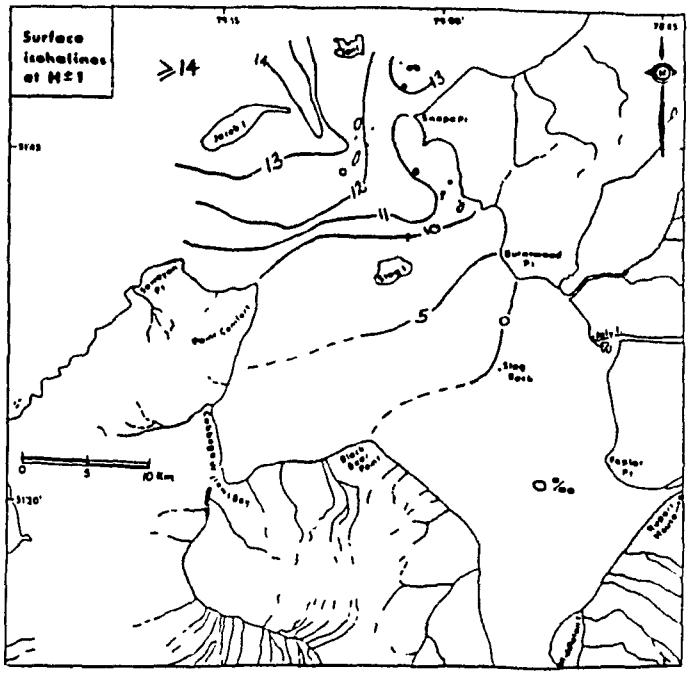

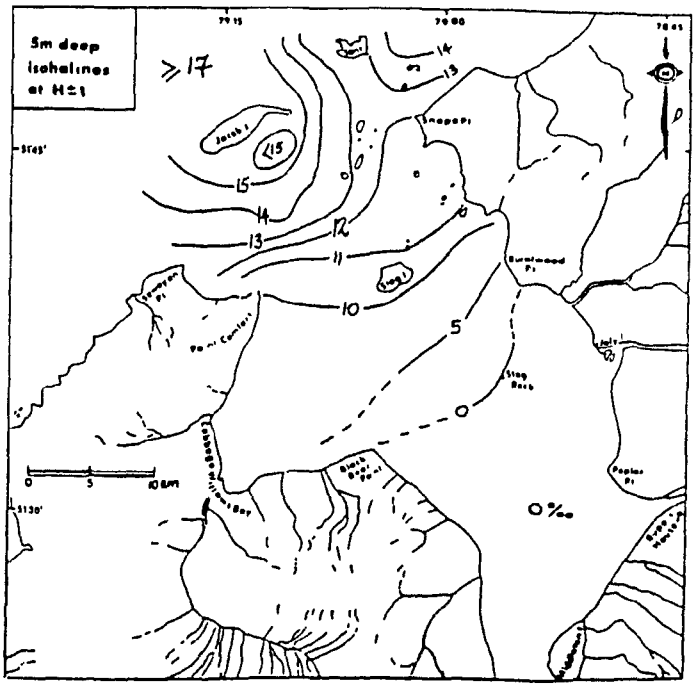

Figure 6. (concluded)

tide (H+1). In general, the salinity distribution varies between three primary zones (Figure 7). In the upstream zone (designated "0" in this study), fresh water is present over the entire semi-diurnal tidal period and the whole water column. In the middle zone (A), between Stag Rock and Gushue Island, salinity profiles show essentially vertically homogeneous conditions, with some lateral discrepancies due to the topography and strong tidal mixing.

In the downstream zone (B), partially mixed conditions prevail, especially in the passages around Jacob and Tent islands.

According to the Hansen and Rattray (1966) estuarine classification method, Rupert Bay is a type 1, well mixed estuary, in which the net flow is seaward at all depths and upstream salt transport is by diffusion. The region between Gushue Island and Stag Rock has only a slight stratification and is of type 1a. An appreciable stratification, type 1b, can be found downstream of Gushue Island (Ingram, 1977).

TIDAL REGIME

The Rupert Bay estuary is a tidally dominated system. The tide range is comparable in magnitude to the local depth, with a mean semidiurnal range at Stag Island of 2 m with spring

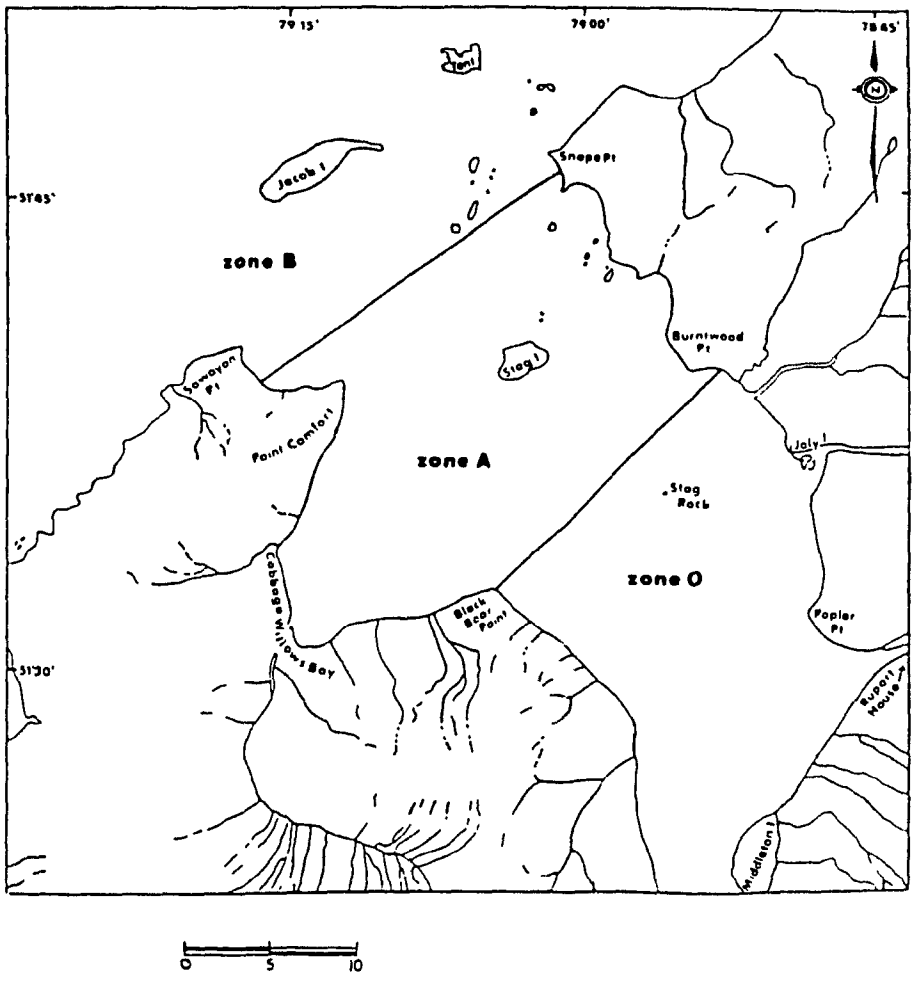

Figure 7. Primary zone designation.

tides up to 3 m. Average tidal current speeds in the central bay area range from 50 to 100 cm/s, which are an order of magnitude greater than the mean flow (5-10 cm/s). The predominance of the semidiurnal components of the tide can be observed in the tidal height analysis (Foreman, 1977) results and in all current meter observations (Tables 1 and 3). Tidal ellipses for the principal lunar constituent (M2) can be seen on Figure 8.

Estimation of the tidal form number (Defant, 1960), which is defined as the ratio (F) of the main diurnal (K1+O1) to the main semidiurnal (M2+S2) constituent amplitudes, also confirms the strong semidiurnal character of the tide. A form number greater than 3 indicates that the tide is of diurnal type and one smaller than 0.25 is considered to represent a semidiurnal tide. Table 4 presents form numbers within the study area for both currents and water level. For those moorings with less than 15 days of recorded data, S2 and O1 components were assumed to be included in, respectively, M2 and K1 components estimation. The average value of F_C computed from tidal currents is 0.10. The value of F_W computed from the water level recorder data is 0.24.

Table 3. Tidal Height Analysis and Tidal Current Analysis (Foreman 1977 and 1978). Predominant terms are underlined.

ANALYSIS OF HOURLY TIDAL HEIGHTS FOR STATION 9
OVER THE PERIOD OF 6HR 16/ 7/76 TO 17HR 18/ 8/76
NO.OBS.= 804 NO.PTS.ANAL.=803 MIDPT=23H 1/ 8/76 SEP.=1.00

	NAME	FREQUENCY	A	G
1	SO	0.00000000	16.1204	0.00
2	MM	0.00151215	0.0137	48.69
3	MSF	0.00282193	0.0264	122.96
4	ALP1	0.03439657	0.0149	285.80
5	2Q1	0.03570635	0.0263	237.72
6	Q1	0.03721850	0.0133	124.17
7	O1	0.03873065	0.0586	102.37
8	NO1	0.04026860	0.0152	119.92
9	K1	0.04178075	0.1702	155.44
10	J1	0.04329290	0.0184	90.99
11	OO1	0.04483084	0.0277	250.67
12	UPS1	0.04634299	0.0159	239.18
13	EPS2	0.07617731	0.0077	87.53
14	MU2	0.07768947	0.0584	153.31
15	N2	0.07899925	0.0963	23.36
16	M2	0.08051140	0.7538	61.14
17	L2	0.08202355	0.0275	101.11
18	S2	0.08333334	0.1761	158.16
19	ETA2	0.08507364	0.0110	241.24
20	MO3	0.11924210	0.0136	98.21
21	M3	0.12076710	0.0049	233.55
22	MK3	0.12229210	0.0133	115.56
23	SK3	0.12511410	0.0057	265.35
24	MN4	0.15951060	0.0099	321.59
25	M4	0.16102280	0.0717	351.79
26	SN4	0.16233260	0.0098	27.89
27	MS4	0.16384470	0.0361	83.29
28	S4	0.16666670	0.0074	135.24
29	2MK5	0.20280360	0.0028	147.17
30	2SK5	0.20844740	0.0021	128.67
31	2MN6	0.24002200	0.0029	110.82
32	M6	0.24153420	0.0155	152.02
33	2MS6	0.24435610	0.0105	253.74
34	2SM6	0.24717810	0.0009	348.07
35	3MK7	0.28331490	0.0032	149.75
36	M8	0.32204560	0.0035	139.13

FINAL ANALYSIS RESULTS IN CURRENT ELLIPSE FORM
FOR STATION 27 , BU23721 AT THE LOCATION 51°41' , 79° 2'
OVER THE PERIOD OF 19HR 0/ 8/76 TO 7HR 18/ 8/76
AMPLITUDES HAVE BEEN SCALED @ ORIGINAL DT=0.0833J HR
FILTERS = 12 12 13 , GREENWICH PHASES ARE FOR TIME ZONE EST

	NAME	CYCLE/HR	MAJOR	MINOR	INC
1	SO	0.00000000	12.392	0.800	23.0
2	K1	0.04178075	6.020	1.128	135.5
3	M2	0.08051140	71.739	3.497	122.5
4	M3	0.12076710	1.850	0.578	67.6
5	M4	0.16102280	7.376	-3.346	36.5
6	2MK5	0.20280360	2.862	1.678	47.6
7	2SK5	0.20844740	3.241	-0.185	112.8
8	M6	0.24153420	10.171	2.174	81.8
9	3MK7	0.28331490	2.286	0.989	89.3
10	M8	0.32204560	2.691	0.331	46.5

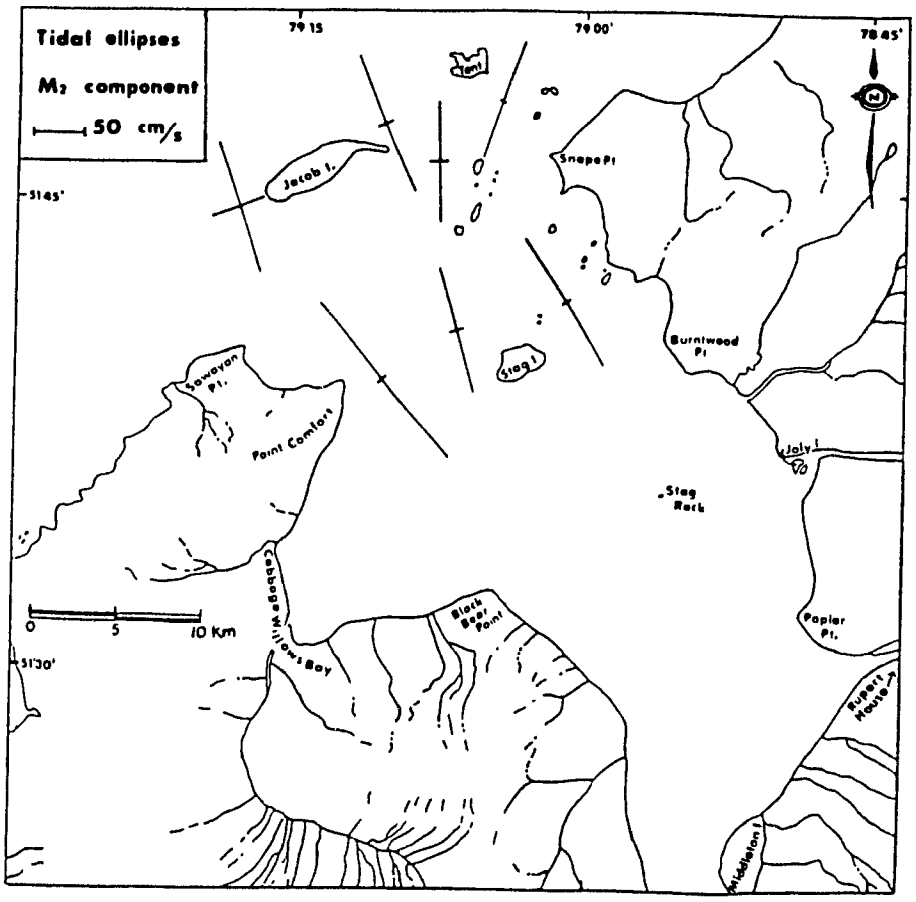

Figure 8. Tidal ellipses for M2 tidal currents in Rupert Bay.

Table 4. Some results from the TCA analysis : h is local station depth, z is instrument depth, F_C is the tidal current form number and M4/M2 is the shallow water effect ratio (depths are in meters).

STATION	h	z	F_C	M4/M2
9	17	4	0.12	0.13
21	14	10	0.10	0.06
38	13	5	0.04	0.14
27	8	3	0.08	0.10
78	12	11	0.10	0.08
40 (surf)	8	3	0.09	0.04
40	8	5	0.12	0.14
25	12	3	0.06	0.10
83	9	4	0.16	0.14 **

Tidal form number for the water level recorder :

F_W = 0.24

Shallow water effect ratio for the WLR :

M4/M2 = 0.10

** moorings moved during sample period

Similar to the observations of semidiurnal tidal currents in the tidal inlets of Mississippi Sound by Seim and Sneed (1988) , the theoretical form number relation, $F_C \approx F_W/2$, is in good agreement with the data presented here. In their article, they explained that continuity causes semidiurnal currents to increase relative to diurnal currents at the inlets and results in the reduced form number (water levels are not affected by the continuity constraint). There are no comparison data in the present study for the offshore tides but the spatial distribution of F_C from Table 4 reveals a progression from maximum values, at the entrance of the bay, to minimum values at stations inshore.

Calculation of the M4/M2 ratio , often called the shallow water effect ratio, gives an idea about the degree of non-linear response of an estuary to tidal forcing. This non-linearity in the tides can be illustrated by comparing offshore tide with the estuary tide. In Rupert Bay, this ratio has a value of 0.10 at the water level recorder station. We do not have offshore tide values outside Rupert Bay but Aubrey and Speer (1985) estimated a shallow water effect ratio of 0.007 for a station outside a similar estuary.

A comparison of the predicted tide in Rupert Bay for the period of the study with the observed water level signal allowed us to determine the non-tidal response in the bay.

Non-tidal forcing within a bay usually includes large scale atmospheric effect, local wind driving and seiches (resonance within the bay). The first step in the analysis of the water level signal was to remove the inverse barometric effect in order to reveal the other non-tidal driving processes. The resulting filtered signal of the water level within which the synodic fortnightly modulation can be seen, is significantly perturbed by the wind.

The dominant wind direction is along the main axis of the bay (from James Bay). Observations show the wind to be an important disturbing factor for the water level signal. This can be seen from a comparison of the U velocity component of the wind with the water level signal (Figure 9). A lagged cross-correlation analysis of the two time series confirmed this hypothesis giving a maximum correlation coefficient (r) of 0.77 , with a 7 hour lag due mainly to the sea level set-up time in response to an imposed wind.

Spectral analysis (Figure 10) of the alongshore velocity data establishes again the strong semi-diurnal nature of the tide. It also reveals the significant presence of shallow water tides constituents, namely M4 and M6 (also called M2 overtides). Both S2 and K1 components also present noticeable amplitudes.

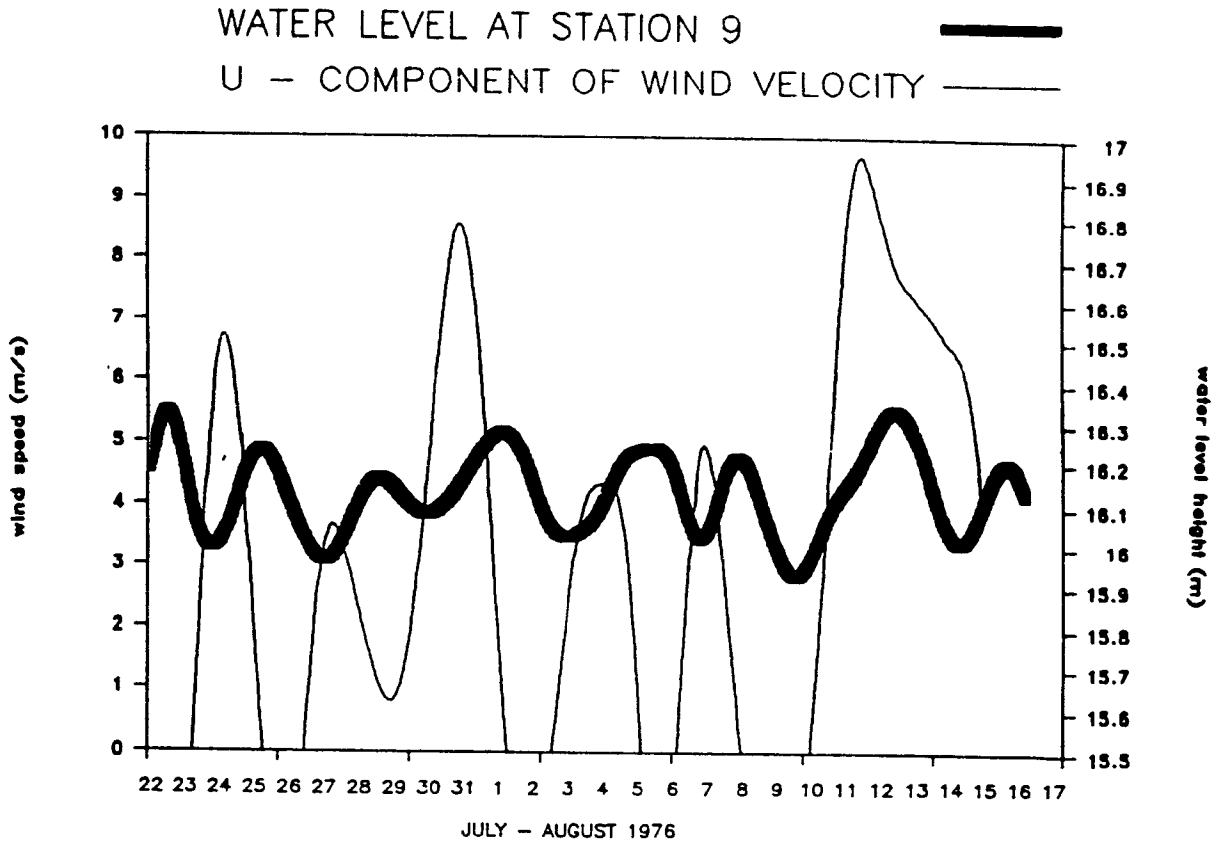

Figure 9. **Comparison of the U velocity component of the wind (recorded on Gushue Island) with the filtered water level signal.**

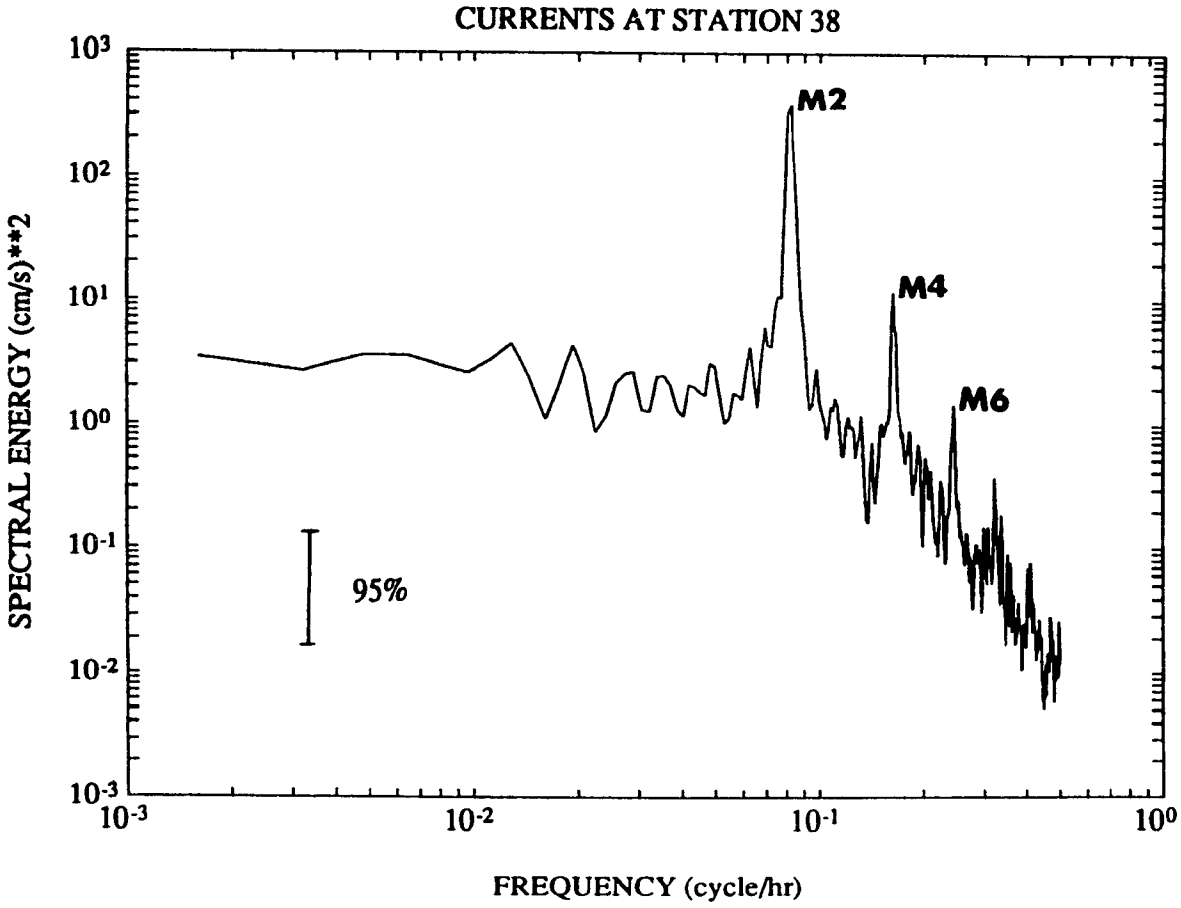

Figure 10. Spectral analysis of moored current meter and water level recorder data.

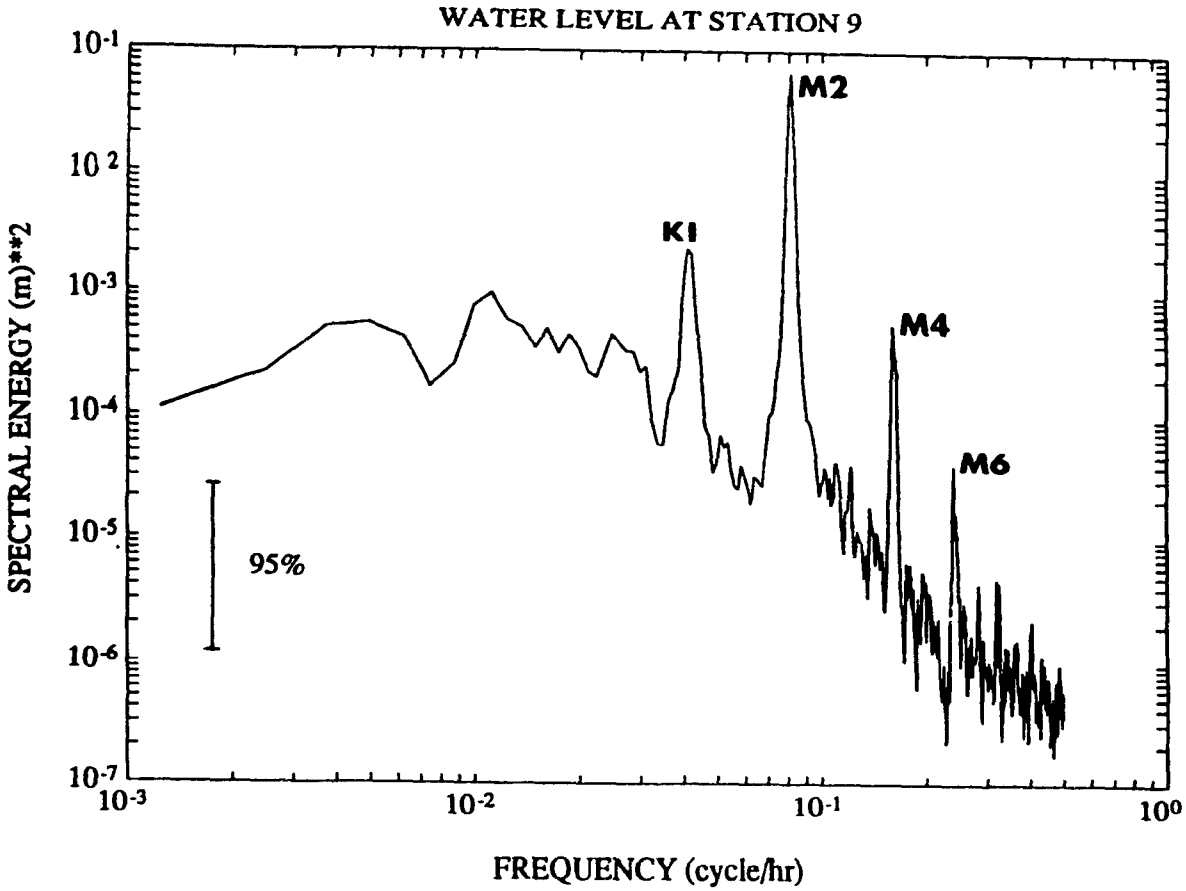

Figure 10. (concluded)

The spectrum of the water level signal also exhibits the most important frequencies i.e. the semi-diurnal principal lunar (M2), the shallow-water quarter-diurnal (M4) and sixth-diurnal (M6) components as well as the diurnal (K1) component which is here significantly more pronounced than in the current spectral analysis.

Two hypotheses could explain the observation of the strong diurnal (K1) component: in the first spectral analysis, the smaller amplitude of the K1 component may be a bias resulting from the discriminating enhancement of the semi-diurnal components. Secondly, the water level signal could be influenced by the land-sea breeze ($T \approx 24$ h) which was observed on 22 of the 43 days of the sampling period (ref. Appendix 3).

The quarter-diurnal component (M4, $T = 6.21$ h), which is significant in both spectra, could also include some seiche effect. The seiche period for Rupert Bay ranges between 6.1 and 7.1 hours, calculated with the equation

$$T = 4*L/(g*D)^{1/2} \qquad [1]$$

where D is the mean depth, g is the acceleration due to gravity and L is the basin length (Forrester, 1983).

The occurence and strength of both the seiche effect and the land-sea breeze are unpredictable. Given the short records available in Rupert Bay, the importance of these wind generated phenomena at periods close to tidal constituents cannot be neglected in analyzing spectra.

FRONTS

Oceanic fronts may be defined as boundaries between horizontally juxtaposed water masses of dissimilar properties (Bowman and Iverson, 1978). They are common features of many estuaries and may significantly affect both the lateral and longitudinal variations in the circulation and mixing. The surface convergent circulation associated with these features bring foam and other floating debris into a line along the position of the front.

Fedorov (1983) defines two types of estuarine fronts, type I - those associated with a "salt wedge" and occupying a position perpendicular to the axis of the estuary, and type II - those related to the interaction of tidal currents with the bottom topography of the estuary and located along the axes of the characteristic features of the bottom topography (mainly along the axis of the estuary). He also indicates that fronts of the second type are encountered more frequently in shallow estuaries of considerable width, with a rugged bottom

topography.

In Rupert Bay, fronts are indeed large in number and similar to Fedorov's type II. They are mostly aligned parallel to the axis of the main channels and around the downstream islands. Figure 11 depicts their approximate distribution from aerial pictures and visual observations (Ingram, 1977). Their presence is also detectable on some unfiltered current meter records, as a quick change of both transverse current velocity and of the salinity and temperature fields occur at maximum ebb.

In Rupert Bay, it is thought that frontogenesis occurs as a result of differential mixing caused by strong tidal flow over variable bottom topography, therefore creating lateral gradients of density (Figure 12).

The same type of frontal formation was reported by Huzzey (1988) and Huzzey & Brubaker (1988) in York River estuary, on the western shore of Chesapeake Bay (Virginia). Klemas and Polis (1977) also observed an extensive network of such fronts, in Delaware Bay, and related them to regions of strong lateral density gradients.

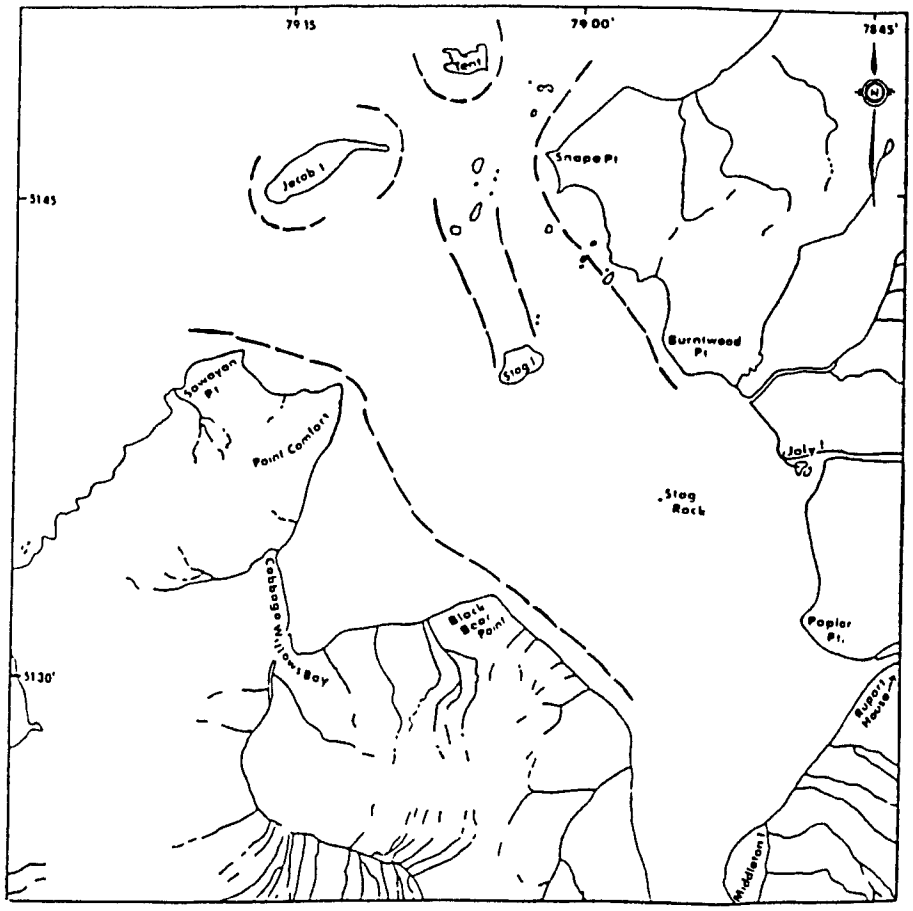

Figure 11. Approximate frontal distribution from aerial pictures and visual observations (Ingram, 1977).

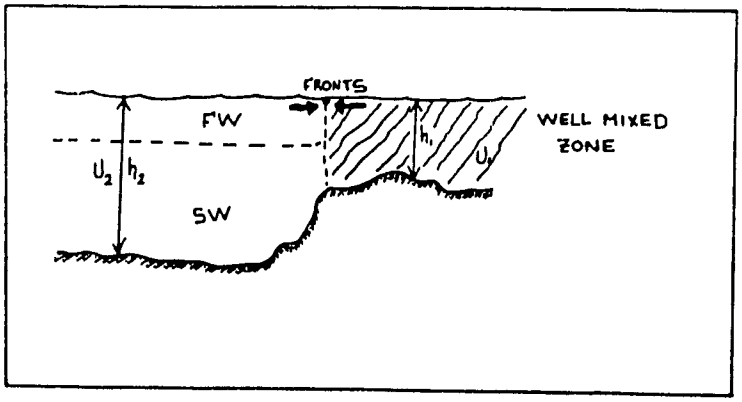

Figure 12. Differential mixing caused by variable bottom topography.

Simpson and Hunter (1974) developed an empirical model to predict frontal position in the Irish Sea according to local tidal currents and bathymetry. They suggested that the energy required to mix the water column was proportional to tidal energy loss and inversely proportional to local depth. As this tidal energy dissipation is also proportional to the cube of tidal current intensity, they integrated their observations and predicted frontal formation when :

$$D / U^3 \approx 55$$

For tidal currents of 0,5 m/s, frontal formation should occur at about 7 m, while tidal currents of 1,0 m/s would correspond to 55 m depth. As tidal currents in Rupert Bay are usually between those limits, fronts should develop around the 15 to 20 m isobath regions. Although this simple criterion predicts depth values that are larger than the actual depths, it still suggests that frontal formation should follow regions of maximum slope (like channel edges). An examination of Figures 3 and 11 confirms this hypothesis.

THE CIRCULATION

In Rupert Bay, the circulation is dominated by the tidal flow ; the displacement of the tidal front is large and currents use different paths for flood and ebb (Figures 13 and 14). In deeper channels (section B), flood currents are dominant, thus creating a strong residual current directed upstream (averaged over a semi-diurnal tidal cycle and for surface and deep moorings). In shallower areas (section O), the ebb current is usually more important, whereas in the middle zone, or section A, residual currents were often found to have a large transverse component (Ingram, 1977). The mean circulation was established from velocity data, taken in the upper 5 m, which have been averaged over time. Figures 13,14 and 15 depict the ebb circulation, the flood circulation and the mean circulation (using mooring data).

The main disturbing influence on the non-tidal mean circulation is believed to be the wind and bottom friction. Indeed, in estuaries with large ratio, Σ , of tidal range to mean water depth (Rupert Bay : $\Sigma = 0.625$), local depth changes appreciably over a tidal cycle and the bottom effect on current magnitude and direction is important in shallow areas (Kjerfve 1975). This bottom effect is due to the frictional stresses arising from bottom drag.

a)

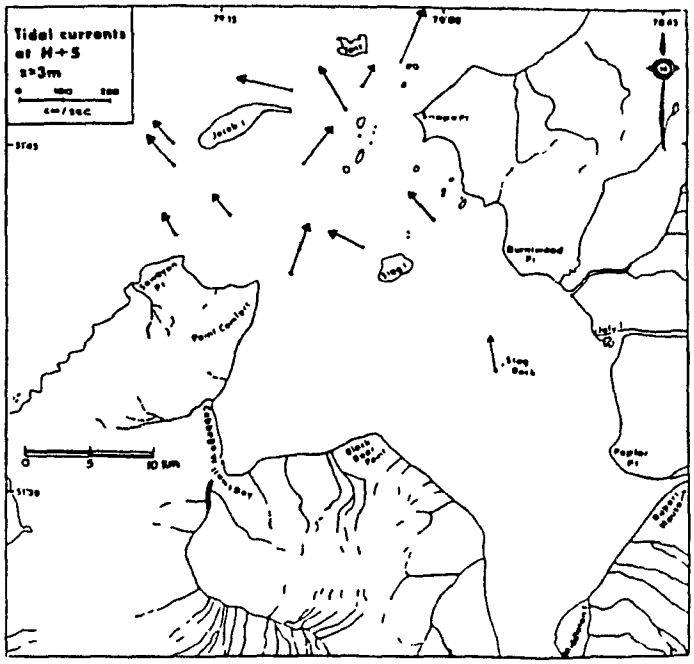

b)

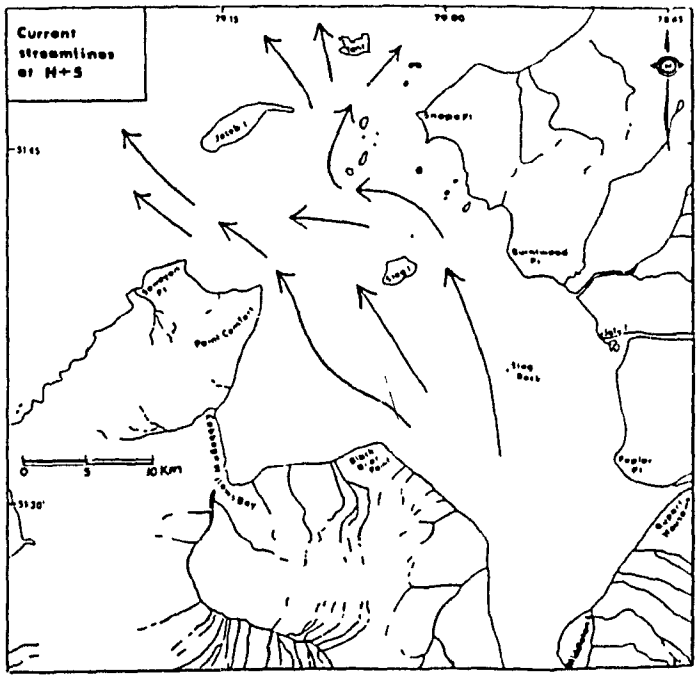

Figure 13. Ebb circulation (H+5) at z = 3 m : a) tidal currents and b) interpolated/extrapolated streamlines.

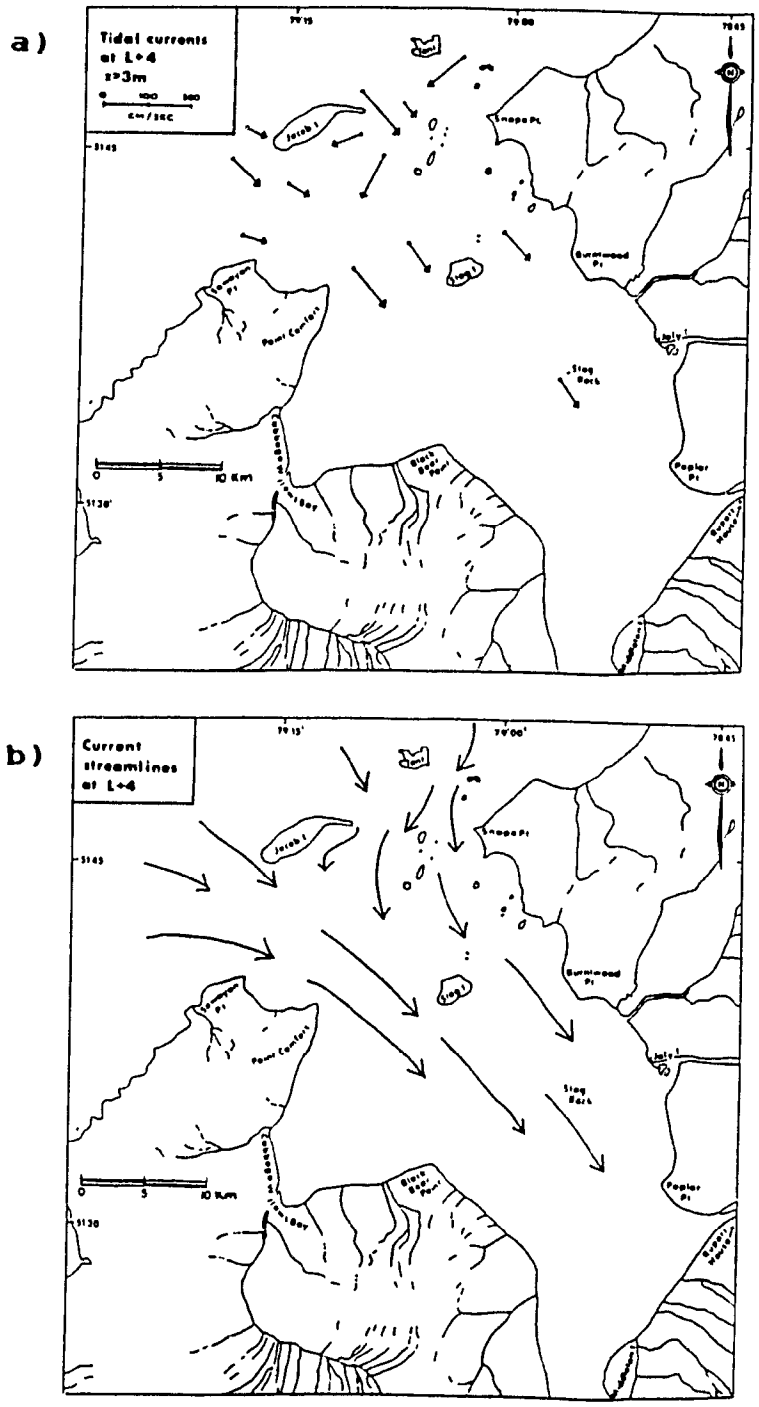

Figure 14. Flood circulation (L+4) at z = 3 m : a) tidal currents and b) interpolated/extrapolated streamlines.

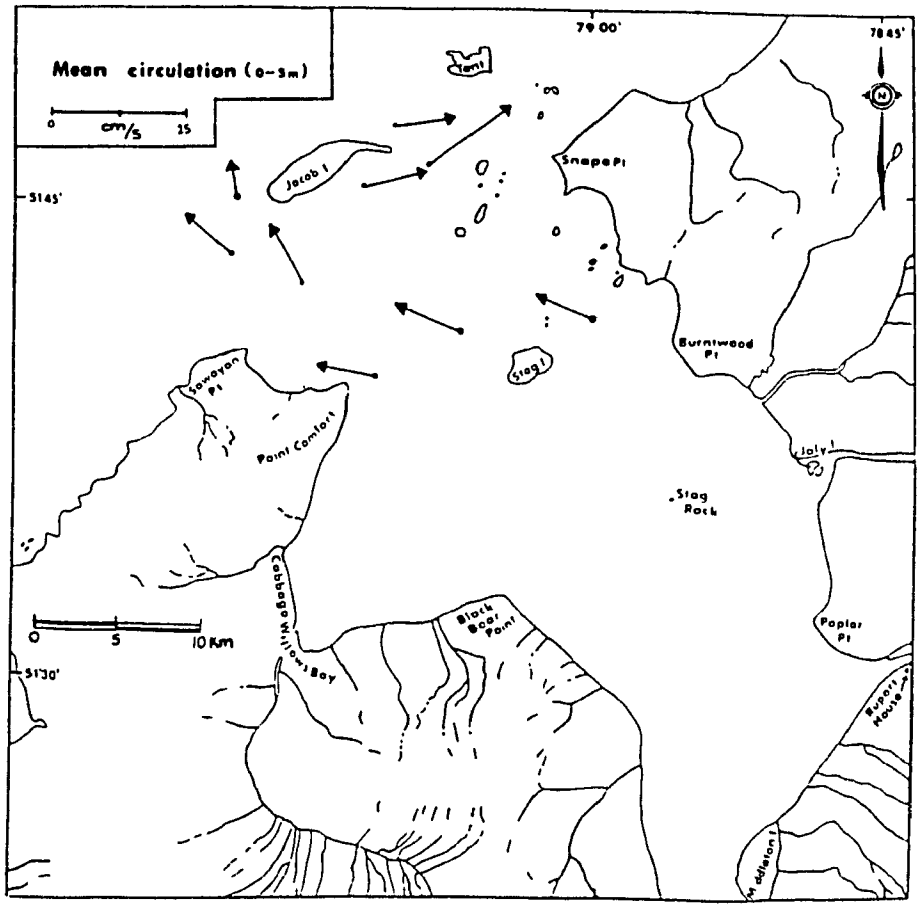

Figure 15. Mean circulation in the surface layer (0-5 m).

The main characteristics of the circulation in Rupert Bay are then : (1) strong tidal current compared to mean flow; (2) residual circulation controlled by the principal channels; (3) tidal currents use different paths at flood and ebb; (4) tidal current magnitude is about 30 % lower at ebb than at flood; (5) surface currents much are affected by wind stress; (6) secondary flows are important.

We have seen that the presence of secondary flows play an important role in Rupert Bay. Similar to Dyer (1977) and Larouche et al. (1987), we will now examine the importance of cross-channel motion within the Bay.

LATERAL DYNAMIC BALANCE AT TRANSECT A

According to Ingram (1977), secondary flows are important in Rupert Bay. The water flows in a spiral fashion and the transverse and vertical components of this flow create what are known as secondary flows in the plane of the cross section. This type of circulation, which is usually caused by variations in bottom topography, produces lateral variations in the salinity and velocity fields (Dyer, 1977).

To demonstrate this effect, variations of the lateral motion along a cross section comprising three stations are analysed. Transect A is located between Point Comfort and

Draulette Island. The bathymetric profile showing the position and depth of the moorings at stations 25,40 and 27 can be seen on Figure 16.

Consider a right handed co-ordinate system, located at the water surface with the tidal mean velocities u, v, and w in the along channel (x), lateral (y), and vertical (z) directions, respectively. The lateral equation of motion is

$$\frac{\partial \bar{v}}{\partial t} + \bar{u}\frac{\partial \bar{v}}{\partial x} + \bar{v}\frac{\partial \bar{v}}{\partial y} + \bar{w}\frac{\partial \bar{v}}{\partial z} = -\frac{\bar{1}}{\rho}\frac{\overline{\partial p}}{\partial y} - g\frac{\overline{\partial \zeta}}{\partial y} - f\bar{u} - \frac{\overline{u^2+U^2}}{R}$$

(1) (2) (3) (4) (5) (6) (7) (8)

$$+ \frac{1}{\rho}\frac{\partial F}{\partial z} - \frac{\partial \overline{(u'v')}}{\partial x} - \frac{\partial \overline{(v'v')}}{\partial y} - \frac{\partial \overline{(w'v')}}{\partial z} \qquad [2]$$

(9) (10) (11) (12)

where overbars denote averaging over a tidal cycle; ρ is the density; p is the pressure; g is the gravity; ζ is the water elevation from mean surface level; f is the Coriolis parameter; U is the longitudinal tidal velocity amplitude; R is the radius of curvature of the streamlines estimated from aerial pictures (Figure 5); F is the lateral frictional force created by the surface and sea bed shear stresses; and u', v', w' are the turbulent high frequency current fluctuations.

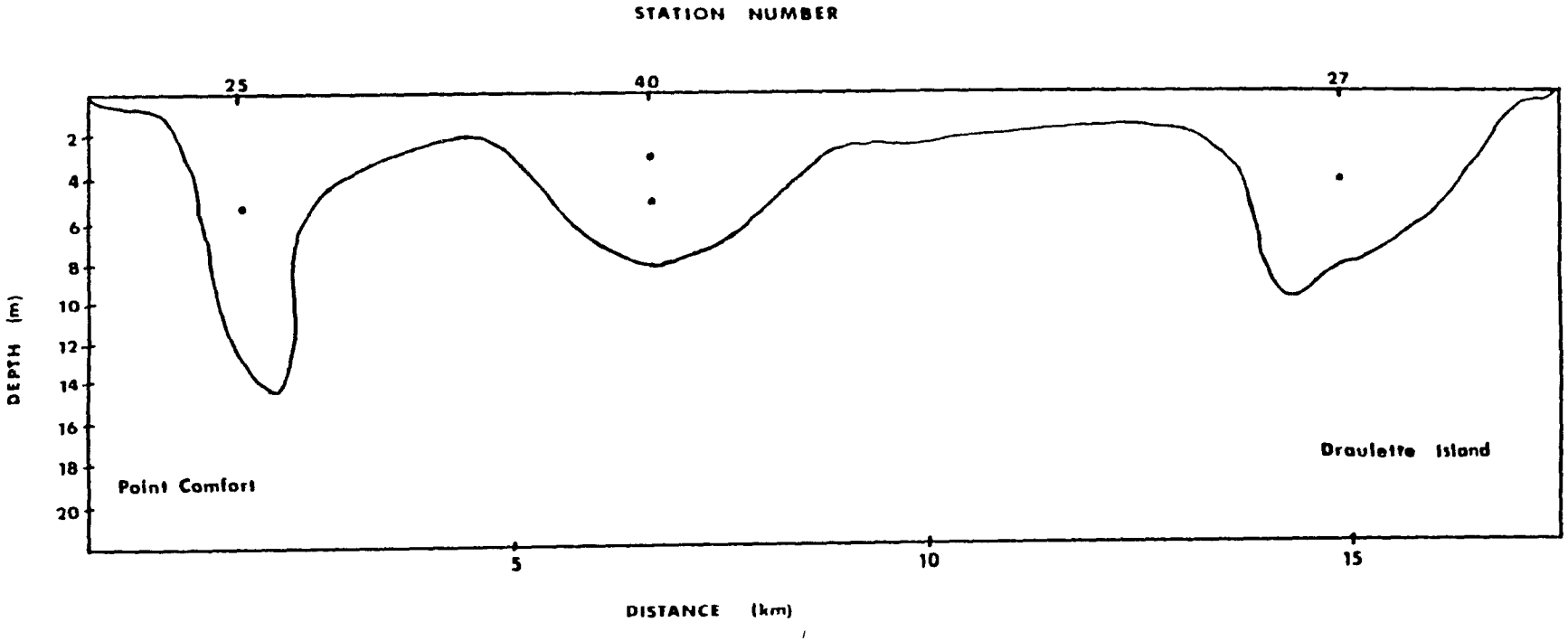

Figure 16. Bathymetric profile of transect A with moorings.

Term (1) is the time rate of change in the lateral velocity. Term (2) - (4) are the field acceleration terms associated with the secondary circulation. Term (5) is the baroclinic pressure gradient while term (6) is the horizontal pressure force resulting from differences in elevation of the water surface across the estuary. The Coriolis force is term (7) and the centrifugal force, arising from the curvature of the streamlines, is term (8). Term (9) is the lateral frictional force created by wind stress on the water surface and bottom friction. Terms (10) to (12) are the turbulent Reynolds stresses (Dyer, 1977).

The relative magnitudes of terms (3),(5),(7),(8) and (9) have been estimated for the three stations along transect A. The other terms i.e.(1),(2),(4),(6) and (10) to (12) have not been calculated either because they are believed to be insignificant in the lateral balance (Dyer, 1977) or because we could not estimate them from the available data.

Pressure measurements were adjusted hydrostatically to the 3 m-level, as follows:

$$P(3\ m) = P(z) - g\rho\,\Delta z \qquad [3]$$

where P(3 m) is the desired pressure, P(z) is the pressure recorded at depth z, ρ is the density measured at depth z, and

Δz is the difference (z - 3) in meters. The mean water density on this transect was set at 1006 kg/m^3 and the radius of curvature of the streamlines (R), which varies between 15 and 30 km according to Ingram (1977), was set at 24 km.

Finally, all calculations were done over the same 10 consecutive semi-diurnal tidal cycles (11/08/76 at 11 h to 16/08/76 at 16 h). Table 5 shows the calculated acceleration terms for the two adjacent pairs 25-40 and 40-27 and for the whole transect.

The results in Table 5 show that, in the terms we are able to estimate, the dominant ones in the lateral dynamic balance are the centrifugal acceleration, the Coriolis force and the baroclinic pressure gradient between stations 25 and 40. The local acceleration term appears to be of secondary importance. The prominence of the centrifugal term (8) was expected due to the strong tidal flow in this region (up to 100 cm/s at sta.25) and from aerial observations. What is surprising is that term (8) was twice as large as the Coriolis term, which was first assumed to be the most important due to the width of the bay (Dyer, 1977). The strength of the baroclinic pressure gradient between stations 25 and 40 results from the fact that fresh water flows mainly on the northern side of the bay (Figure 5).

Table 5. Lateral Dynamic Balance in Rupert Bay at Transect A. Terms 3,5,7,8,9 from equation [2] are estimated from hourly smoothed velocity and density measurements at stations 25,27 and 40. Units are 10^{-6} m/s² and the curvature of streamlines (R) is given in km.

STATION PAIRS :	(25-40)	(40-27)	(25-27)
TERMS			
(3) : $\bar{v}(\partial\bar{v}/\partial y)$	1.83	-0.58	0.27
(5) : $\overline{(\partial P/\partial y)/\rho}$	-16.70	2.40	-4.72
(7) : $(f\bar{u})$	-6.78	-5.65	-5.65
(8) : $(\overline{u^2} + \overline{U^2})/R$	16.10	10.51	18.33
TOTAL : (3)+(5)+(7)+(8)			
(residual contribution)	-5.55	6.68	8.23
(9) : $(\partial F/\partial z)/h\rho$			
for station 25 ...	-1.35		
for station 40 ...	-5.48		
for station 27 ...	-3.41		

The " total " shown in Table 5 represents the "residual" contribution arising from other terms in equation [2]. Although this contribution is of the same order of magnitude as the Coriolis term, it is thought that those other terms are individually less significant than terms (5), (7) and (9).

Dyer (1977) pointed out that, of all terms in equation [2], wind stress is potentially the most significant, especially in shallow estuaries. He defined this lateral frictional term (9) by :

$$(F_S - F_B)/\rho h \qquad [4]$$

where F_S and F_B were the surface and sea bed shear stresses and h the water depth. Following onset of wind forcing, the whole mass of water tends to be driven across the estuary. An induced water circulation is then created, giving downwelling on the downwind side and upwelling on the upwind side of the estuary. This secondary circulation leads to negative values of the sea bed shear stress (F_B) and an increase in the frictional term. In Rupert Bay, we could not confirm this relationship for two main reasons : first, the dominant winds are mainly longitudinal ; secondly, strong tidal flows and the bottom topography restrain such a cross-sectional wind induced circulation. Consequently, the values calculated for the lateral frictional term (9) on transect A are probably not

significant. The higher range at station 40 is probably due to the lack of precision in the measurements needed in the calculation.

CONCLUSION

Rupert Bay estuary is characterized by its shallow topography, strong tidal flow and numerous fronts. Mixing is intense in the first two-thirds of its length, creating homogeneous conditions in many areas. Spectral analysis of observed water level and current velocity confirmed the strong semidiurnal character of the tide and the presence of important shallow water constituents. Most of the observed non-tidal water level variations were well correlated with wind forcing. Finally, an examination of the lateral dynamic balance equation at a mid-bay transect showed that the centrifugal force, the Coriolis acceleration and the baroclinic pressure gradient between the south shore station and the middle bay one, were the most important terms of those we were able to estimate. Results are in general agreement with aerial observations.

ACKNOWLEDGEMENTS

The authors would like to thank Jean-Claude Deguise for his work in collecting the data. This work was supported by research grants from SEBJ and Hydro-Québec to GIROQ and by an NSERC operating grant to R.G.Ingram.

REFERENCES

Aubrey, D.G. and P.E. Speer, 1985. A study of non-linear tidal propagation in shallow inlet/estuarine systems. Part I: Observations. Estuarine, Coastal and Shelf Science, 21 : 185-205.

Bowman, M.J. and R.L. Iverson, 1978. Estuarine and plume fronts. in Oceanic Fronts in Coastal Processes, edited by M.J. Bowman and W.E. Esaias, Springer-Verlag, New York : 87-104.

Canadian Hydrographic Service, 1972. Chart 5414, scale 1:73000, Ottawa.

d'Anglejan, B., 1977. Etudes sédimentologiques et géochimiques de la Baie de Rupert en 1966 et 1977. GIROQ, rapport à la SEBJ. 92 p., (unpublished).

d'Anglejan, B., 1980. Effects of seasonal changes on the sedimentary regime of a subarctic estuary, Rupert Bay (Canada). Sedimentary Geology, 26 : 51-68.

Defant, A., 1960. Physical Oceanography. Vol.2. Pergamon Press, London, 598 p.

Dunbar, M.J., 1982. Oceanographic research in Hudson and James Bays. Naturaliste Canadien, 109 : 677-683.

Dyer, K.R., 1977. Lateral circulation effects in estuaries. In : Estuaries, Geophysics, and the Environment. National Academy of Sciences, Washington DC : 22-29.

Fedorov, K.N., 1983. The Physical Nature and Structure of Oceanic Fronts. in Lecture Notes on Coastal and Estuarine Studies. No.19, Springer-Verlag, New York, 333 p.

Foreman, M.G.G., 1977. Manual for Tidal Heights Analysis and Prediction. Pacific Marine Science Report 77-10, Institute of Marine Sciences, Patricia Bay, Victoria, B.C. 97 p. (unpublished).

Foreman, M.G.G., 1978. Manual for Tidal Currents Analysis and Prediction. Pacific Marine Science Report 78-6, Institute of Marine Sciences, Patricia Bay, Victoria, B.C., 70 p. (unpublished).

Forrester, W.D., 1983. Manuel Canadien des Marées. Ministère des Pêches et des Océans, Service Hydrographique du Canada, Ottawa (Ontario),148 p.

Godin, G.G., 1972. The Analysis of Tides. University of Toronto Press, 264 p.

Hansen, D. and M. Rattray, 1966. New dimensions and estuary classification. Limnology and Oceanograph, 11(3) : 319-325.

Huzzey, L.M., 1988. The lateral density distribution in a partially mixed estuary. Estuarine, Coastal and Shelf Science, 9 : 351-358.

Huzzey, L.M. and J.M. Brubaker, 1988. The formation of longitudinal fronts in a coastal plain estuary. Journal of Geophysical Research, Vol. 93, C2 : 1329-1334.

Ingram, R.G., 1977. Océanographie physique de l'estuaire de la baie de Rupert. GIROQ, rapport à la SEBJ :44 p., (unpublished).

Ingram, R.G. and V.H. Chu, 1987. Flow around islands in Rupert Bay : an investigation of the bottom friction effect. Journal of Geophysical Research, vol.92, C13 : 14521-14533.

Kjerfve, B., 1975. Velocity averaging in estuaries characterized by a large tidal range to depth ratio. Estuarine and Coastal Marine Science. 3 : 311-323.

Klemas, V. and D.F. Polis, 1977. A study of density fronts and their effect on coastal pollutants. Remote Sensing and Environment, 6 : 95-126.

Larouche, P., Koutitonsky, V.G., Chanut, J.-P. and M.I.El-Sabh, 1987. Lateral Stratification and Dynamic Balance at the Matane Transect in the Lower Saint Lawrence Estuary. Estuarine Coastal and Shelf Science, 24 : 859-871.

Ouellet, Y., 1977. Etudes à l'aide d'un modèle mathématique de la circulation hydrodynamique, de la propagation de la marée et de la distribution de la salinité dans la baie de Rupert. GIROQ, rapport à la SEBJ : 115 p., (unpublished).

Seim, H.E. and J.E. Sneed, 1988. Enhancement of semidiurnal tidal currents in the tidal inlets to Mississippi Sound. in Lecture Notes oc Coastal and Estuarine Studies, Vol.29. D.G. Aubrey, L. Weishar (Eds), Hydrodynamics and Sediment Dynamics of Tidal Inlets, Springer-Verlag, New York : 157-168.

Simard, Y. and L. Legendre, 1977. Complexe NBR. Etude sur la baie de Rupert: Synthèse des études de 1976. GIROQ, rapport à la SEBJ : 80 p., (unpublished).

Simpson, J. and J. Hunter, 1974. Fronts in the Irish Sea. Nature, 250 : 404-406.

CHAPTER 3 : RIVER PLUME LIFT-OFF UNDER A COMPLETE ICE COVER IN HUDSON BAY

ABSTRACT

Measurements of the temperature and salinity fields were made at the mouth of Great Whale River, southeastern Hudson Bay, during a period of complete sea ice cover and rising river discharge. The aim of the experiment was to characterize the lift-off region of the freshwater plume as a function of tidal phase, bathymetry and discharge rate. Comparison of field data for the under ice case and predictions based on recent laboratory and analytical studies show disagreement. Discussion of the processes at work and evidence for supercooled water masses under the plume immediately offshore of the lift-off point are presented.

INTRODUCTION

As a part of an extensive oceanographic study of the Great Whale River plume in southeastern Hudson Bay (Canada), a field investigation was undertaken at the mouth of the river to examine the hydrodynamic behaviour of the plume. The survey took place during the period of complete sea ice cover, just before spring break up, when discharge levels were rising rapidly.

Major rivers flowing into a body of denser sea water often form surface buoyant jets and plumes. The less dense

river water is characterized by an initial discharge, a specific momentum and a buoyancy flux. Momentum dominates at the initial stage within the river mouth and the jet is attached to the bottom. At a certain distance offshore, buoyancy acts to detach the jet from the ocean floor and, as strong horizontal spreading takes place, the jet becomes a surface buoyant plume. The point where the jet leaves the bottom has been termed the lift-off point. Its location depends on the relative strength of the momentum and buoyancy fluxes at the source (Luketina and Imberger 1987a,b).

There are several criteria for estimating the location of the lift-off point. Earlier work on this subject includes that of Safaie (1979), Jirka et al. (1981), Baddour and Dance (1983), Hauenstein (1983), Hearn et al. (1985), Chu and Jirka (1986), Luketina and Imberger (1987a and b). Only Hearn et al. (1985) and Luketina and Imberger (1987a and b) have established a relationship for the lift-off point based on field observations. All others obtained their criteria from laboratory experiments. Both Hearn et al. (1985) and Luketina and Imberger (1987a and b) used field data from Koombana Bay, Western Australia during open water conditions.

The objective of this study was to describe the characteristics of the Great Whale River under-ice plume in the lift-off region, to estimate the location of the lift-off

point for varying momentum and buoyancy fluxes and to compare the observations with existing models.

The conclusions of this study are expected to be helpful in understanding the behaviour of plumes and jets in subarctic coastal areas. Plume features are closely linked with the formation of fronts and convergence zones, which in turn may have ecological significance to local productivity. The depth of the lift-off point may also be instrumental in determining the salt intrusion characteristics upstream of the river mouth.

THE STUDY AREA

With a mean annual river runoff exceeding 700 m^3/s, the Great Whale River is one of the major rivers entering Hudson Bay in northern Canada (Figure 1). Low water depths over sandbar located near the river mouth are about 2 m, while within 2 km offshore the depth falls to over 60 m. Hudson Bay is almost completely covered by sea ice from January to April each year. The ice break up in the river usually occurs in mid-May and subsequently in the offshore area (Lepage and Ingram, 1988). River discharge is subject to large seasonal fluctuations : annual minima and maxima are usually attained in mid-April and late May, respectively. Figure 2 illustrates three years of discharge data from the Great Whale River.

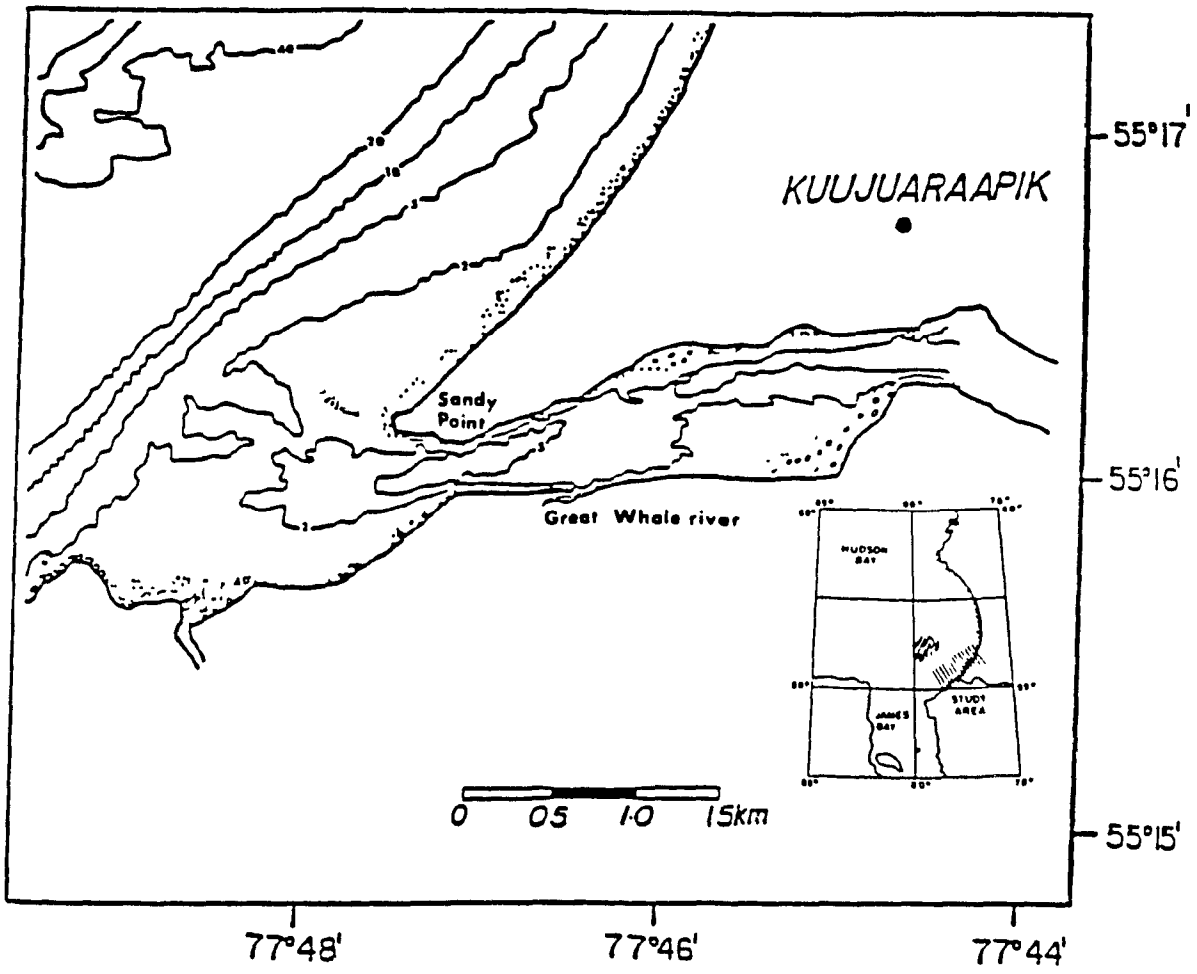

Figure 1. Place map of the study area.

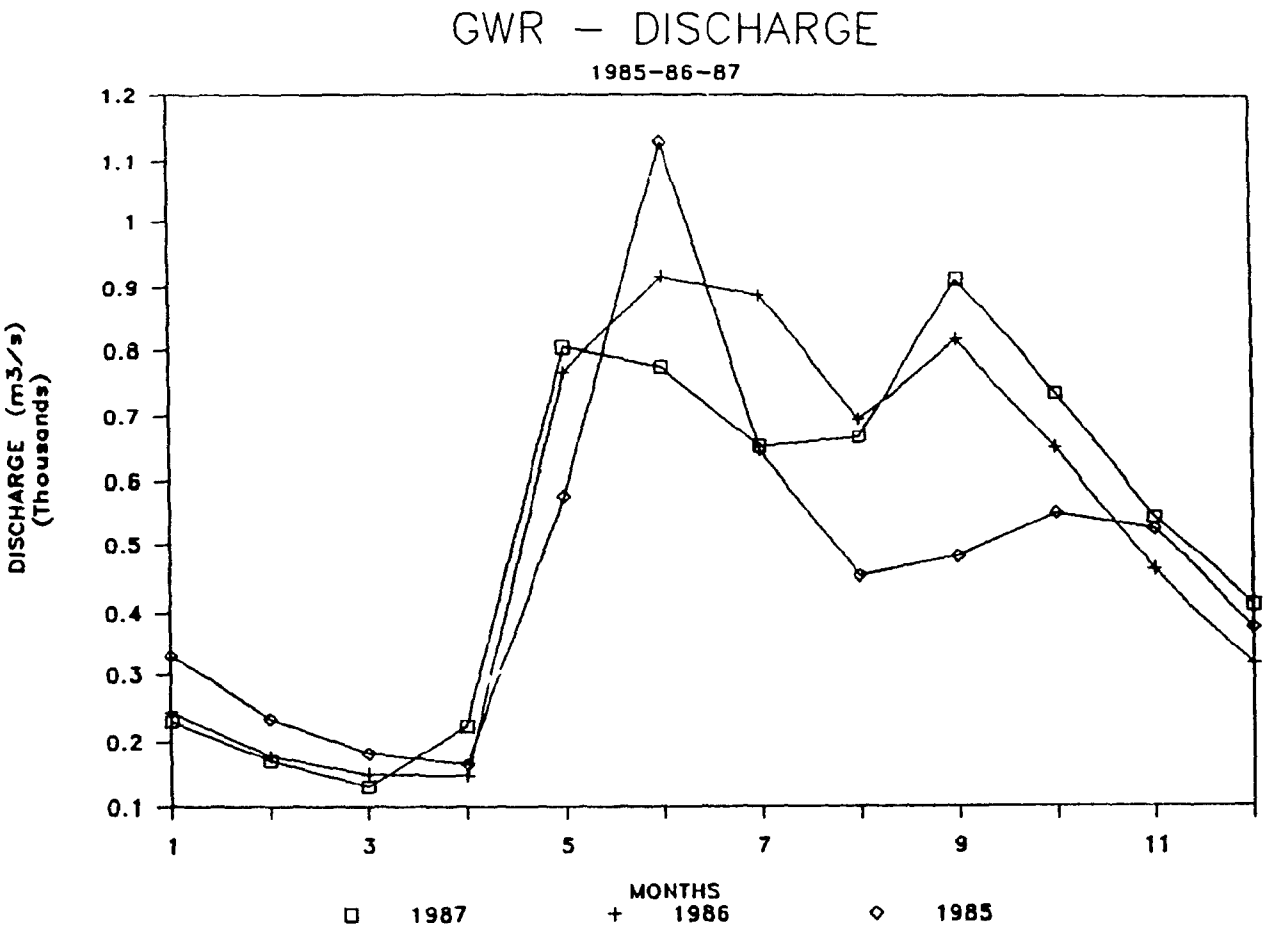

Figure 2. Great Whale River annual hydrograph for the years 1985, 1986 and 1987.

CHARACTERISTICS OF GREAT WHALE RIVER UNDER-ICE PLUME

Recent interest in the oceanography of Hudson Bay and James Bay and adjacent estuaries has been related principally to the Québec government's decision in the early seventies to dam or divert a number of rivers for the purposes of hydro-electric development. The Great Whale River (GWR) is one of those proposed for development in the 1990's.

Previous work on Great Whale River plume includes that of Ingram (1981), who presented observations of the GWR plume motion field and dilution effects in summer, and a limited data set for winter; Freeman et al. (1982) and Freeman (1982) who described and modelled the spreading and mixing of La Grande and Great Whale river plumes; Ingram and GIROQ (1977 and 1979) published two technical reports on the general physical oceanography of Manitounuk Sound and the Great Whale and Little Whale estuaries; and, finally, Ingram and Larouche (1987), Lepage and Ingram (1988) and Ingram et al. (in press) who studied the variability of the GWR under-ice plume.

From the above studies, the general characteristics of the GWR plume can be outlined as follows : the river forms an extensive plume at all times of the year because of the large ratio of mean freshwater discharge velocity to tidal current at its mouth. The plume is, according to Ingram (1981) and

Freeman et al. (1982), in hydrostatic equilibrium and is decoupled from the velocity field underneath. The summer plume covers a surface area of approximately 100 km² and is between 1 to 2 m in depth. Typical velocities within the plume are about 60 cm/s in amplitude and north-westerly in direction, whereas tidal currents in the underlying waters are generally less than 10 cm/s (Lepage and Ingram 1988). Under the sea ice cover, from January to mid-May, a much larger plume develops compared to open water conditions with a sharp pycnocline between 3 and 5 m in depth (Ingram and Larouche 1987). The larger aerial extent of the plume in the period of reduced freshwater flow (ref. Figure 2) has been related by Ingram (1981) to the absence of direct wind and wave mixing and also to the reduced tidal motion on the under side of the ice near the river mouth. Ingram and Larouche (1987) showed that the late winter-early spring plume area varied as a power of the discharge and that differences in plume geometry were related to elapsed time since ice formation and low-frequency variability of the coastal circulation.

THE LIFT-OFF REGION : METHODS and OBSERVATIONS

During the 3-week program, current velocity was monitored continuously (5-min sampling) upstream of the river sill with an Aanderaa recording current meter (RCM model 4), while CTD profiles were taken along a transect of eight stations near

the mouth of the river (Figure 3). These stations, consisting of ice holes (about 40 cm in diameter), were spaced at about 150 m intervals across the river sill. The deepest offshore station had a depth of 26 m, while the shallowest inshore site was about 2 m in depth. The complete transect was sampled on nine occasions at different tidal phases (including neap and spring tides). A Seabird Seacat CTD instrument and an ice thickness gauge were used. Sampling took place between April 23rd and May 7th 1988. The break up of the river ice occurred on May 8th. To complete this set of data (CTD and current meter data), discharge values were obtained from the Ministère de l'Environnement du Québec (MENVIQ).

Along with the MENVIQ values, the river mouth discharge rates were calculated with the single-velocity method (Strilaeff and Bilozor, 1975) i.e. from the current velocity data and the cross-sectional area at the river mooring. The area of the river at the mooring site (located at a constriction) was estimated, assuming a 1 m thick ice layer. The discharge, Q, was then calculated by using the simple formula

$$Q = A * \bar{u} \qquad [1]$$

where A is the cross-sectional area at the current meter location and $\bar{u}$ is the daily mean longitudinal velocity. The current meter was recovered on May 1.

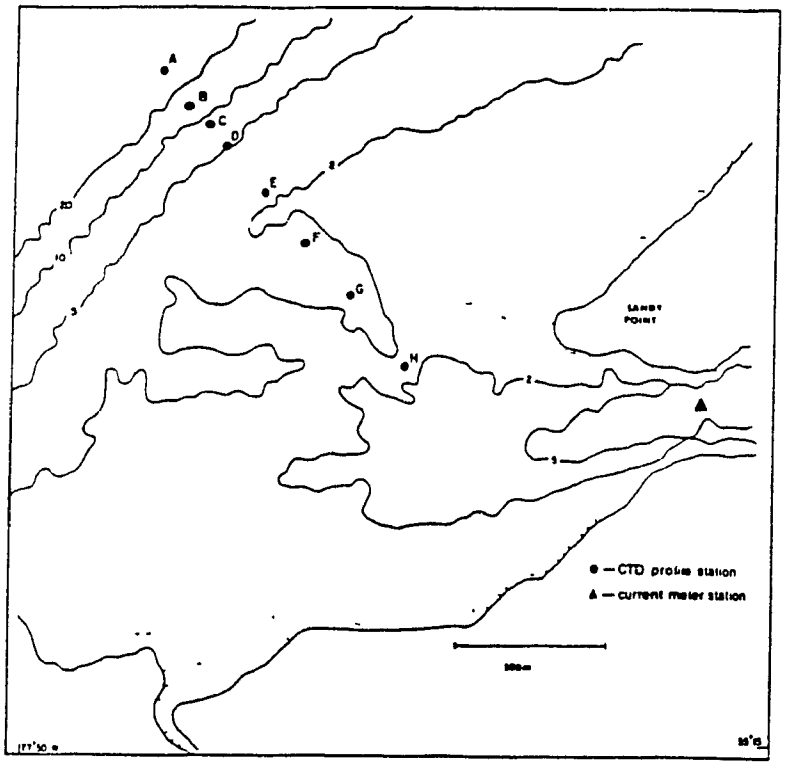

Figure 3. Place map showing bathymetry and location of both current meter mooring and CTD profiling stations.

The resulting values of discharge were subsequently plotted against the MENVIQ daily discharge data (to which an ice effect and a river mouth factor had been applied) to evaluate the accuracy of the above method. These curves can be seen on Figure 4. It seems that the two methods are in good agreement in spite of a possible large error on the river cross-section area due to the "constant ice thickness" assumption. The lower values of the single-velocity method after April 26 are probably due to the extremely mild weather conditions and the ensuing ice melt.

The river mouth freshwater runoff for the months of April and May 1988 (from MENVIQ data) are plotted on Figure 5 while Table 1 gives the conditions (tidal phase, discharge rate, mean and tidal along channel velocities at the RCM mooring) on the profiling days. Note the sharp increase of discharge rate during the sampling period and the weak values (compared to summer) of the tidal current at the RCM station. During the sampling period, the tidal current amplitude was below 5 cm/s.

An along channel bathymetric profile along the transect can be seen in Figure 6. Examples of vertical salinity profiles at stations A,C,D and E are shown in Figure 7. Note that there was no above zero salinity values at stations F,G and H during the whole sampling period.

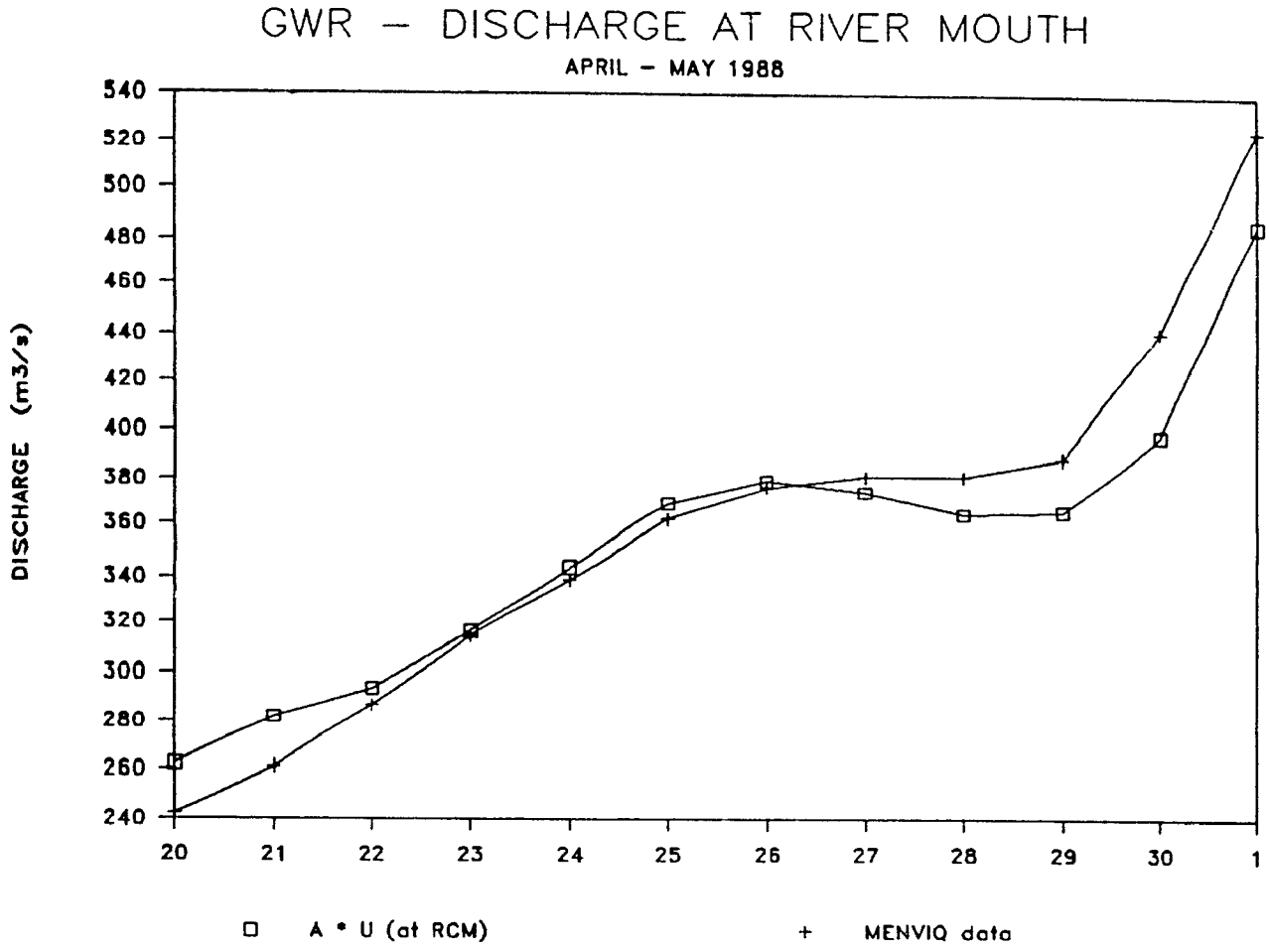

Figure 4. Comparison of the daily river mouth discharge a) from Ministère de l'Environnement du Québec data and b) calculated with equation (1).

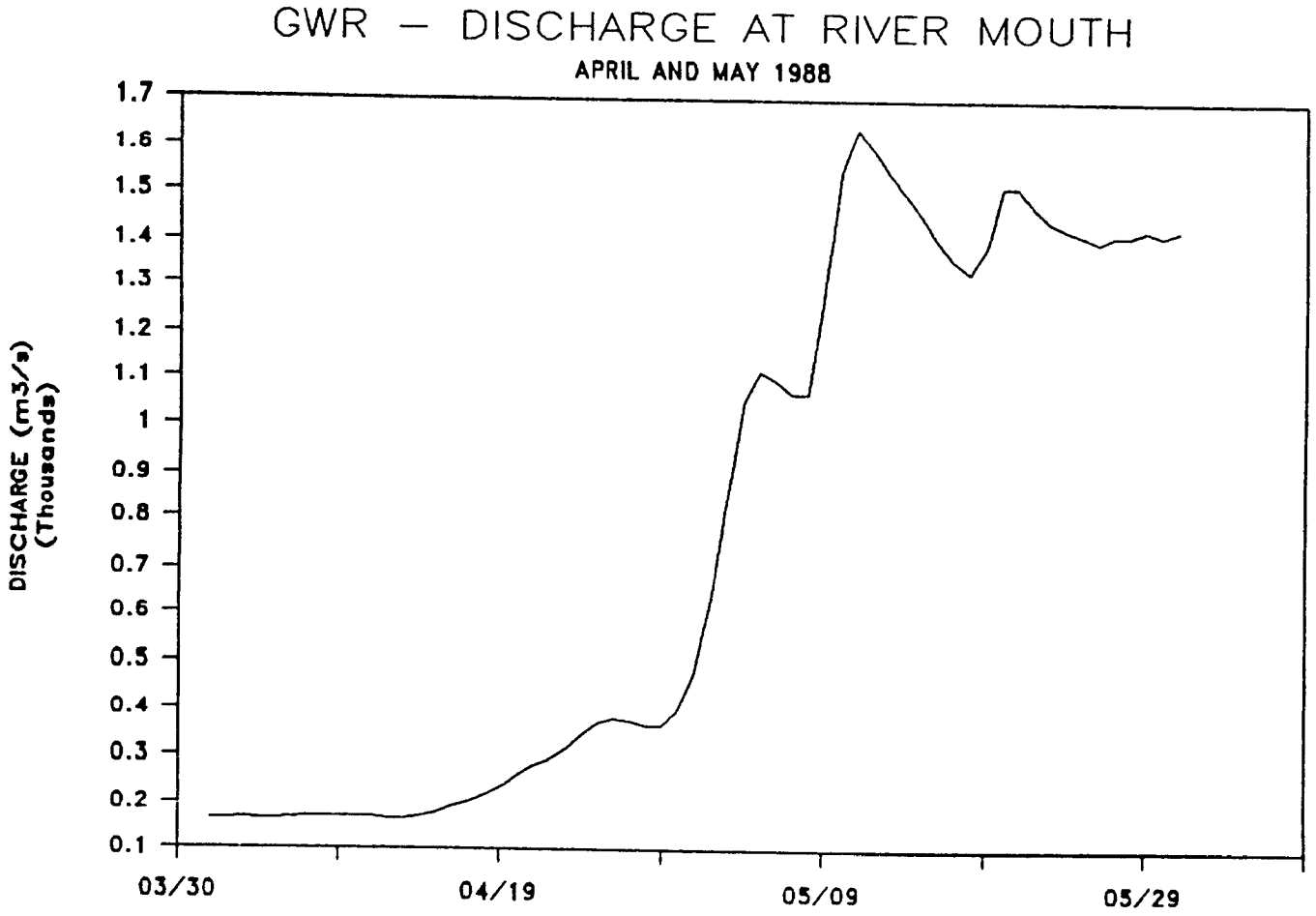

Figure 5. Daily Great Whale River mouth discharge for April and May 1988.

Table 1. **Tidal phase, river mouth discharge rate, mean and tidal along channel velocities at river mouth mooring for each profiling day.**

date	tidal phase	discharge (m^3/s)	$\bar{u}$ (cm/s)	U (cm/s)
23-04-88	H+1	316 (314)	30.2	4.8
25-04-88	H+1	369 (362)	34.8	2.8
27-04-88	L+1 (neap)	374 (381)	36.7	2.9
28-04-88	L+2	364 (381)	36.7	3.4
29-04-88	H+3	365 (389)	37.4	3.6
01-05-88	H+2	486 (525)	50.5	3.5
02-05-88	L+5	627 (NA)	60.3**	NA
05-05-88	L+6 (spring)	1117 (NA)	107.4**	NA

* values of discharge in ( ) are from RCM current measurements.

** values estimated from MENVIQ discharge rate and cross-sectional area at river mooring.

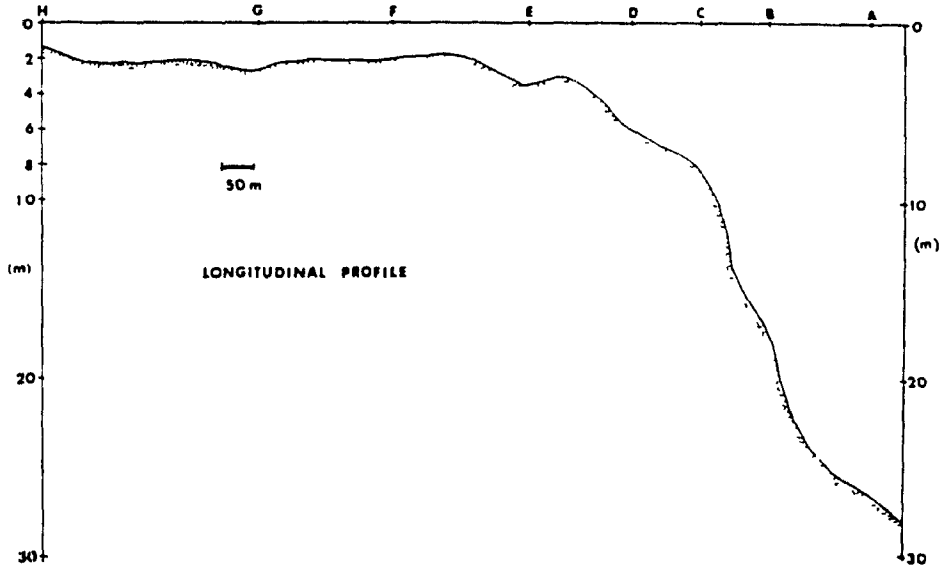

Figure 6. Longitudinal bathymetric profile of the transect.

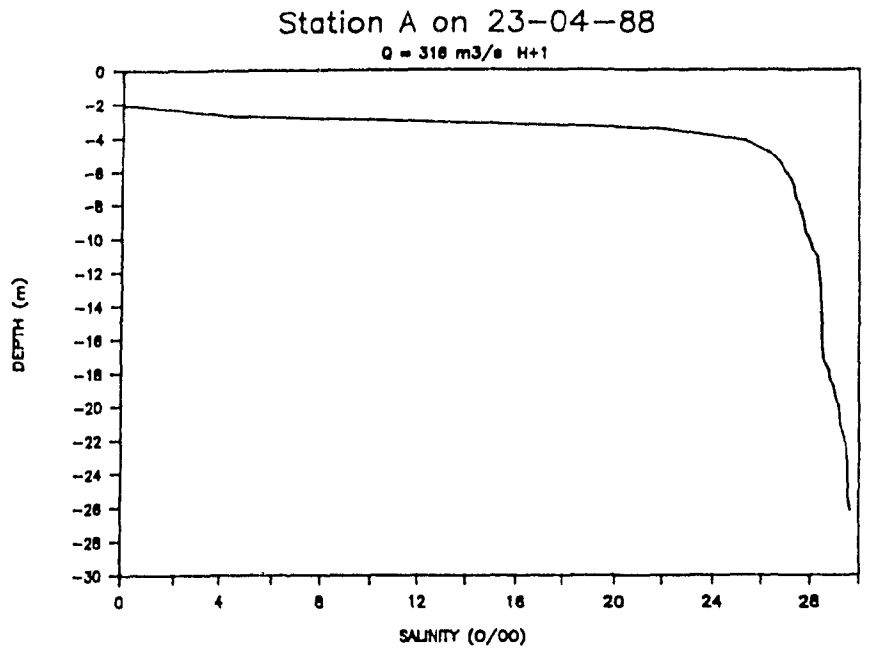

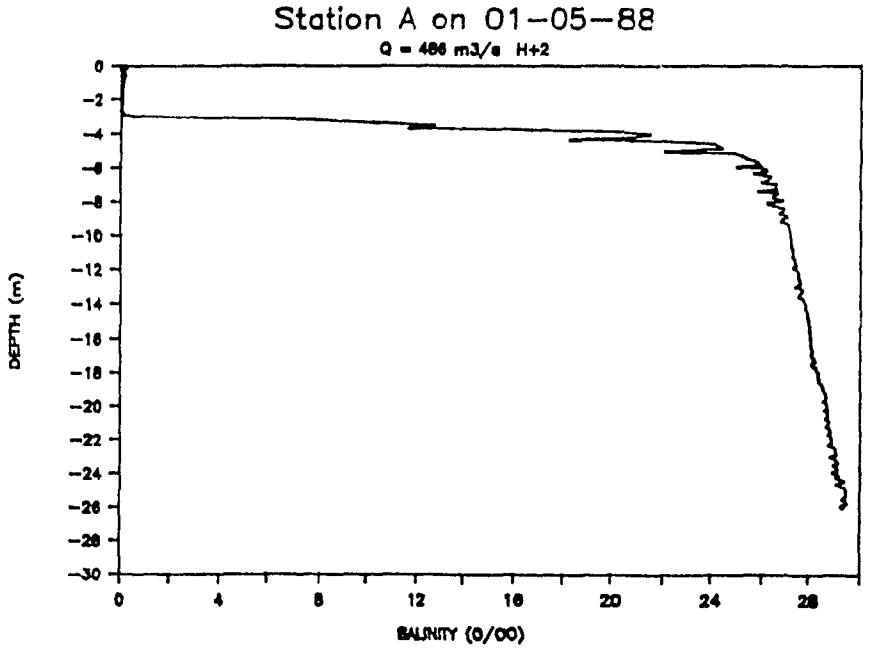

Figure 7. a) Vertical salinity profiles. Discharge rates and tidal phases are indicated on each graph.

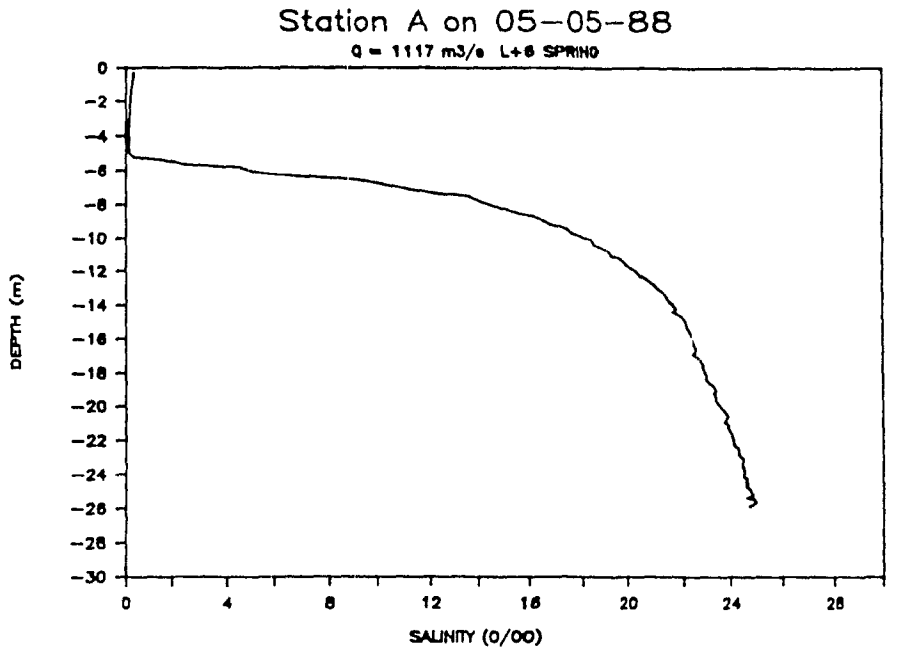
Station A on 05-05-88
Q = 1117 m3/s L+6 SPRING
DEPTH (m)
0
-2
-4
-6
-8
-10
-12
-14
-16
-18
-20
-22
-24
-26
-28
-30
0
4
8
12
16
20
24
28
SALINITY (0/00)

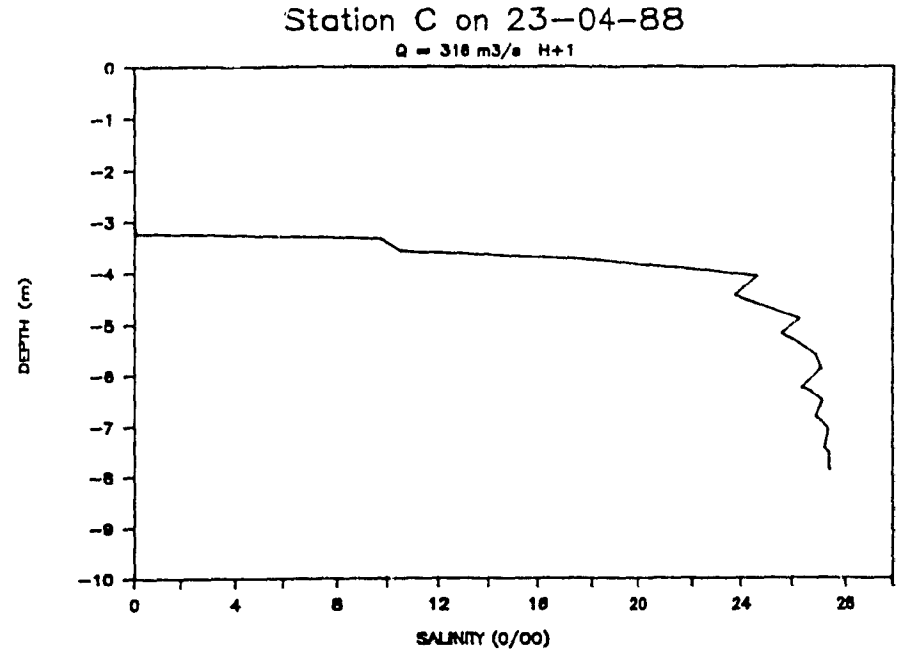
Station C on 23-04-88
Q = 316 m3/s H+1
DEPTH (m)
0
-1
-2
-3
-4
-5
-6
-7
-8
-9
-10
0
4
8
12
16
20
24
28
SALINITY (0/00)

Figure 7 b)

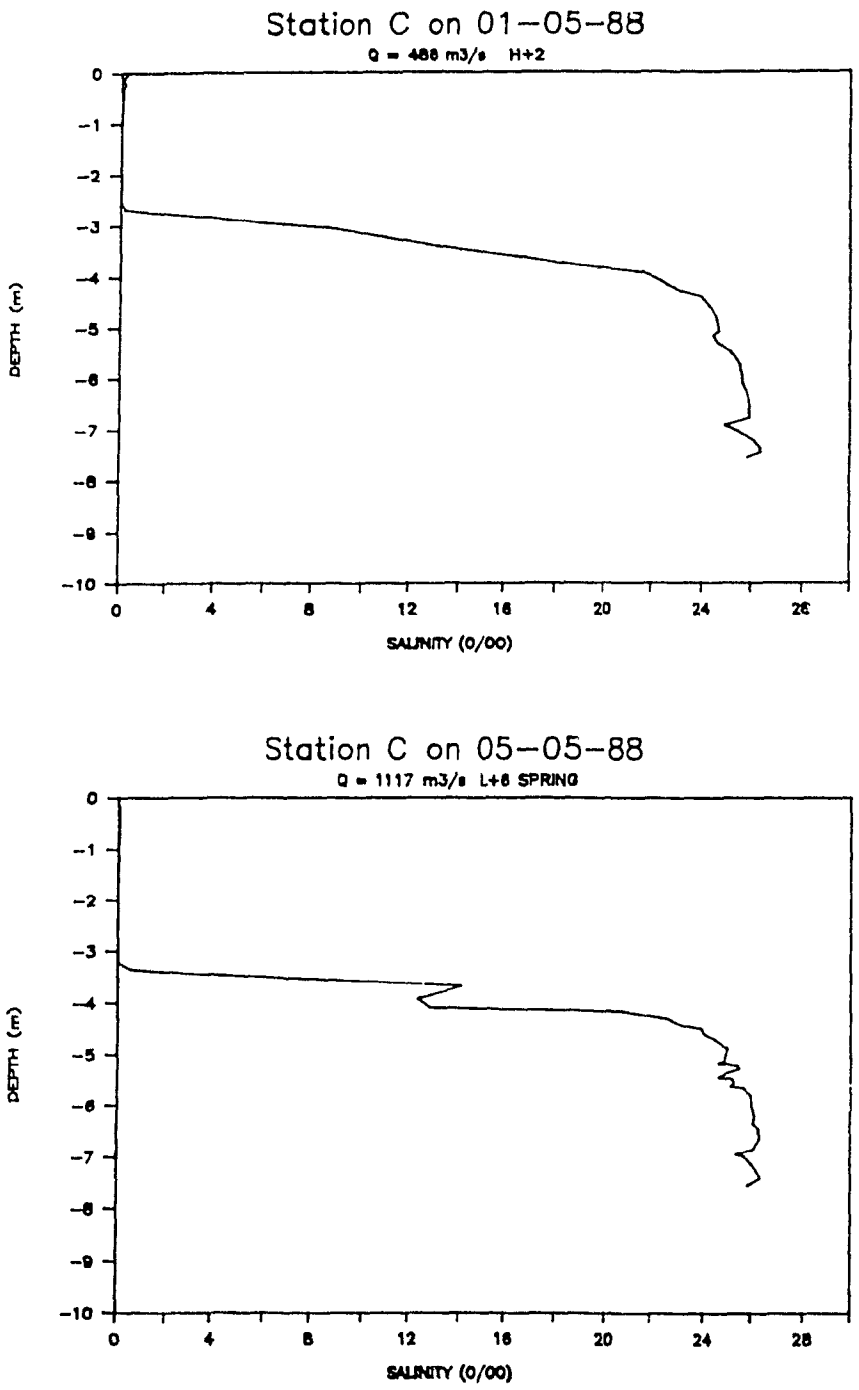
Station C on 01-05-88
Q = 486 m3/s H+2
DEPTH (m)
0
-1
-2
-3
-4
-5
-6
-7
-8
-9
-10
0
4
8
12
16
20
24
28
SALINITY (0/00)
Station C on 05-05-88
Q = 1117 m3/s L+6 SPRING
DEPTH (m)
0
-1
-2
-3
-4
-5
-6
-7
-8
-9
-10
0
4
8
12
16
20
24
28
SALINITY (0/00)

Figure 7 c)

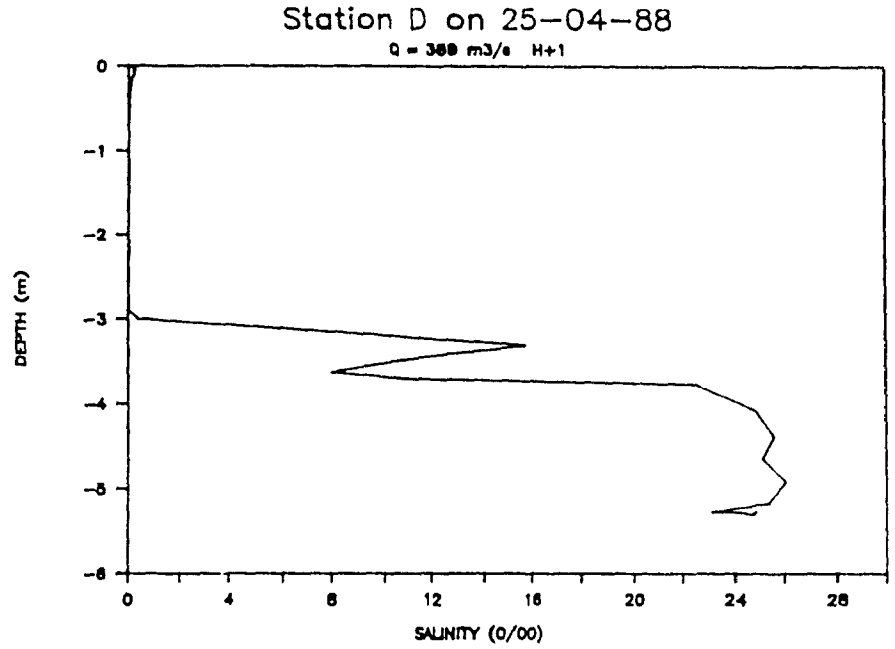
Station D on 25-04-88
Q = 388 m3/s H+1
DEPTH (m)
0
-1
-2
-3
-4
-5
-6
0
4
8
12
16
20
24
28
SALINITY (0/00)

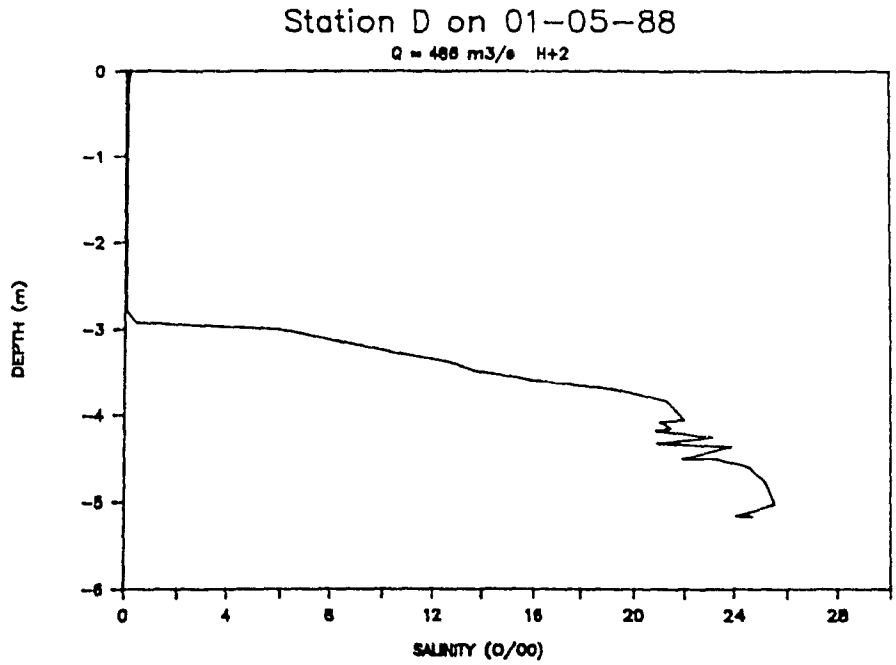
Station D on 01-05-88
Q = 486 m3/s H+2
DEPTH (m)
0
-1
-2
-3
-4
-5
-6
0
4
8
12
16
20
24
28
SALINITY (0/00)

Figure 7 d)

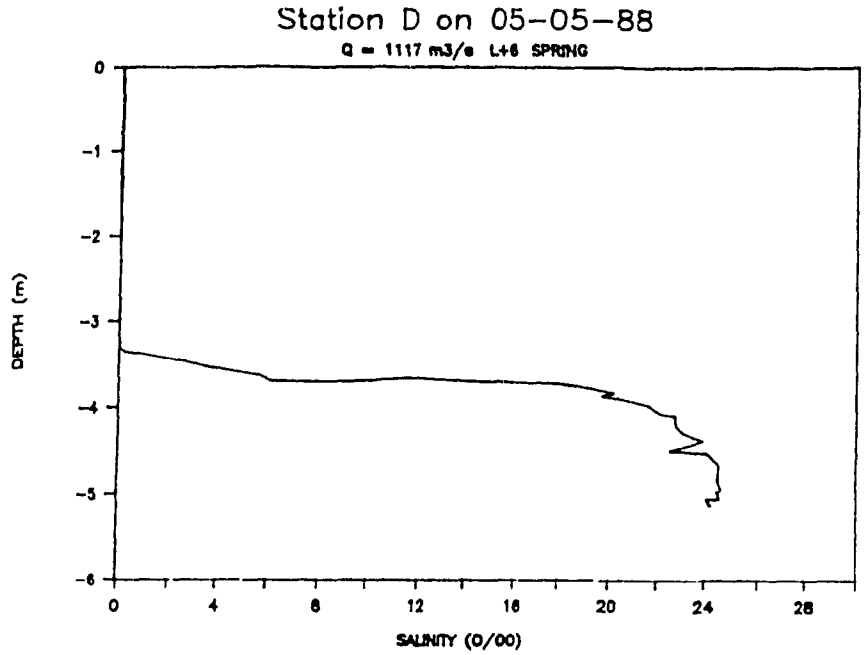
Station D on 05-05-88
Q = 1117 m3/s L+6 SPRING
DEPTH (m)
0
-1
-2
-3
-4
-5
-6
0
4
8
12
16
20
24
28
SALINITY (0/00)

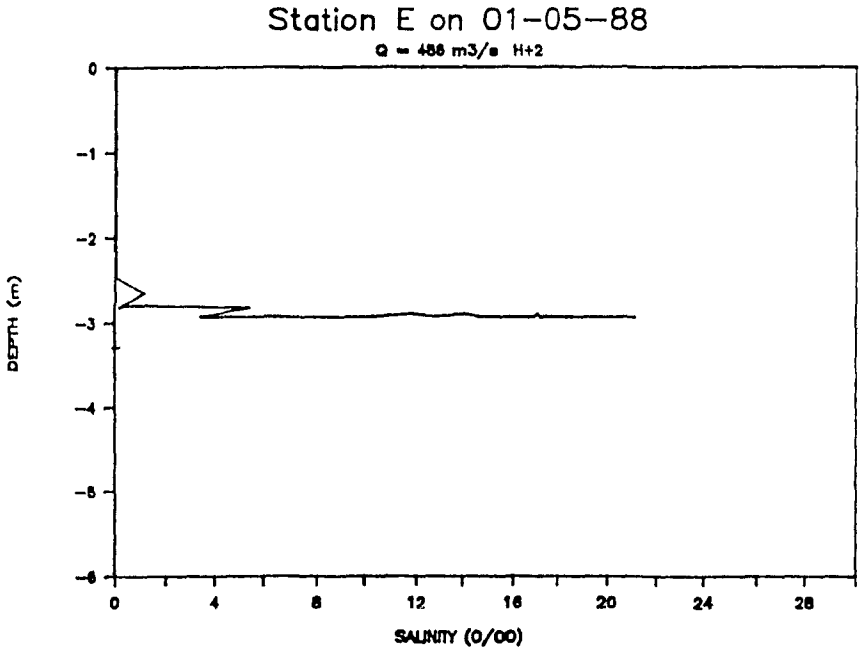
Station E on 01-05-88
Q = 486 m3/s H+2
DEPTH (m)
0
-1
-2
-3
-4
-5
-6
0
4
8
12
16
20
24
28
SALINITY (0/00)

Figure 7 e)

On one occasion (ref. Figure 7 e), a thin layer of seawater (S > 16 $^{\circ}/_{\circ\circ}$) was observed at the bottom of station E. It may be presumed, from the orientation of the freshwater isohaline at station D, that the same intrusion was also present on 02-05-88. Unfortunately, this CTD profile did not include the bottom layer.

Salinity sections along the transect were drawn for each sampling day on a logarithmic vertical scale. Selected diagrams can be seen on Figure 8. The fresh water layer thicknesses (S < 1 $^{\circ}/_{\circ\circ}$) for station A and D are given in Table 2. The vertical reference level was taken as the water surface.

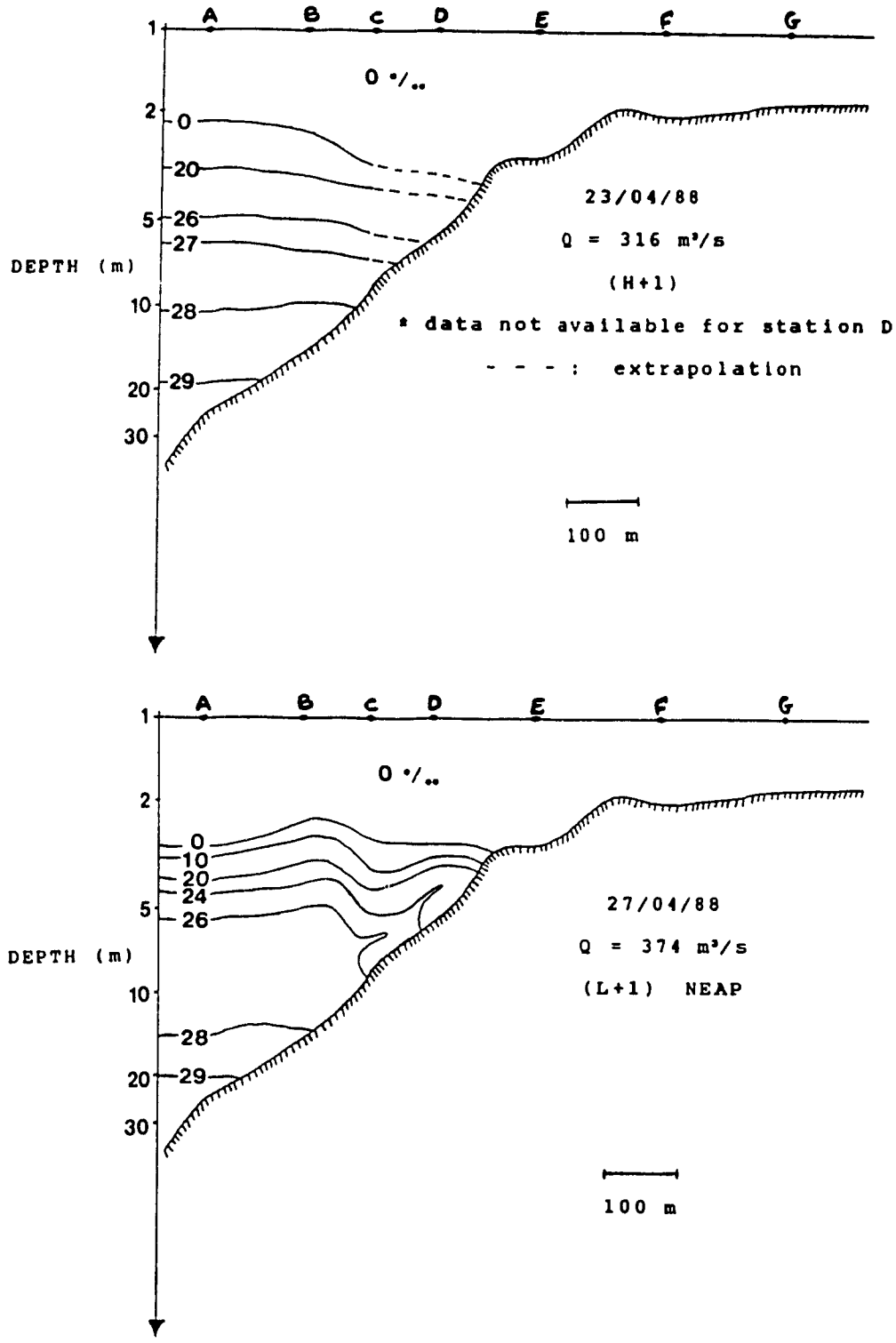

Figure 8. Longitudinal salinity transects.

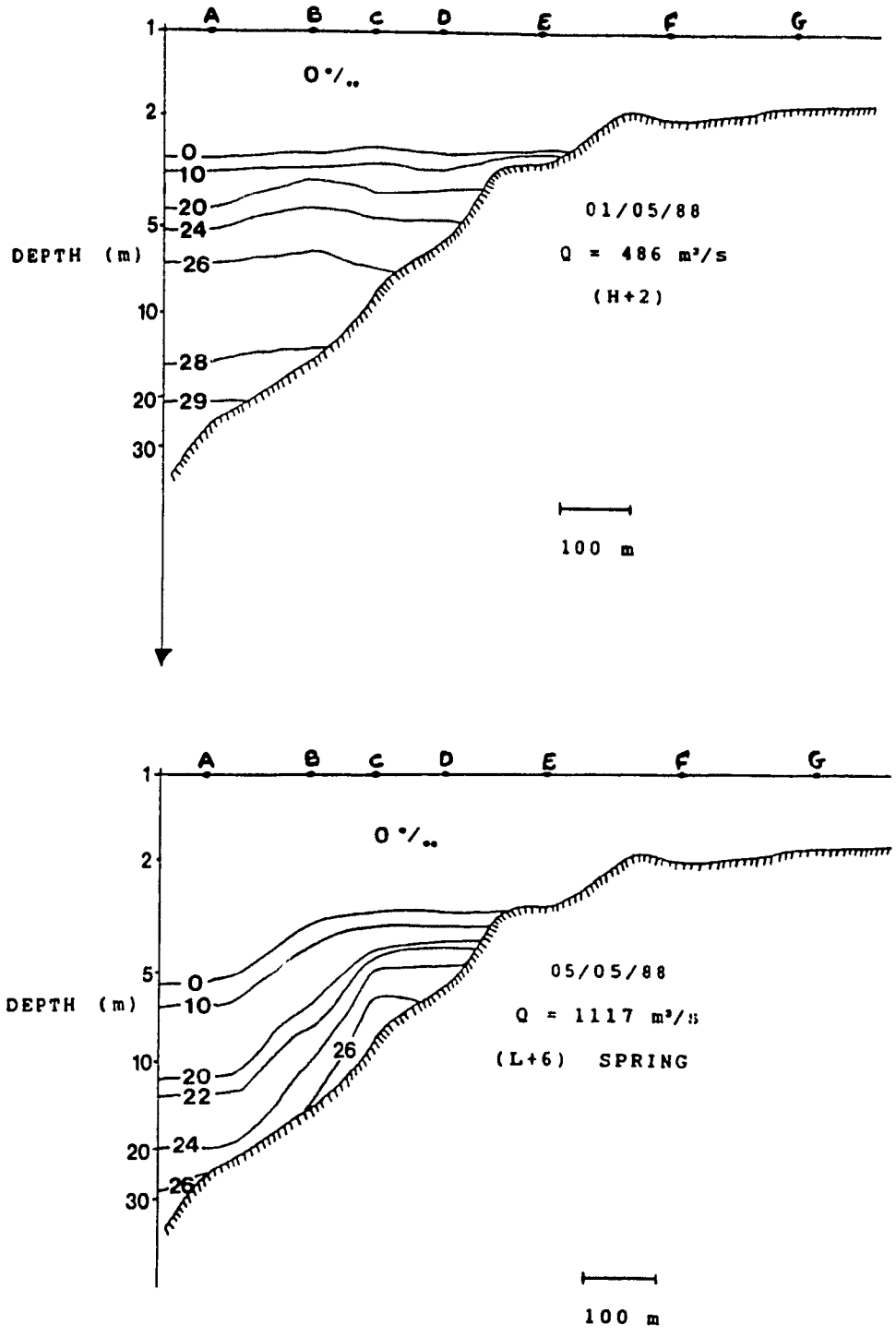

Figure 8. (concluded)

Table 2. Fresh water layer thickness (S < 1 ‰) for station A and D. The depths are given in metres below the surface of water.

date	discharge (m^3/s)	tidal phase	d_A (m)	d_D (m)
23-04-88	316	H+1	2.7	-
25-04-88	369	H+1	3.0	2.9
27-04-88	374	L+1 (neap)	3.1	3.0
29-04-88	365	H+3	2.7	3.0
01-05-88	486	H+2	3.0	2.9
02-05-88	627	L+5	3.1	2.6
05-05-88	1117	L+6 (spring)	5.2	3.3

DISCUSSION

a) Froude number

The buoyant outflow regime into a deeper and denser mass of water is determined by the relative strengths of the momentum and buoyancy fluxes from the source. Momentum flux at the source leads to a narrow well-defined turbulent jet, whilst buoyancy inhibits vertical turbulent mixing and causes lateral spreading of the flow (Chu and Jirka, 1986). The outflow near the GWR river mouth is a well-mixed jet attached to the seabed, but as it passes over the sandbar and into deeper water, the jet is lifted off the sloping bottom and becomes a surface buoyant plume.

The ratio of the momentum forces to buoyant forces at the source is usually described by the local densimetric Froude number Fr :

$$Fr = u / (g' * h)^{1/2} \qquad [2]$$

and

$$g' = g * (\rho_a - \rho_o) / \rho_a \qquad [3]$$

where g' is the effective acceleration due to gravity, ρ_a is the ambient ocean water density, ρ_o is the river water density, u is the discharge velocity and h is the outflow depth.

Resulting densimetric Froude numbers for GWR outflow at stations E and D during the fieldwork can be seen in Table 3.

The Froude number is used as an indicator of the potential for vertical mixing in stratified waters. Increasing Froude number implies stronger vertical mixing. Dyer (1973) reported some interesting results related to the Froude number in stratified flows : "...entrainment of salt water from below increases the thickness of the upper layer for F less than about 0.5. For F greater than 0.5 and less than unity, the thickness of the fresh surface layer decreases" and "...at an F = 1 there is a general erosion of the density interface causing an increase in the thickness of the upper layer." (Dyer, 1973, page 24). The Froude number is also used to characterize a flow ; if $F < 1$ it is subcritical and the stratification is stable, if $F > 1$ the flow is supercritical and mixing can develop (Figure 9).

b) lift-off point from observations

From the observations of the salinity field at the river mouth (the temperature variations are insignificant compared with the salinity variations and are, therefore, neglected in the discussion), it was determined that the lift-off region over the sampling period was located between stations D and E or in the 3.0 to 3.5 m deep area seaward of the sandbar. The only exception was on May 1 and 2, when it was observed

Table 3. Station depth (including the ice thickness and tidal phase), reduced gravity, estimated along channel velocity in the lift-off area and densimetric Froude number based on discharge depth.

station/date	h (m)	g' (m/s²)	u (m/s)	Fr
C : 23-04-88	6.7	0.20	0.25	0.22
D : 25-04-88	4.2	0.19	0.30	0.34
D : 27-04-88	3.5	0.19	0.30	0.37
D : 29-04-88	3.5	0.16	0.50	0.67
D : 01-05-88	4.1	0.18	0.50	0.58
E : 01-05-88	1.9	0.15	0.50	0.94
D : 02-05-88	4.1	0.19	0.60	0.68
E : 02-05-88	1.9	0.15	0.60	1.12
D : 05-05-88	4.1	0.18	1.10	1.28

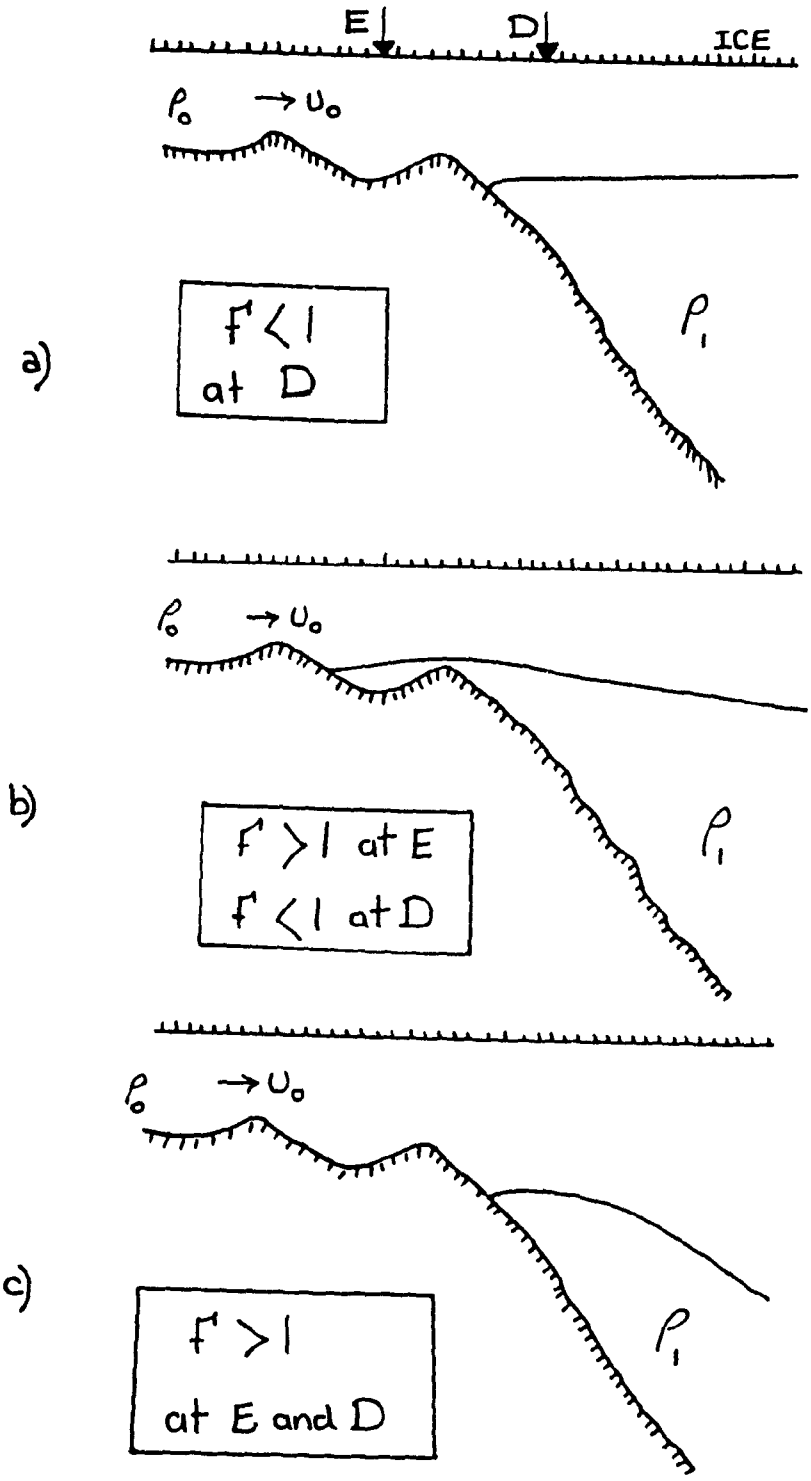

Figure 9. Schematic of the Great Whale River under-ice plume lift-off region from observations on a) 25-04-88, b) 01-05-88 and c) 05-05-88.

between stations E and F (2.5-3 m deep). The typical thickness of the fresh water layer (ref. Table 2) at station A and D was about 3 m [2.6-3.3 m], except for May 5 when it reached a depth of 5 m at station A. However, the variations were quite different at these stations, even though the distance between them was only 300 m. It seems that, as the discharge and exit velocity increased, a larger mixing rate developed in the lift-off area, restricting its displacement offshore. This response is similar to that predicted by theory and will be discussed further in the next section. A general picture of this lift-off region and its variations are sketched in Figure 9.

It also appears from the examination of the salinity profiles (Figure 7) that the effect of discharge variations on the fresh water layer thickness is more important than tidal variations. This can be seen by comparing the halocline behaviour on 23-04 and on 05-05-88 at station A (Figure 7 a and b). The plume thickness expands from 2.2 m to 5.2 m while the abrupt pycnocline found on 23-04-88 is replaced by smoothly varying (in depth) salinity gradient on 05-05-88. The influence of different tidal phase is revealed by the presence of intrusion features on the halocline at flooding tide (especially at station D) and by bottom salinity differences during the ebb and flood phases. The observed intrusion features could be related to Kelvin-Helmhotz instabilities as

they usually occur in the same conditions i.e. in presence of strong stratification and shear flow (when the two fluids are flowing in opposite directions) (Tritton, 1977).

c) lift-off models.

As mentioned above, many criteria exist for estimating the location of the lift-off point of a surface buoyant jet, but only few of them are based on field work and none of these with ice covered conditions and large vertical density gradients. For the present study, the Safaie (1979) and Hearn et al.(1985) criteria were retained for comparison.

Safaie's (1979) relationship, based on an empirical fit to laboratory data, gives a lift-off depth h_1 of

$$h_1 = 0.914 \frac{u_o h_o}{g'} \qquad [4]$$

in which u_o is the discharge velocity and h_o is the discharge height at the source point. Along with this criterion, he defined the discharge aspect ratio which is the ratio of the discharge height h_o to the discharge half-width, b_o . For his experiment, this discharge aspect ratio was in the range of [0.2 to 3.0] whereas the estimated one for the present study was 0.04 (at the river mouth constriction) and 0.002 (between stations E and F).

Hearn et al.(1985) were the first to report a field based comparative study. They investigated a tidally induced jet in the coastal waters off South-West Australia. This jet is generated by the ebb tide flowing from Leschenault Inlet, through a man-made channel called The Cut, into Koombana Bay. Leschenault Inlet is a shallow estuarine system with an average depth of 1 m at mean sea level. The buoyant jet is attached to the seabed over the initial 2 km of its trajectory, which lies in shallow coastal water of less than 10 m depth. The aspect ratio near the source is 0.04, which is much lower than for most of the reported bottom-attached jet studies. The criterion that they introduced was based on a lateral balance of buoyancy and frictional forces. The relationship involves bottom friction acting to suppress buoyancy-induced lift-off until the jet reaches a critical water depth. They obtained a lift-off depth h_2 such that

$$h_2 = \frac{(2\, C_D\, \alpha_j^2\, u^2\, b^2)^{1/4}}{g'} \qquad [5]$$

where b is the half width of the jet, C_D is the bottom friction coefficient, α_j is the jet entrainment coefficient, and u, b, and g' are local values at the lift-off point.

Values taken from our observations on 25-04-88 with a discharge depth of 2 m gave a lift-off depth (h_1) of 1.3 m with Safaie's (1979) criteria. This is consistent with his theory that for a buoyant surface jet with a densimetric Froude number smaller than 3, there should be no attachment region and the spread of the jet dominates. Using the Hearn et al. (1985) model with a jet half-width of 900 m (in the lift-off area), C_D = 0.0025, Fr = 0.3 (Ri > 1), which leads to a_j = 0.002 (Jirka, 1982, Figure 10), the lift-off depth (h_2) would be at 1.6 m. As the observed lift-off region was in the 3.0 to 3.5 m deep area, both models underestimate the lift-off depth. Similarly, for conditions on 05-05-88 , using C_D = 0.0025 and a_j = 0.005 yields h_1 = 2.5 m and h_2 = 5 m, results which are somewhat closer to observations .

Both models predicted an increase in lift-off depth for increasing discharge but they failed to predict the exact observed lift-off depths. Surely, the above models need adjustments for our special conditions : ice cover and large vertical density gradient. Both terms, C_D and a_j , the bottom friction and the jet entrainment coefficients, require correction factors in order to be able to predict correctly the lift-off depth of the freshwater plume.

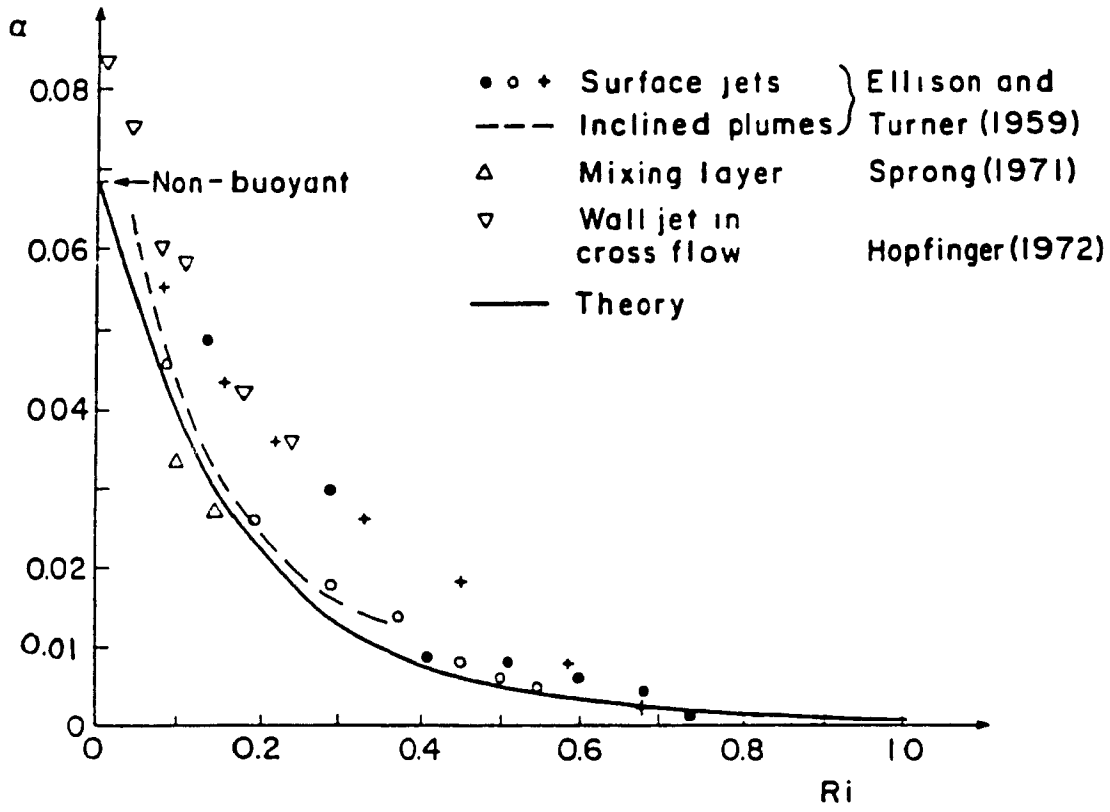

Figure 10. Entrainment rate into horizontal buoyant shear flow as a function of bulk Richardson number (adapted from Jirka, 1982).

d) T-S diagrams in the lift-off area

While examining the data set, an interesting feature was observed upon plotting T-S diagrams. For most station D data, and stations A,B and C on 05-05-88, the curves showed an inflexion below the freezing point line (Figure 11). The explanation for this could be either a malfunction of the CTD instrument or the presence of supercooled water.

The response time of the CTD temperature sensor cannot be at fault because the temperature would be warmer instead of colder with increasing salinity. The observation of supercooled water on the records then suggests the possible presence of frazil ice crystals in the pycnocline region and above (although we did not make such an observation during the field work).

Frazil ice is one of the first stages in ice formation. It consists of accumulations of ice crystals in the form of small spicules or disks (with maximum dimensions of approximately 2.5 cm * 0.5 mm) which form in the top few centimetres of the water column (Pounder, 1965). They are also found in swiftly flowing streams and turbulent sea water in which sheet ice formation is prevented (U.S.Navy Hydrographic Office, 1952). Weeks and Ackley (1986) discussed some mechanisms for the generation of oceanic frazil ice. They suggested that one necessary condition for the growth of fine

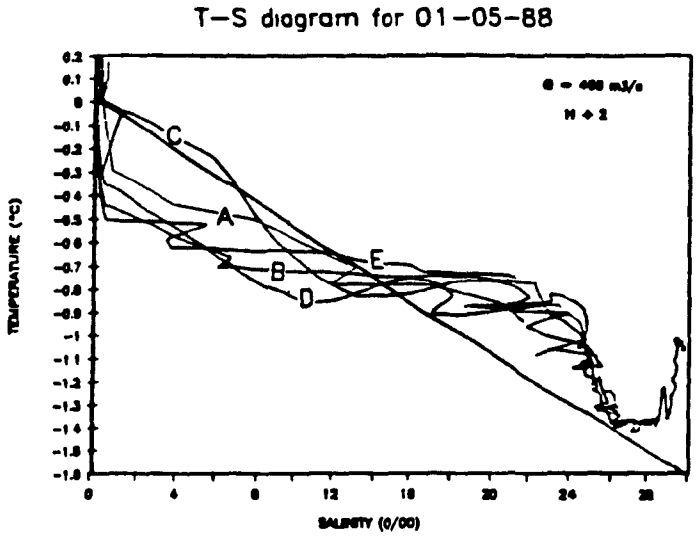

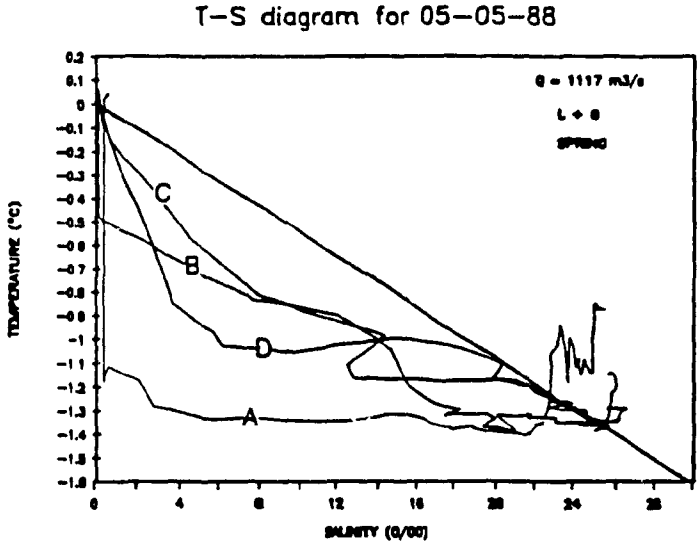

Figure 11. Temperature-Salinity diagram on 01-05-88 and 05-05-88. Freezing point line is indicated.

grained frazil ice in rivers,lakes and oceans was the presence of turbulence. Frazil generation originates as a result of the large-scale (> cm scale) mixing of waters and efficient heat transfer between either the cold atmosphere and the surface water or between two water masses of significantly different salinity. In the latter case, freezing occurs due to double diffusion phenomenon (transfer of heat at a faster rate than salt for S < 24.7 $^{o}/_{oo}$) from the cold (< -1°C) seawater to the freshwater above it.

The presence of nearshore supercooled water at, and above the pycnocline, and the potential formation of frazil crystals, could perhaps explain the intermittent problems of moored near-surface instruments that has been observed by our group in previous research work. Weeks and Ackley (1986) reported that a threshold velocity of about 0.6 m/s is necessary under freezing conditions to allow the onset of frazil formation. Indeed, this assumption corresponds quite well with the larger area of supercooled water masses that were observed in the T-S diagram of all stations on May 5 1988, when $\bar{u}$ > 0.6 m/s.

CONCLUSIONS

This study documented the salinity field in the lift-off region of Great Whale River under-ice plume during the period of increasing discharge, just before spring break up. Along with the description of the observations and their relationship with the flow characteristics (Froude number), calculation of the lift-off depths using existing models were done. Comparison of observed and calculated lift-off depths showed them to be inadequate in explaining the field results. Reasons for this failure may be related to the uncertainties in estimating the various parameters such as the "source" location, the drag caused by bottom and ice friction and the entrainment rate in atypical conditions (ice cover, strong outflow velocities, large vertical density gradients, etc). Nevertheless, these calculations imply that the lift-off point of an under-ice surface buoyant plume cannot be accurately predicted with the existing models and more work needs to be done on the subject. Finally, it is to be mentioned that, in spite of the limited number of observations and the lack of comparisons, the present survey revealed a number of features such as the relationship between the stratification conditions at the river mouth and the approximate location of the plume lift-off point, and the presence of supercooled water in the lift-off area, which are observations that could be useful for future investigations.

ACKNOWLEDGEMENTS

The authors would like to thank Dr.V. Chu, Sofia Babarutsi, Paul Peltola, Michel Cloutier, Jean Richard and the people at the Centre d'Études Nordiques. Financial support was provided by GIROQ (Groupe Interuniversitaire de Recherches Océanographiques du Québec), a Northern Scientific Training Grant from the Department of Indian and Northern Affairs to L.V. (through the Centre for Northern Studies and Research of McGill University), NSERC and Fonds FCAR grants for research to R.G.I..

REFERENCES

Baddour, R.E. and Dance, P.G., 1983. Surface Buoyant Discharge in a Vertically Confined Ambient Environment. ASME Publications 83-WA/FE-1, 7 p.

Chu, V.H. and Jirka, G.H., 1986. Surface Buoyant Jets and Plumes. Encyclopedia of Fluid Mechanics, Volume VI, Section 4, Chap. 27 : 1053-1084.

Dyer, K.R., 1973. Estuaries : a Physical Introduction. Wiley, New York, 140 p.

Freeman, N.G., 1982. Measurements and modelling of freshwater plumes under an ice cover. Ph.D. Thesis, University of Waterloo, Waterloo, Ontario, 155 p.

------ , Roff, J.C. and Pett, R.J., 1982. Physical, Chemical, and Biological Features of River Plumes Under an Ice Cover in James and Hudson Bays. Le Naturaliste Canadien, Vol. 109, 4 : 745-764.

Godin, G.G., 1972. The Analysis of Tides. University of Toronto Press, 264 p.

Hauenstein, W., 1983. Zuflussbedingte Dichtestromungen in Seen. Institute for Hydromechanics, ETH, Zurich, Tech.Rep. No. R20-83.

Hearn, C.J., Hunter, J.R., Imberger, J., and van Senden, D., 1985. Tidally Induced Jet in Koombana Bay, Western Australia. Aust. J. Mar. Fresw. Res., 36 : 453-479.

Ingram, R.G., 1977. Océanographie Physique du détroit de Manitounuk et de l'estuaire de Grande Rivière de la Baleine. Tech. Rep., GIROQ, Québec.

------, 1979. Circulation et caractéristiques des masses d'eau du détroit de Manitounuk et des estuaires de la Grande Rivière de la Baleine et de la Petite Rivière de la Baleine. Tech. Rep., GIROQ, Québec.

------, 1981. Characteristics of Great Whale River Plume. J. of Geophy. Res., Vol.86, C3 : 2017-2023.

------ and Larouche, P., 1987. Variability of an under-ice river plume in Hudson Bay. J. of Geophy. Res., Vol. 92, C9 : 9541-9548.

------, Lepage, S. and Shirasawa, K., 1988. Under-Ice Plume Dynamics. Proceedings of Stratified Fluids Symposium, Pasadena, California (in press).

----- , Adams, E.E. and Stolzenbach, K.D., 1981. Buoyant Surface Jets. J. of Hydraulic Div., ASCE, Volume 107 (HY11) : 1467-1487.

Lepage, S. and Ingram, R.G., 1988. Modification of the Great Whale River plume during ice breakup. ACUNS Stud. Res. in Canada's North, Ottawa : 120-127.

Luketina, D.A. and Imberger, J., 1987a. Characteristics of a Surface Buoyant Jet. J. of Geophysical Res., Volume 92, C5 : 5435-5447.

-------, 1987b. Turbulent Motions in a Surface Buoyant Jet. Proceedings of Stratified Fluids Symposium, Pasadena, California (in press).

Pounder, E.R., 1965. The Physics of Ice. Pergamon Press, Oxford, 151 p.

Safaie, B., 1979. Mixing of Buoyant Surface Jet Over Sloping Bottom. J. of Waterway Port, Coastal and Ocean Engineering Division, ASCE, Vol. 105 (WW4) : 357-373.

Strilaeff, P.W. and Bilozor, W., 1973. Single-Velocity Method in Measuring Discharge. Technical Bulletin No.75, Inland Waters Directorate, Water Resources Branch, Ottawa, Canada, 6 p.

Tritton, D.J., 1977. Physical Fluid Dynamics. Van Nostrand Reinhold, 200 p.

Weeks, W.F. and Ackley, S.F., 1986. The Growth, Structure, and Properties of Sea Ice.(Chapter 1, pp.9-164). in The Geophysics of Sea Ice, edited by Norbert Untersteiner. NATO ASI Series, Series B : Physics, Vol.146.

U.S. Navy Hydrographic Office, 1952. A Functional Glossary of Ice Terminology. H.O.Pub. 609, Washington D.C. 50 p.

APPENDIX 1 : RECORDING CURRENT METER DATA

INTRODUCTION

A survey of an estuary must include observations of the salinity, temperature and current velocity distribution in horizontal space and depth. There are two methods for direct current measurements : the flow method uses the Eulerian principle i.e. measurements taken at a fixed location over a certain time period and the drift method which exploits the Lagrangian principle of measuring the successive locations of a moving object (Pond and Pickard, 1986).

The Eulerian method, which was used in the two preceding studies, comprises measurements by current meters used either from an anchored vessel or below a moored buoy. A number of current meters moored in a predetermined pattern will provide information about the three-dimensional distribution of horizontal currents as a function of time.

A series of Aanderaa recording current meters , model RCM-4, were moored within two sections of Rupert Bay and upstream of the river sill in the Great Whale River, to monitor (10- or 20-min sampling) current speed and direction, temperature, conductivity, and pressure or instrument depth.

THE INSTRUMENT

The Aanderaa Recording Current Meter used in the present study (Figure A1.1.) records digital data internally on 1/4 inch reel to reel magnetic tape (the new Aanderaa current meters, RCM-7, have a solid state memory) and a quartz clock which triggers the measuring cycle at the chosen interval. The characteristics of the instrument and of the different sensors are given at Table A1.1. The technique used for open water moorings are shown in Figure A1.2.

DATA TREATMENT

After the recovery of the instrument, the tapes are read with an Aanderaa tape translation interface, then the raw data are converted into physical units. To do this, one needs to know the calibration for each sensor i.e. the mathematical formula expressing the relationship between the readings and the corresponding physical quantity. Calculations of the salinity and sigma-t values from the conductivity, pressure and temperature data are also done. Later, all current vectors are usually decomposed into along-channel (or E-W) components, positive into the river, and cross-channel (or N-S) components, 90° counterclockwise.

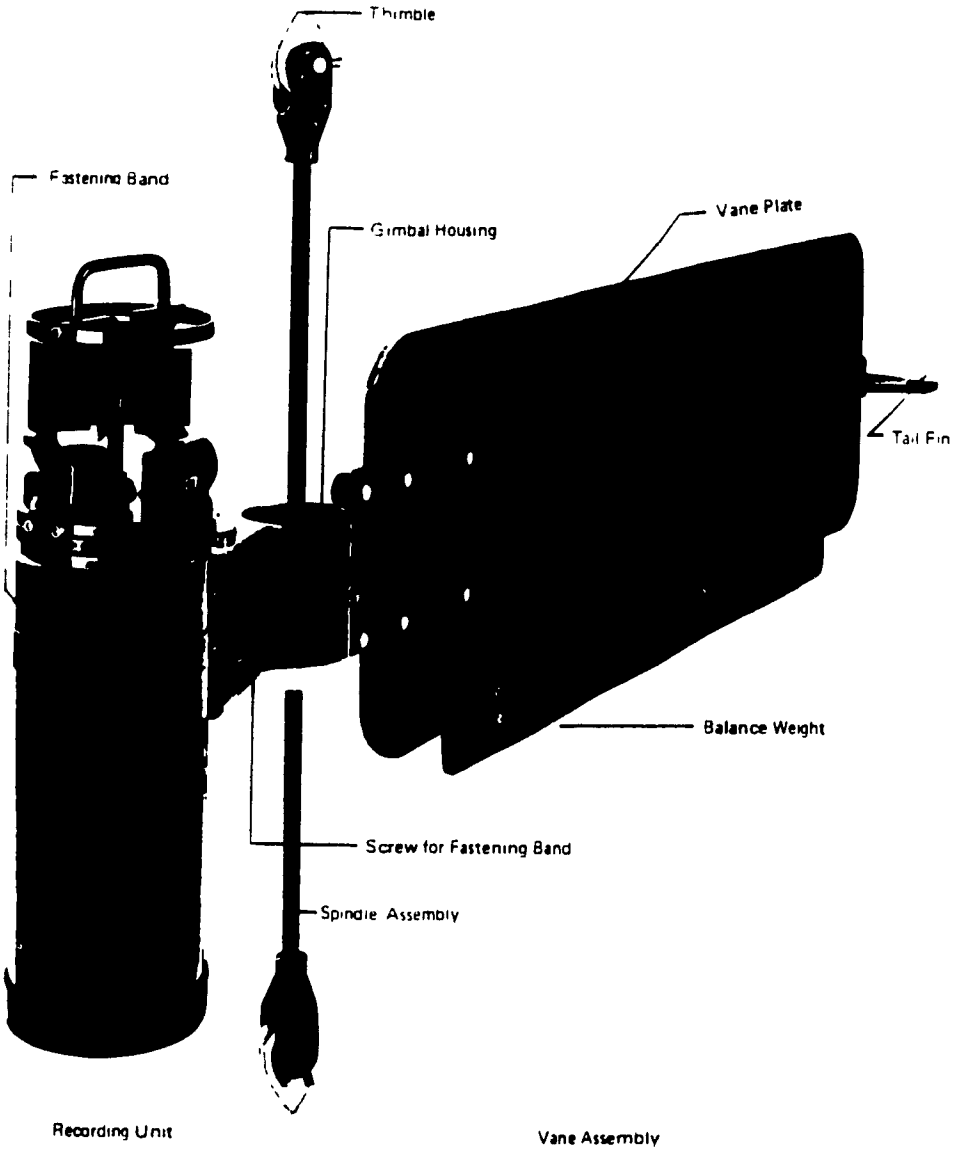

Figure A1.1. Aanderaa Recording Current Meter (RCM) unit.

Table A1.1. Characteristics of current meters

MODEL : Aanderaa recording current meter, model 4.

MEASURING SYSTEM : Self balancing bridge with sequential measuring of six channels and recording on magnetic tape. A ten bit binary word is used for each channel.

SENSOR	SCALE	PRECISION
TEMPERATURE	-2,46°C to 21,48°C	± 0,05°C
CONDUCTIVITY	0 to 77 mmho/cm	± 0,025 mmho/cm
PRESSURE	0 to 200 psi	2 psi
DIRECTION	0 to 36°	± 7,5° for v = 2,5 to 5 cm/s and v = 100 to 200 cm/s ± 5,0° for v = 5 to 100 cm/s
SPEED	2,5 to 250 cm/s	± 1 cm/s for v = 2 to 100 cm/s ± 2 cm/s for v > 100 cm/s starting velocity : 2 cm/s

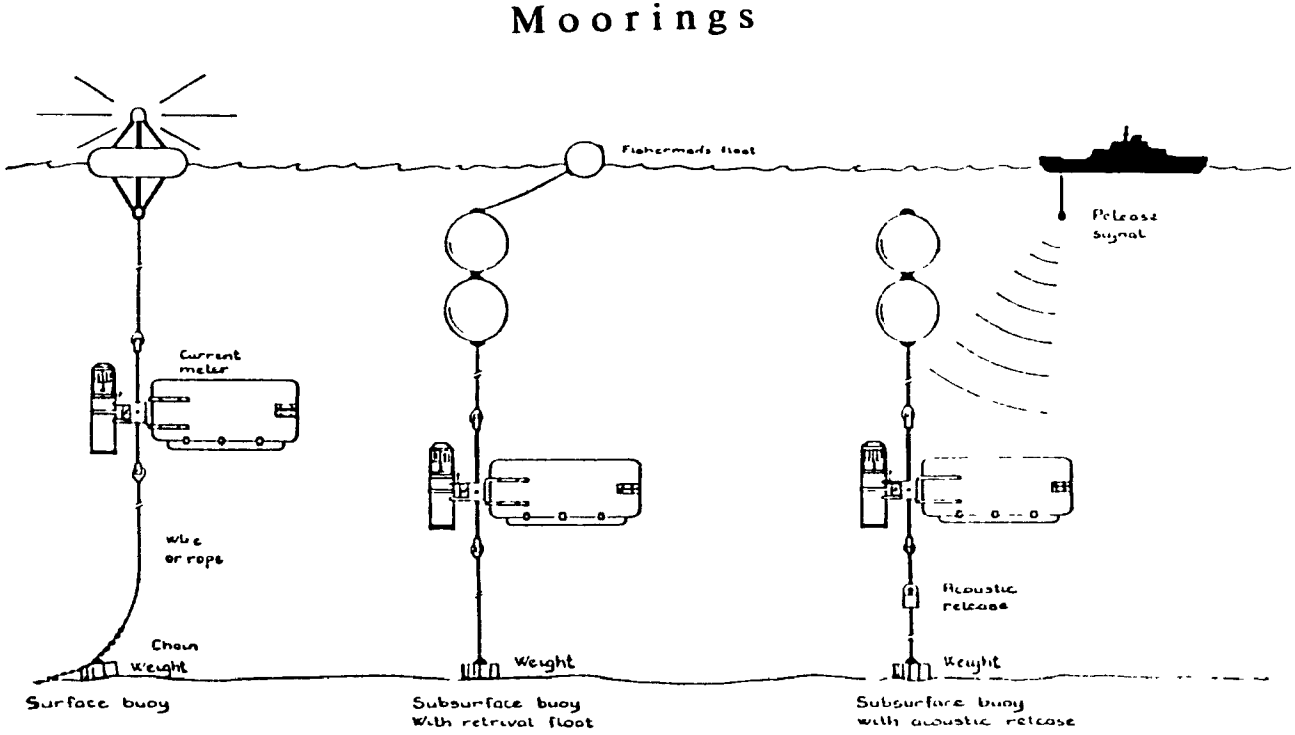

Figure A1.2. Mooring techniques for recording current meter instrument.

Current meter data are then filtered with an $a_6a_6a_7/6*6*7$ type moving mean (Godin, 1972) to reduce the relative frequency of observations to hourly values. In the present application, the decimated time series were also filtered with an $a_{24}a_{24}a_{25}/24*24*25$ filter (Godin, 1972) to eliminate diurnal and semidiurnal fluctuations (leaving a signal representative of "low-pass" flow).

The smoothed and low-pass filtered data are then plotted as time series. Appendix 3 presents the time series obtained from the current meter moorings of Rupert Bay study.

Other current meter data analysis methods used in the present thesis included the following:

* **spectral analysis** : the aim of spectral analysis is to represent a function by a sum of weighted sinusoidal functions called spectral components. The reason for representing a function by its spectrum is that the spectrum can be an efficient and often revealing description of the function (Gardner, 1988) i.e. it shows how the variance of a stochastic process is distributed with frequency. The method used herein to obtain the power spectrum of current and wind velocity, as well as for water level fluctuations, is the Fourier Transform Method.

The 95 % confidence intervals for the spectral estimates have been calculated with the technique described in Jenkins and Watts (1968). One of the resulting graphs for the north-south component of current velocity at sta.38 is shown in Figure 10 (Chapter 2).

* **tidal current harmonic analysis** : " Tides are displacements of the particles in a celestial body caused by the attraction of a neighbouring body. Terrestrial tides are known to be related to the phases of the moon and to the seasons, and are created mainly by the moon and the sun. (...) The regularity of astronomical motion implies the presence of known periodicities in the tidal records, and a search for these is the primary task of the analysis. A series of measurements on the tidal displacements at a given point can usually be fitted by a sum of harmonics. " (from Godin, 1972).

Based on the above definition of tidal analysis, we used the tidal current analysis (TCA) and tidal height analysis (THA) programs developed by Foreman (1977, 1978). The TCA program analyzes hourly current meter data for a given period of time. Current ellipse parameters and Greenwich phase lags are calculated via a least squares fit method coupled with nodal modulation. Results of a tidal current analysis are shown in Table 3 of Chapter 2. The ellipses of Figure 8 are drawn from TCA results for the M2 constituent.

* **correlation analysis** : the correlation analysis is a statistical method that permits one to determine a coefficient of correlation which measures the amount of association between variables. This coefficient is large when the variables are closely related and small when there is little association. In our case, cross-correlation analysis have been performed on time series with a STATGRAF software package. Results for the correlation analysis between the filtered tidal signal and the u-component of the wind velocity in the bay were presented earlier in the Rupert Bay study (Fig.9, Chapter 2).

* **variance analysis** : this last analysis can be performed on all three different time-series (analysed, smoothed and low-pass filtered data) by calculating the mean and the variance of each set and by separating the results depending on their frequency characteristics. This technique was applied on the current meter data set of Rupert Bay study (ref. Table 2 of Chapter 2).

APPENDIX 2 : WATER LEVEL RECORDER DATA

THE INSTRUMENT

The Aanderaa Water Level Recorder (WLR) is a high precision recording instrument for determining water level in the open sea. The water level is measured by evaluating the hydrostatic pressure with a precise quartz pressure sensor. Knowing the density of water and atmospheric pressure, the water level can then be established.

The water level recorder contains a clock circuitry that triggers the measuring cycle at preset time intervals. The instrument records data on magnetic tape, and this tape has the same recording format as for other Aanderaa recording instruments (which allows for use of the same tape reading equipment, ref. Appendix 1).

The instrument is usually moored on the sea bottom with a concrete anchor or with any fixture available that keeps the instrument at the bottom and which makes it easy to retrieve (Figure A2.1).

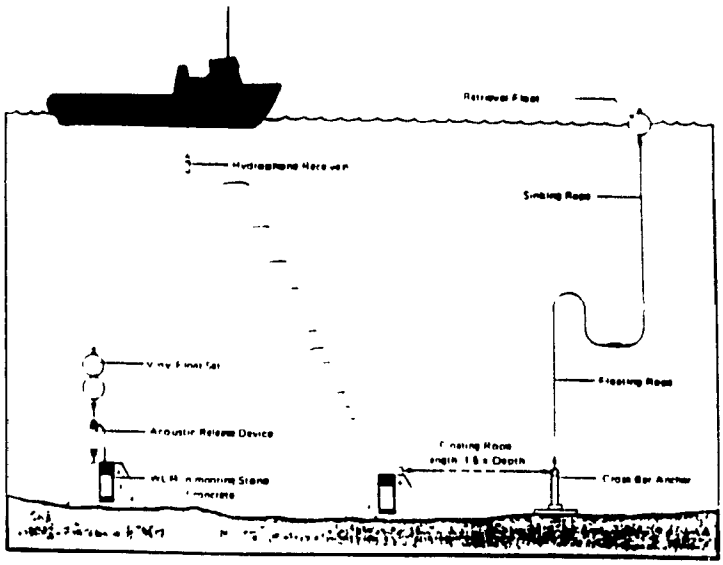

Figure A2.1. Mooring techniques for water level recorder instrument.

DATA TREATMENT

After the recovery of the instrument, the tapes are read with an Aanderaa tape translation interface, then the raw data are converted into physical units. To do this, one needs to know the calibration for each sensor i.e. the mathematical formula expressing the relationship between the readings and the corresponding physical quantity.

Similar to the current meter data processing methods, the water level signal can be filtered with an $a_6 a_6 a_7/6*6*7$ type moving mean to reduce the relative frequency of observations to hourly values and with an $a_{24} a_{24} a_{25}/24*24*25$ filter (Godin, 1972) to eliminate diurnal and semidiurnal fluctuations. The smoothed and low-pass filtered data are then plotted as time series.

In the Rupert Bay study, an additional data handling process had to be done on the water level signal ; from the low-pass filtered version of the water level data set, it appeared that on July 28/1976, when the field expedition crew changed the instrument tapes at station 9, the mooring location, on which was anchored WLR # 58, was displaced and the instrument was turned off for five hours.

Consequently, the water level signal was analysed and filtered in two different parts i.e. from July 16 to July 28 and from July 29 to August 18. Then, in order to obtain a longer data set (which was preferable for statistical analysis), a standardization of the whole water level signal was carried out. It included : 1) finding the mean level for both parts; 2) taking the difference of level between the two time series; 3) adding this difference to the shortest of the two time series; 4) joining the two parts (of which, one had been normalized) and filling, by interpolation, the missing interval (5 hours); 5) analyzing this new water level time series.

Aside from the filtering process, which permits us to assess qualitatively other disturbing factors (i.e. wind, river discharge or sea level pressure), the additional WLR data analysis methods include :

* **removal of inverse barometric effect** : after removing the major tidal components on a water level signal (with a "low-pass" filter), the dominant time scales for the non-tidal fluctuations are usually between 2-5 days and are related to meteorological forcing. In order to study the response of the signal to other disturbing factors, namely the wind driven transport, the usual approach is to remove the inverse barometric effect from the signal.

This can be done by transforming the water level data into sea level pressure data with the hydrostatic equation and, by comparing the sea level pressure recorded at a meteorological station, corrections can made.

* **Tidal Height Analysis** : similar to the TCA analysis (ref.Appendix 1.), the tidal height analysis (THA) program developed by Foreman (1977) was used. The THA program analyzes hourly water level data for a given period of time. Amplitudes and Greenwich phase lags are calculated via a least squares fit method coupled with nodal modulation. Results of the THA analysis performed on the WLR of Rupert Bay station 9 are shown on Table 3 of Chapter 2.

APPENDIX 3 : RUPERT 1976 TIME SERIES PLOTS

1) Filtered time series produced from recording current meter data. The extension " SM " designate the smoothed time series i.e. that have been filtered with an $a_6 a_6 a_7/6*6*7$ type moving mean to reduce the relative frequency of observations to hourly values. The extension " LP " stands for those which have been filtered with an $a_{24} a_{24} a_{25}/24*24*25$ filter (low-pass filter) to eliminate diurnal and semidiurnal fluctuations.

2) Time series produced from the water level recorder data and tidal prediction in Rupert Bay on the same period.

3) Rupert Bay total freshwater discharge, in m^3/s, for July and August 1976.

4) Examples of sea-land breeze patterns in Rupert Bay.

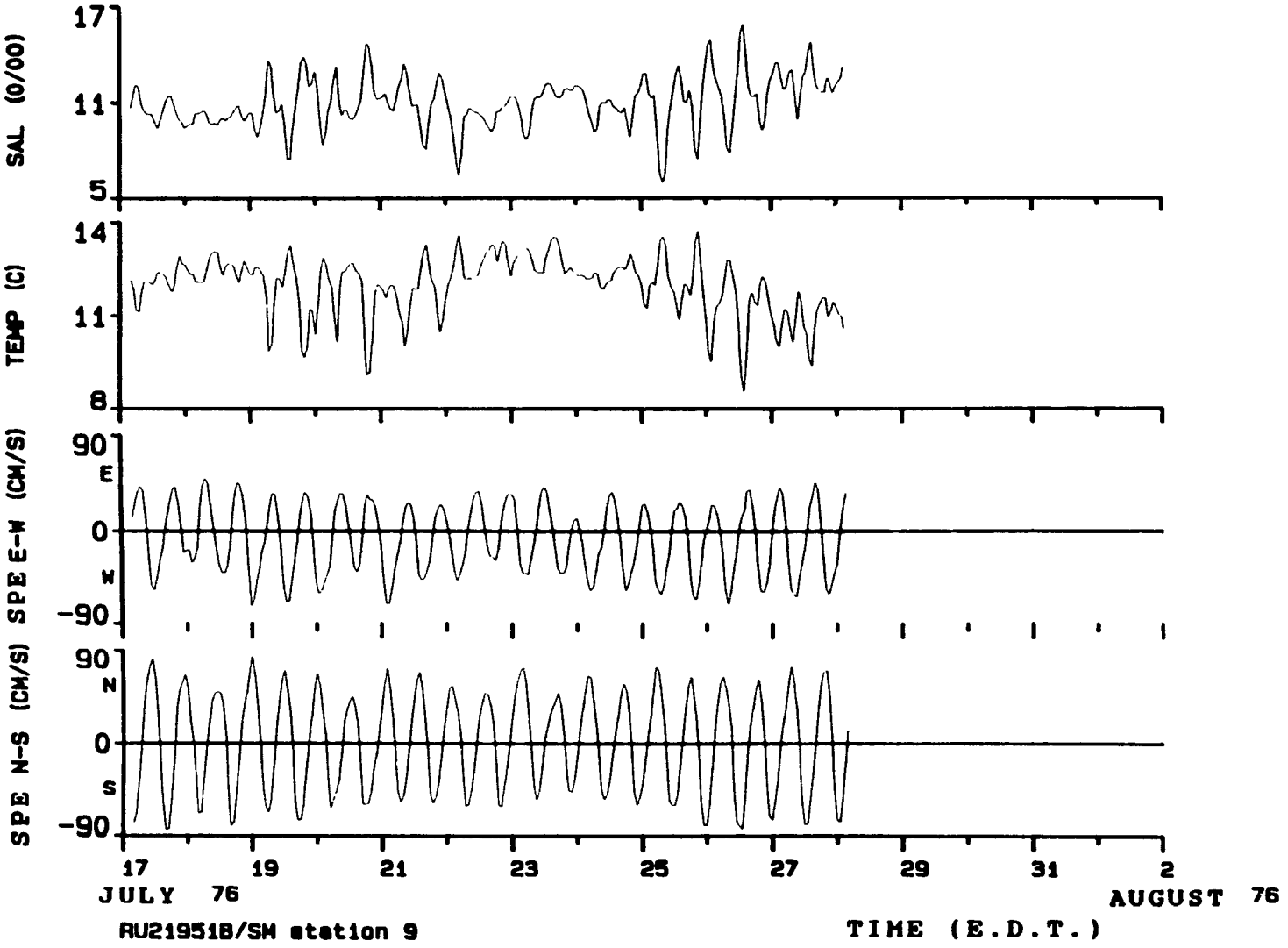
SAL (0/00)
17
11
5
TEMP (C)
14
11
8
SPE E-W (CM/S)
90
E
0
W
-90
SPE N-S (CM/S)
90
N
0
S
-90
17
19
21
23
25
27
29
31
2
JULY 76
AUGUST 76
RU21951B/SM station 9
TIME (E.D.T.)

Figure A3.1

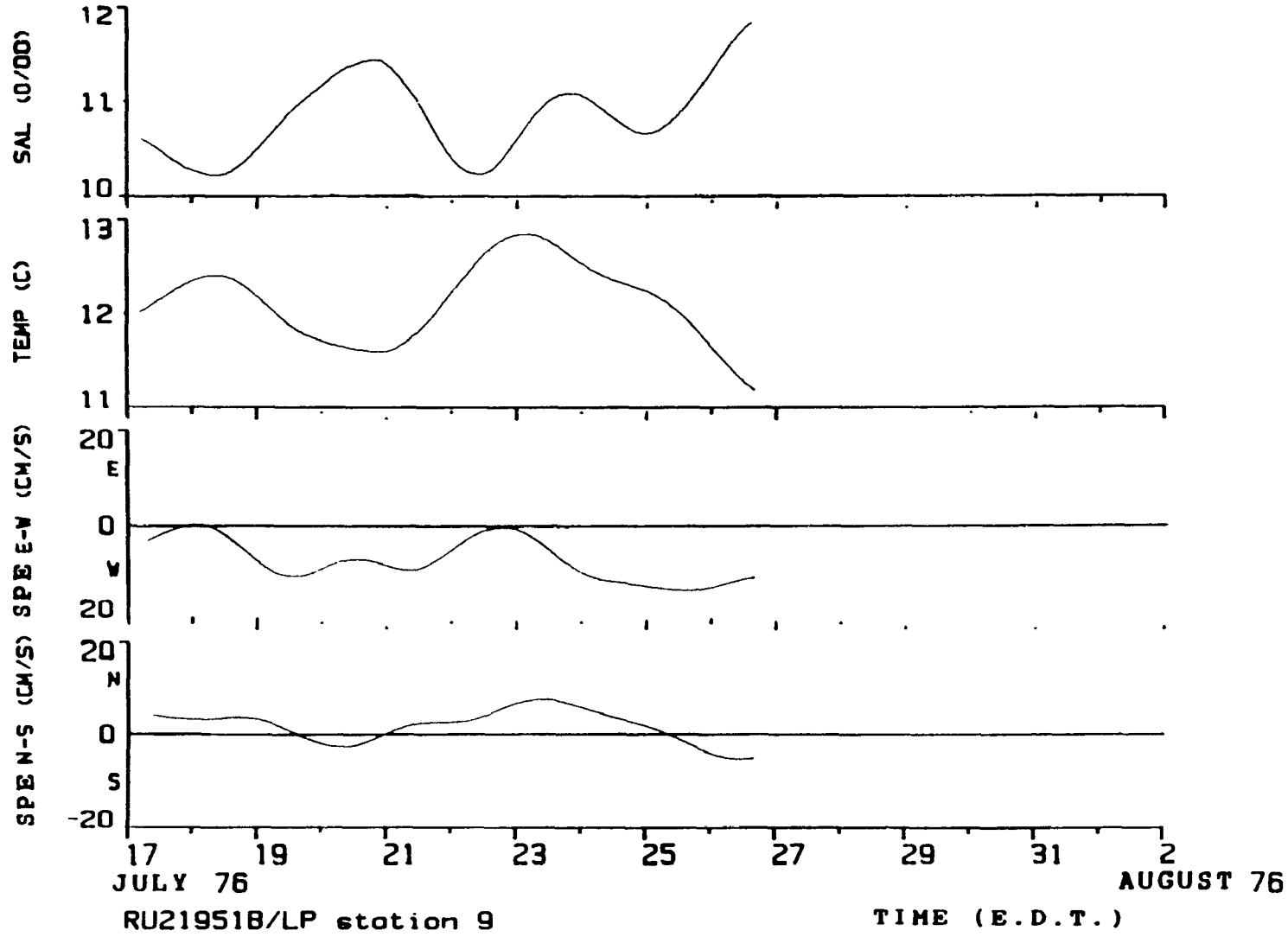
SAL (0/00)
12
11
10
TEMP (C)
13
12
11
SPD E-W (CM/S)
20
E
0
W
20
SPD N-S (CM/S)
20
N
0
S
-20
17
19
21
23
25
27
29
31
2
JULY 76
AUGUST 76
RU21951B/LP station 9
TIME (E.D.T.)

Figure A3.2

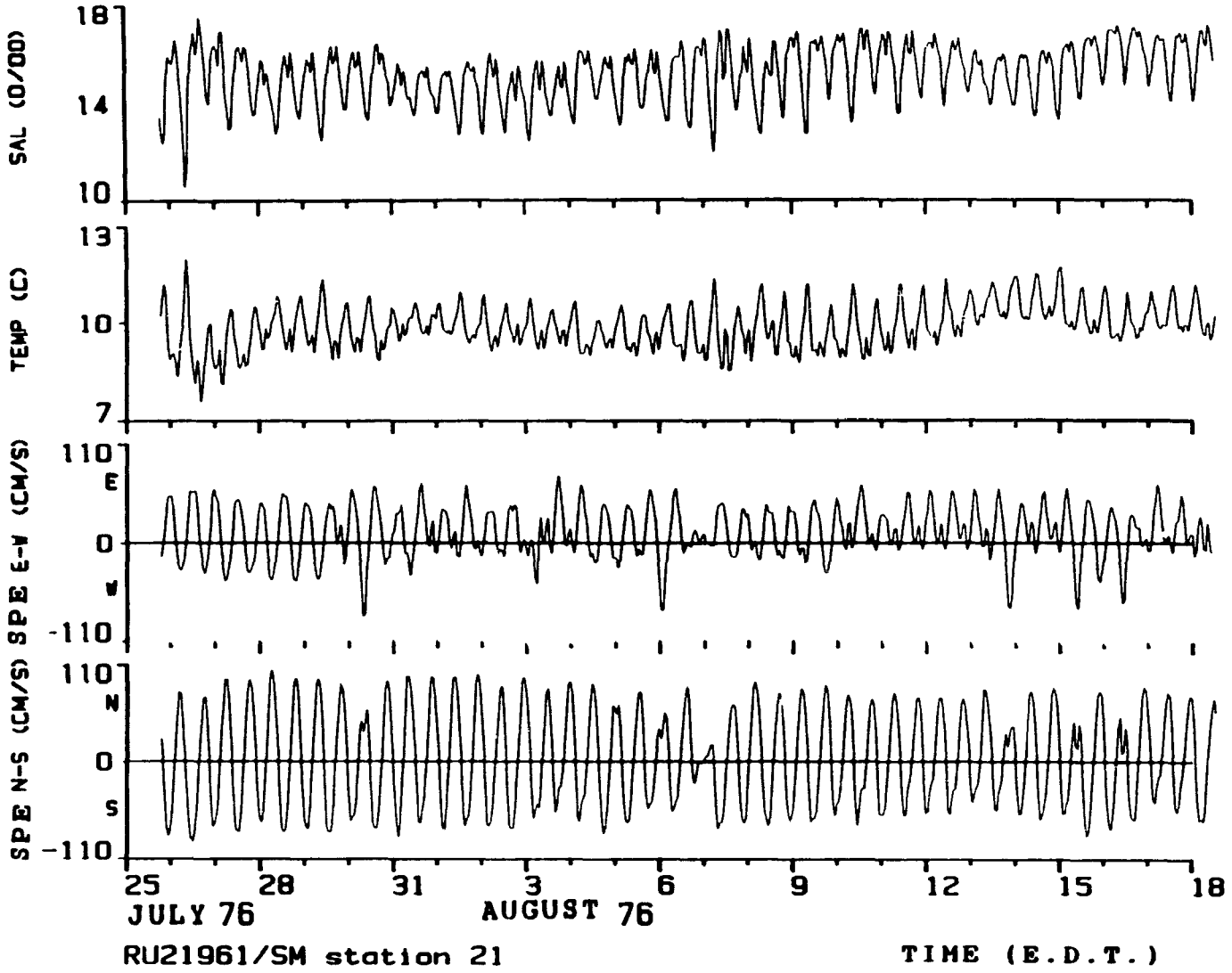
SAL (O/OO)
18
14
10
TEMP (C)
13
10
7
SPE E-W (CM/S)
110
E
0
W
-110
SPE N-S (CM/S)
110
N
0
S
-110
25
28
31
3
6
9
12
15
18
JULY 76
AUGUST 76
RU21961/SM station 21
TIME (E.D.T.)

Figure A3.3

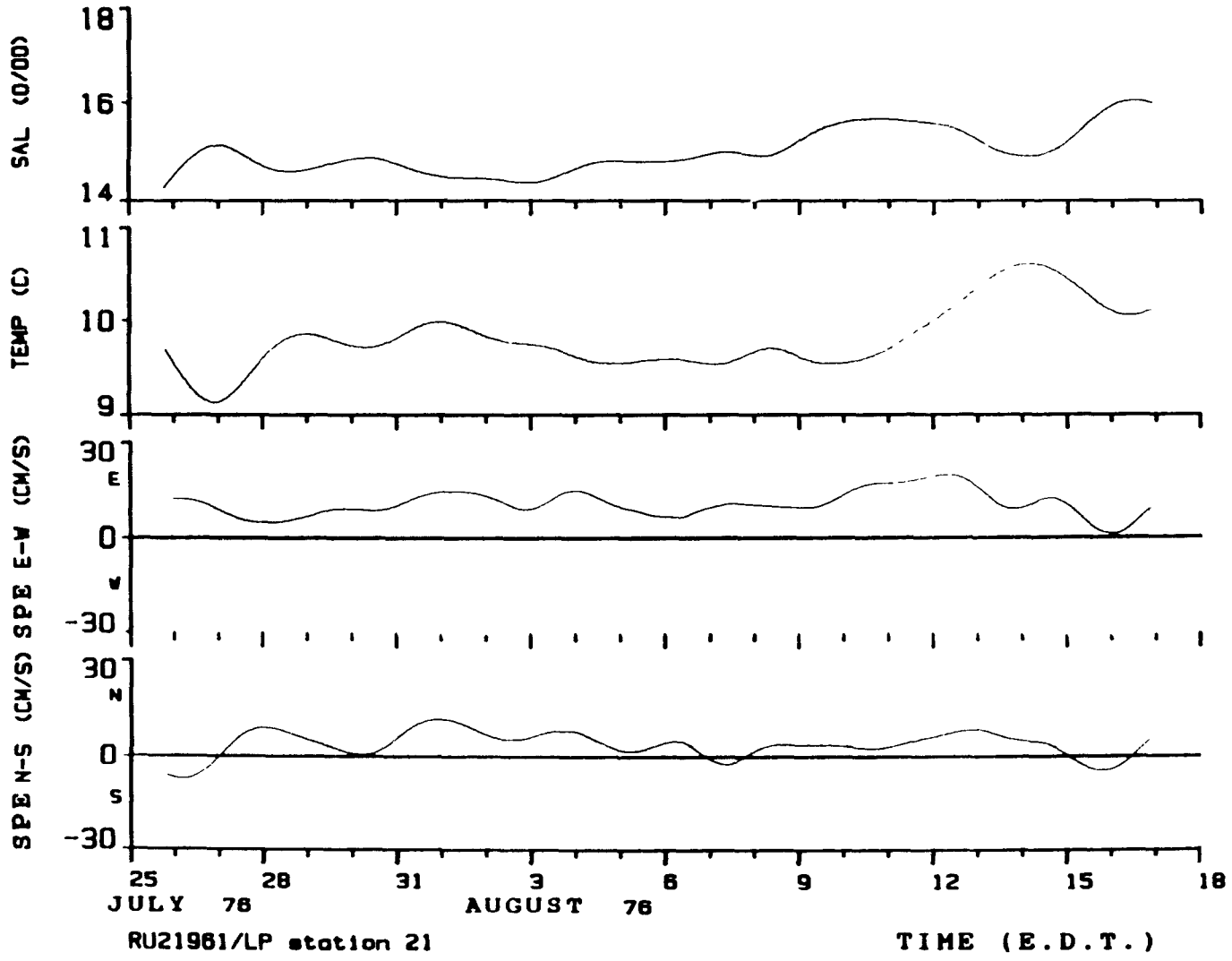
SAL (O/OO)
18
16
14
TEMP (C)
11
10
9
SPE E-W (CM/S)
30
E
0
W
-30
SPE N-S (CM/S)
30
N
0
S
-30
25
28
31
3
6
9
12
15
18
JULY 76
AUGUST 76
RU21961/LP station 21
TIME (E.D.T.)

Figure A3.4

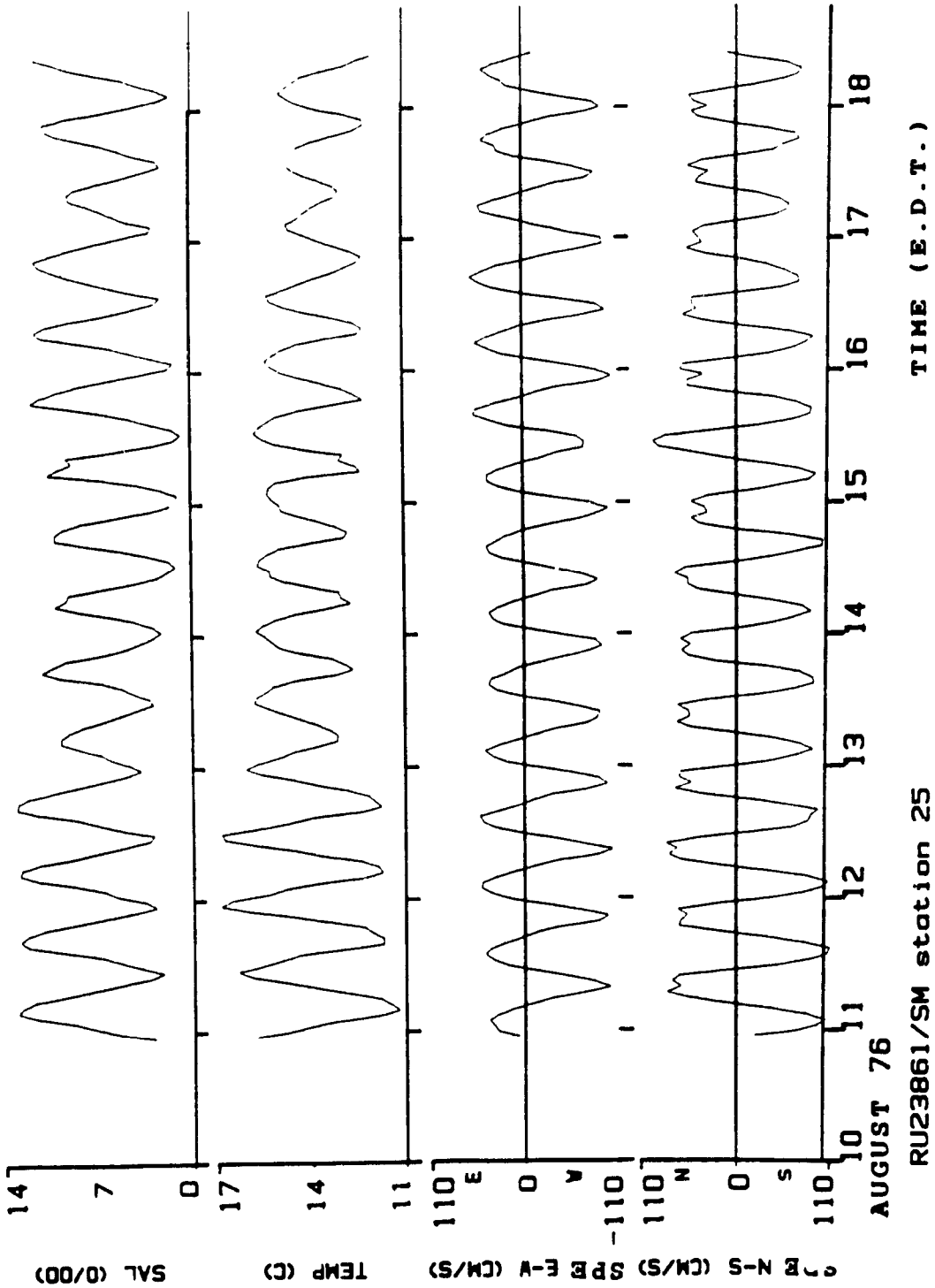
SAL (0/00)
14
7
0
TEMP (C)
17
14
11
SPD E-W (CM/S)
110
0
-110
SPD N-S (CM/S)
110
0
-110
10
11
12
13
14
15
16
17
18
AUGUST 76
TIME (E.D.T.)
RU23861/SM station 25

Figure A3.5

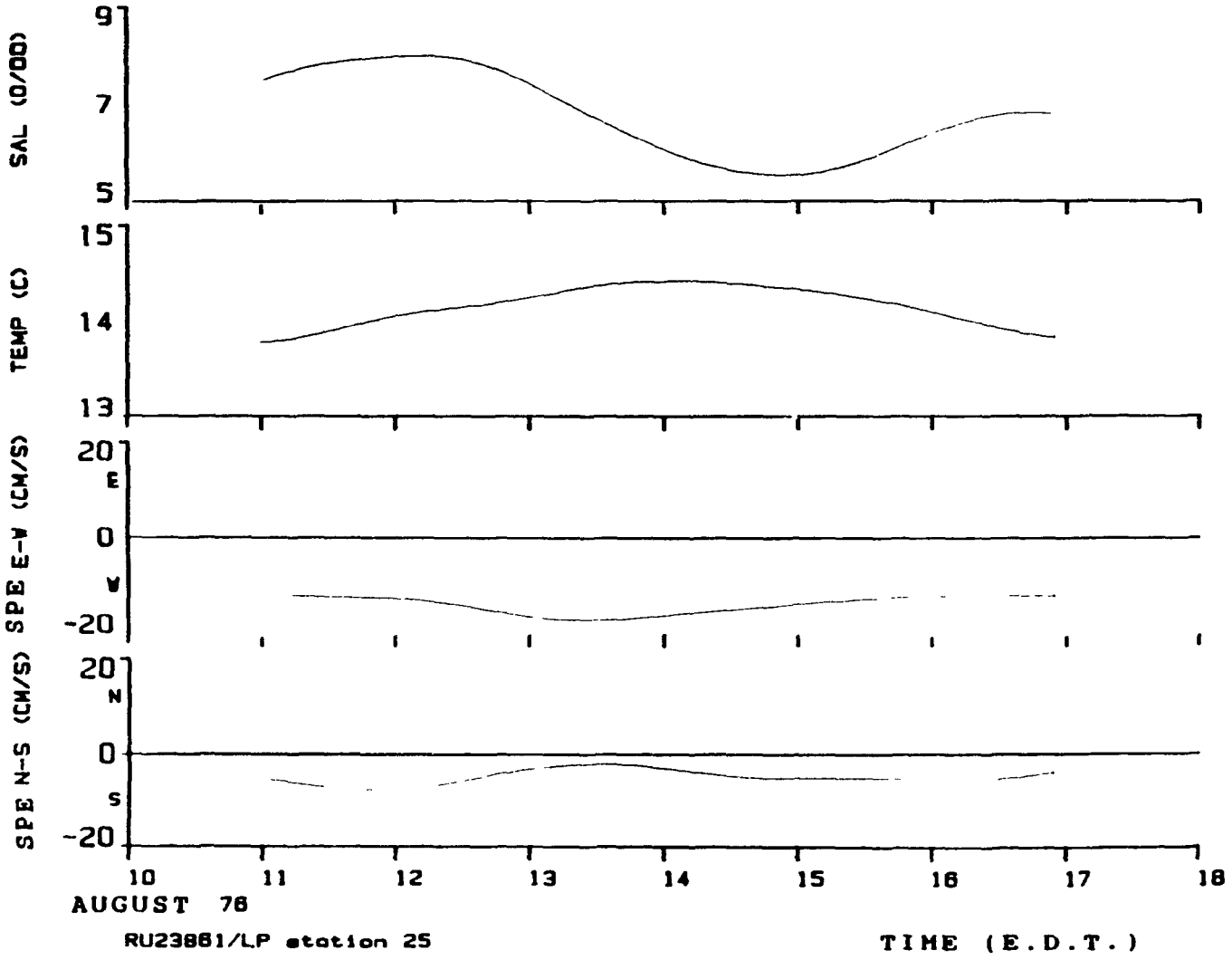
SAL (0/00)
9
7
5
TEMP (C)
15
14
13
SPE E-W (CM/S)
20
E
0
W
-20
SPE N-S (CM/S)
20
N
0
S
-20
10
11
12
13
14
15
16
17
18
AUGUST 78
RU23861/LP station 25
TIME (E.D.T.)

Figure A3.6

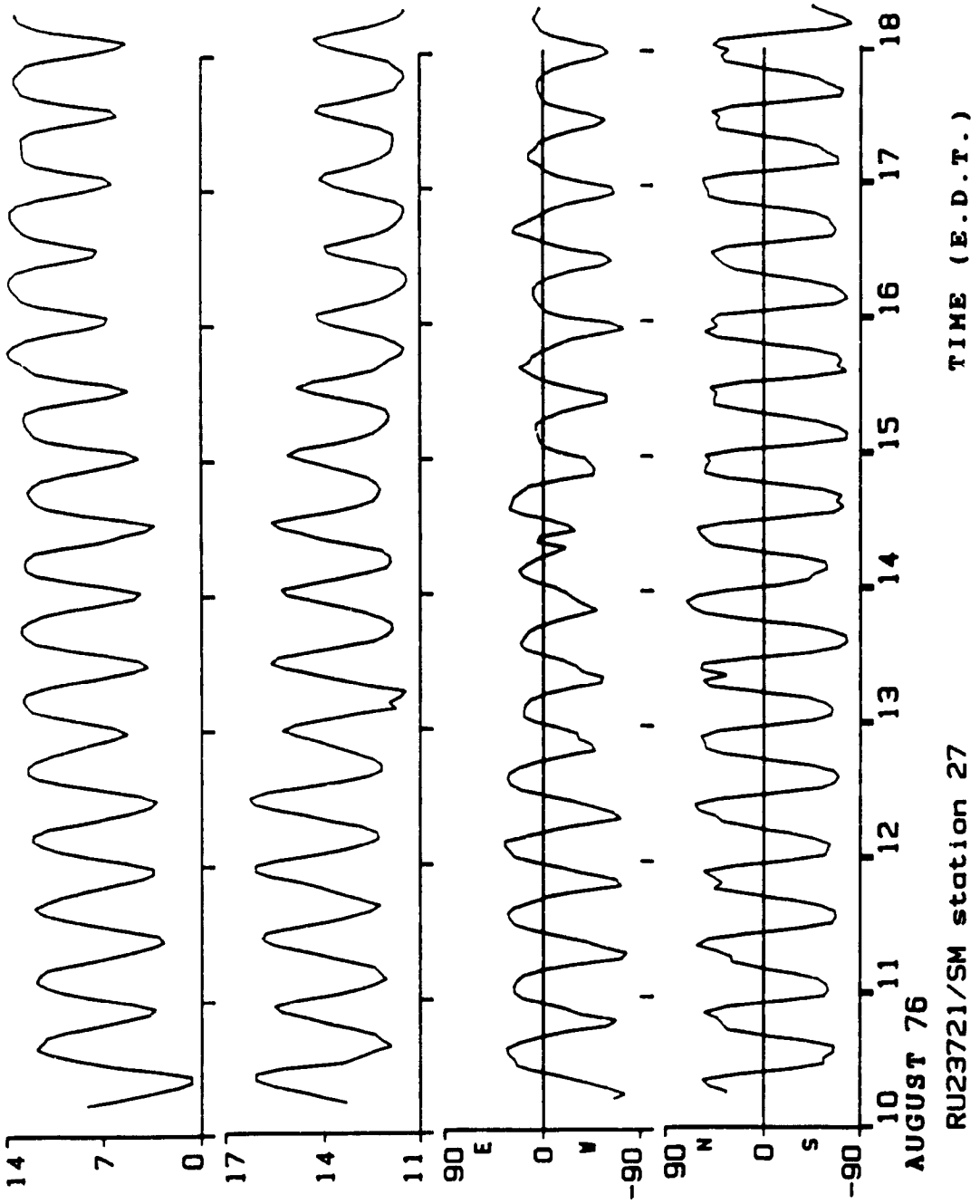
SAL (0/00)
14
7
0
TEMP (C)
17
14
11
SPEED E-W (CM/S)
90
E
0
W
-90
SPEED N-S (CM/S)
90
N
0
S
-90
10
11
12
13
14
15
16
17
18
AUGUST 76
RU23721/SM station 27
TIME (E.D.T.)

Figure A3.7

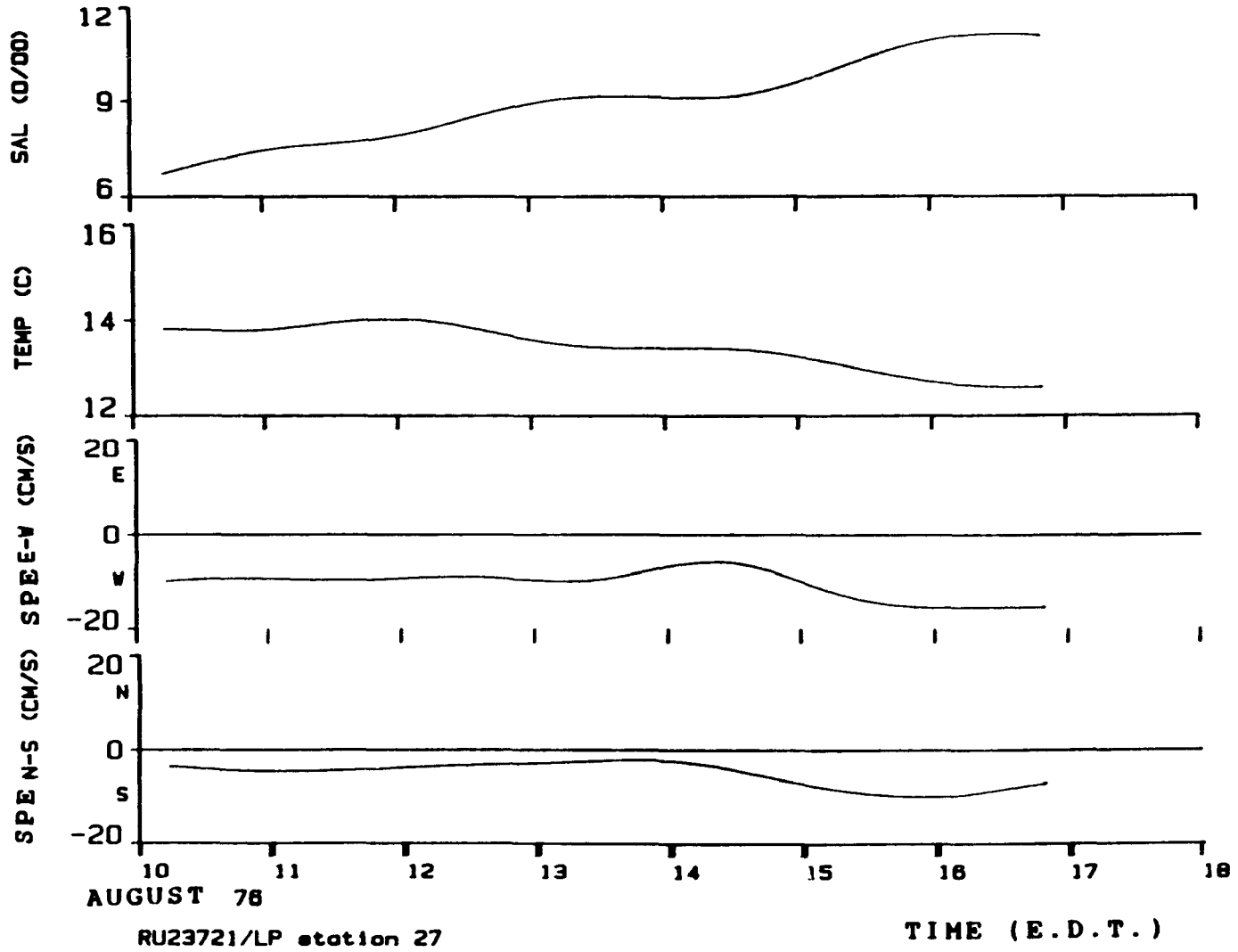
SAL (O/OO)
12
9
6
TEMP (C)
16
14
12
SPEE-W (CM/S)
20
E
0
W
-20
SPE N-S (CM/S)
20
N
0
S
-20
10
11
12
13
14
15
16
17
18
AUGUST 78
RU23721/LP station 27
TIME (E.D.T.)

Figure A3.8

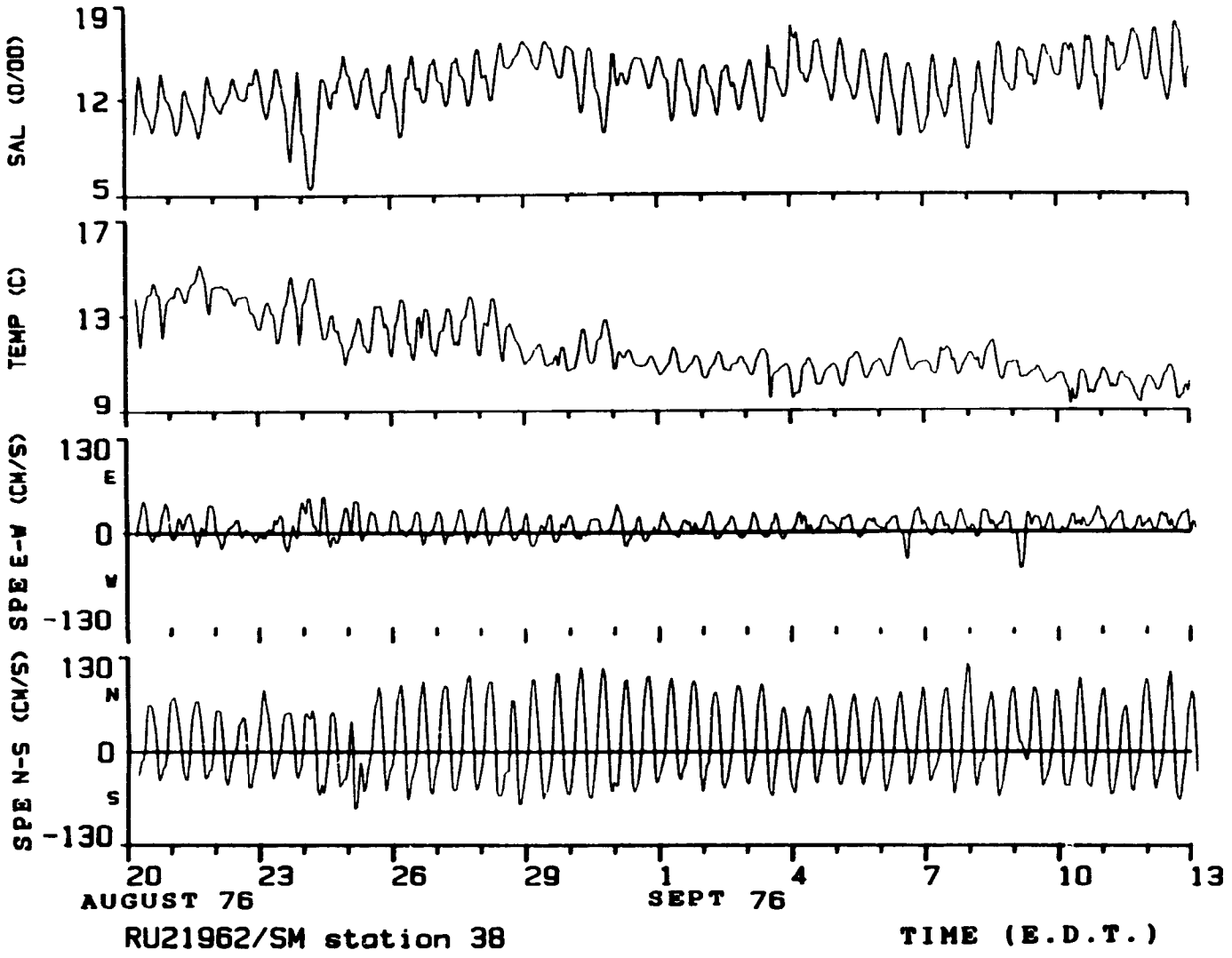
19
12
5
SAL (0/00)
17
13
9
TEMP (C)
130
E
0
W
-130
SPE E-W (CM/S)
130
N
0
S
-130
SPE N-S (CM/S)
20
23
26
29
1
4
7
10
13
AUGUST 76
SEPT 76
RU21962/SM station 38
TIME (E.D.T.)

Figure A3.9

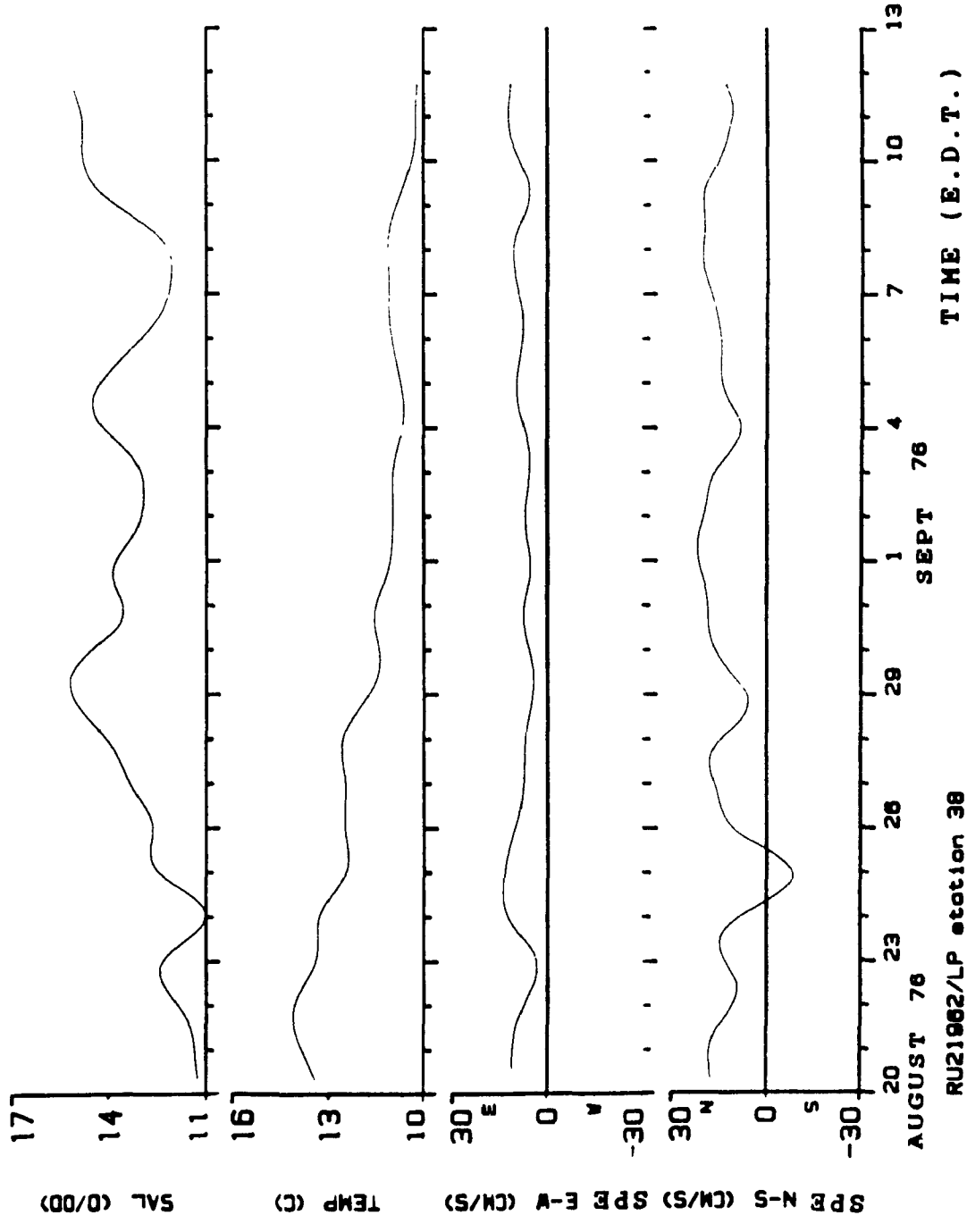
SAL (0/00)
17
14
11
TEMP (C)
16
13
10
SPE E-W (CM/S)
30
E
0
W
-30
SPE N-S (CM/S)
30
N
0
S
-30
20
23
26
29
1
4
7
10
13
AUGUST 76
SEPT 76
TIME (E.D.T.)
RU21002/LP station 38

Figure A3.10

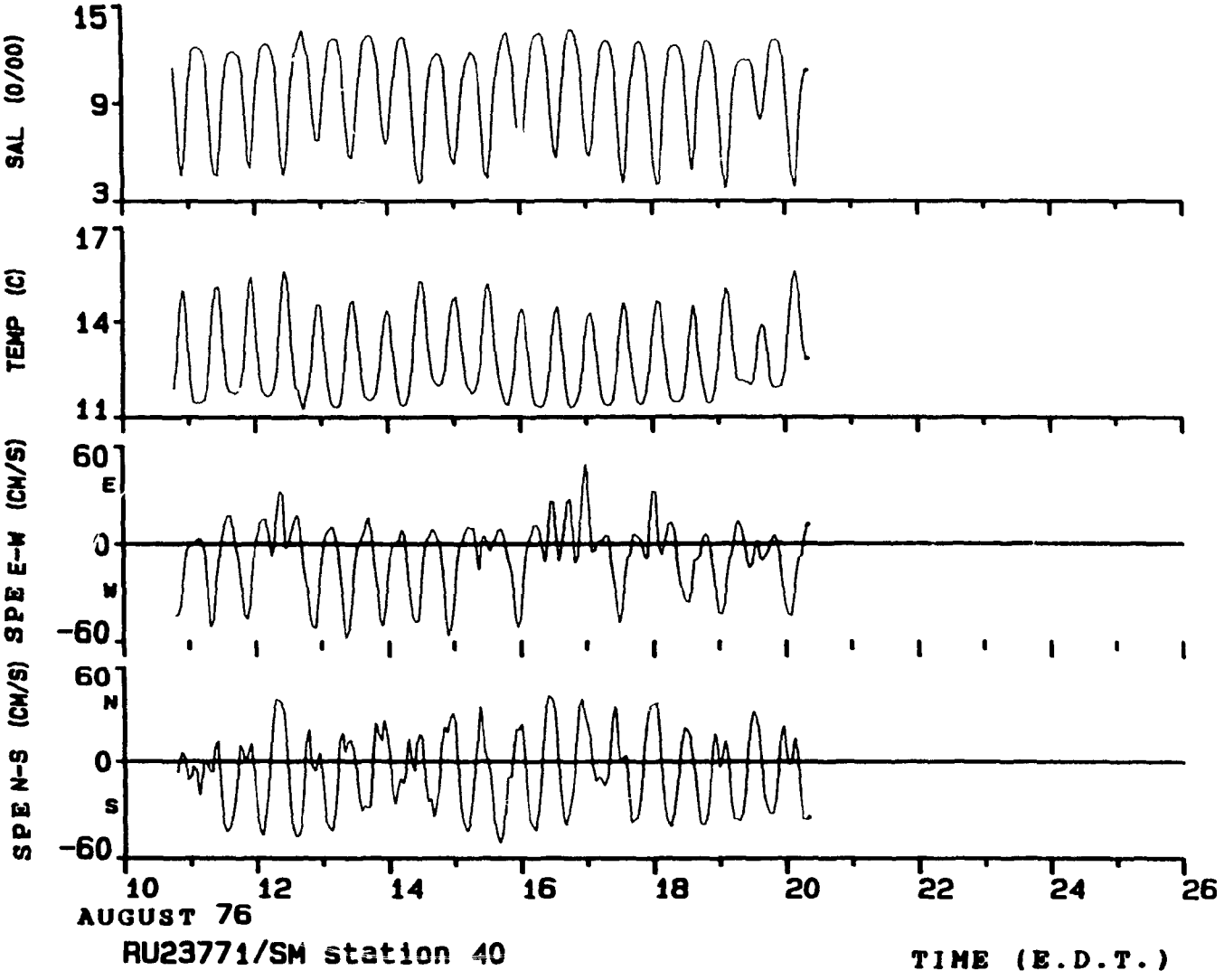
SAL (0/00)
15
9
3
TEMP (C)
17
14
11
SPE E-W (CM/S)
60
E
0
W
-60
SPE N-S (CM/S)
60
N
0
S
-60
10
12
14
16
18
20
22
24
26
AUGUST 76
RU23771/SM station 40
TIME (E.D.T.)

Figure A3.11

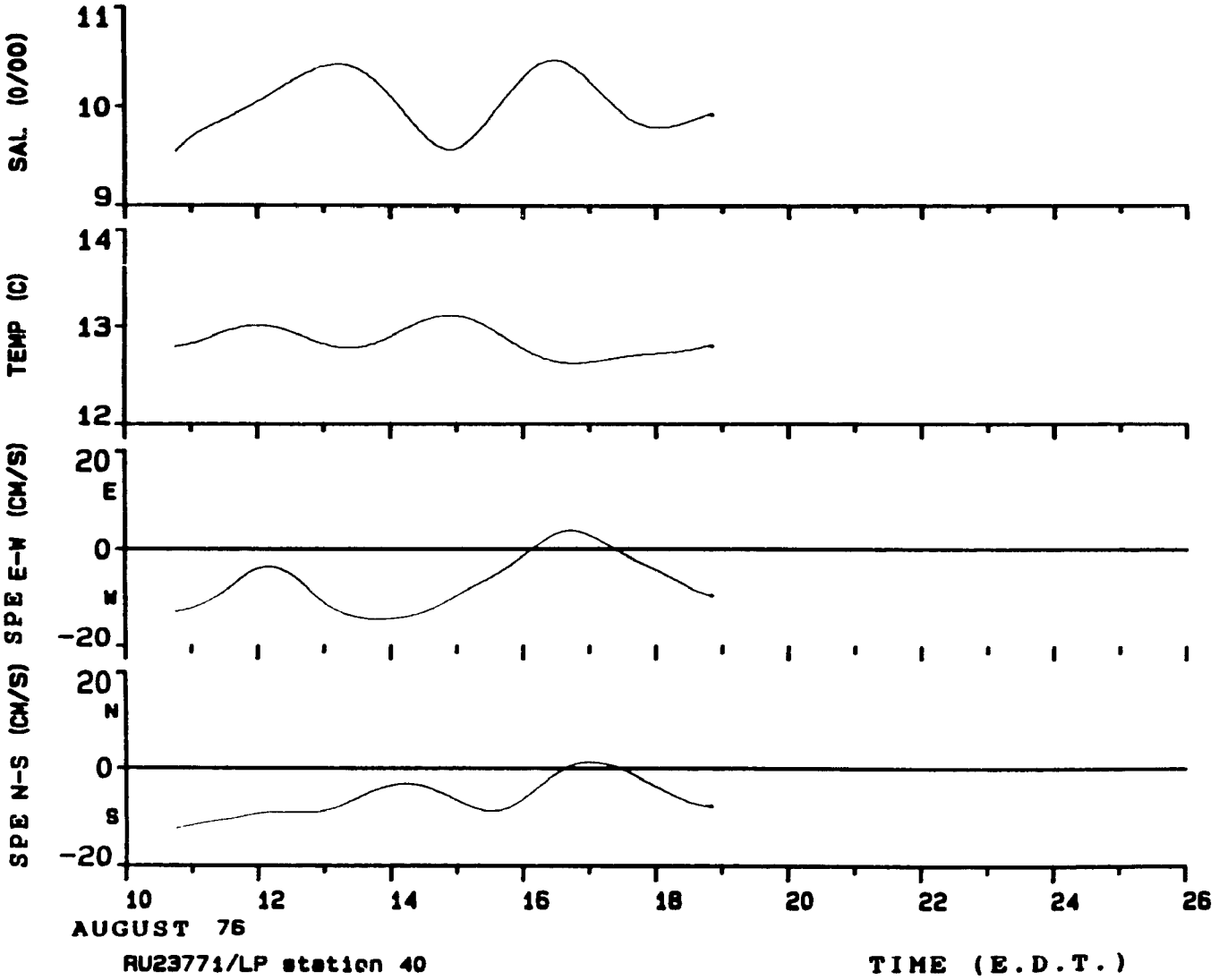
SAL (0/00)
11
10
9
TEMP (C)
14
13
12
SPE E-W (CM/S)
20
E
0
W
-20
SPE N-S (CM/S)
20
N
0
S
-20
10
12
14
16
18
20
22
24
26
AUGUST 76
RU23771/LP station 40
TIME (E.D.T.)

Figure A3.12

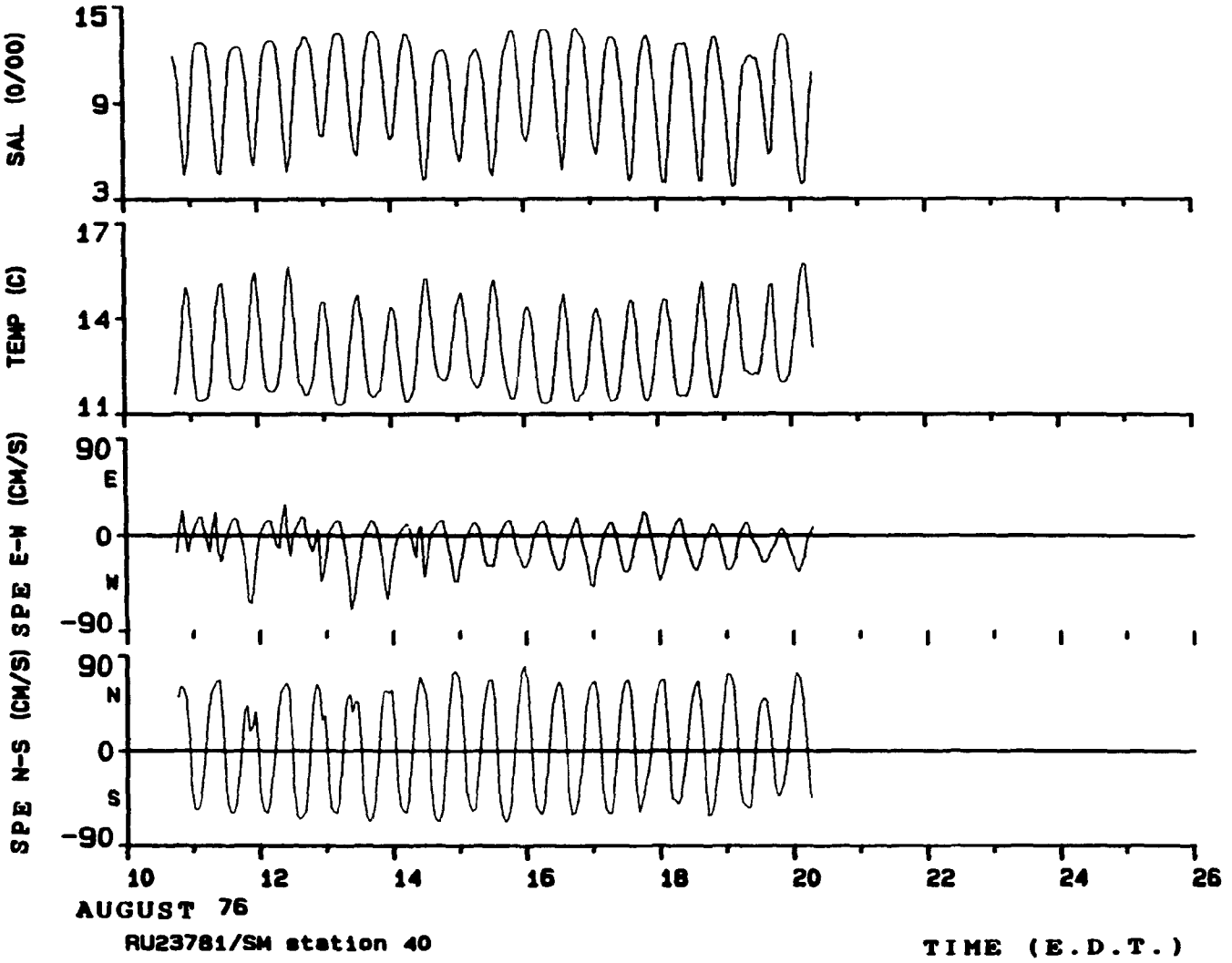
SAL (0/00)
15
9
3
TEMP (C)
17
14
11
SPE E-W (CM/S)
90
E
0
W
-90
SPE N-S (CM/S)
90
N
0
S
-90
10
12
14
16
18
20
22
24
26
AUGUST 76
RU23781/SM station 40
TIME (E.D.T.)

Figure A3.13

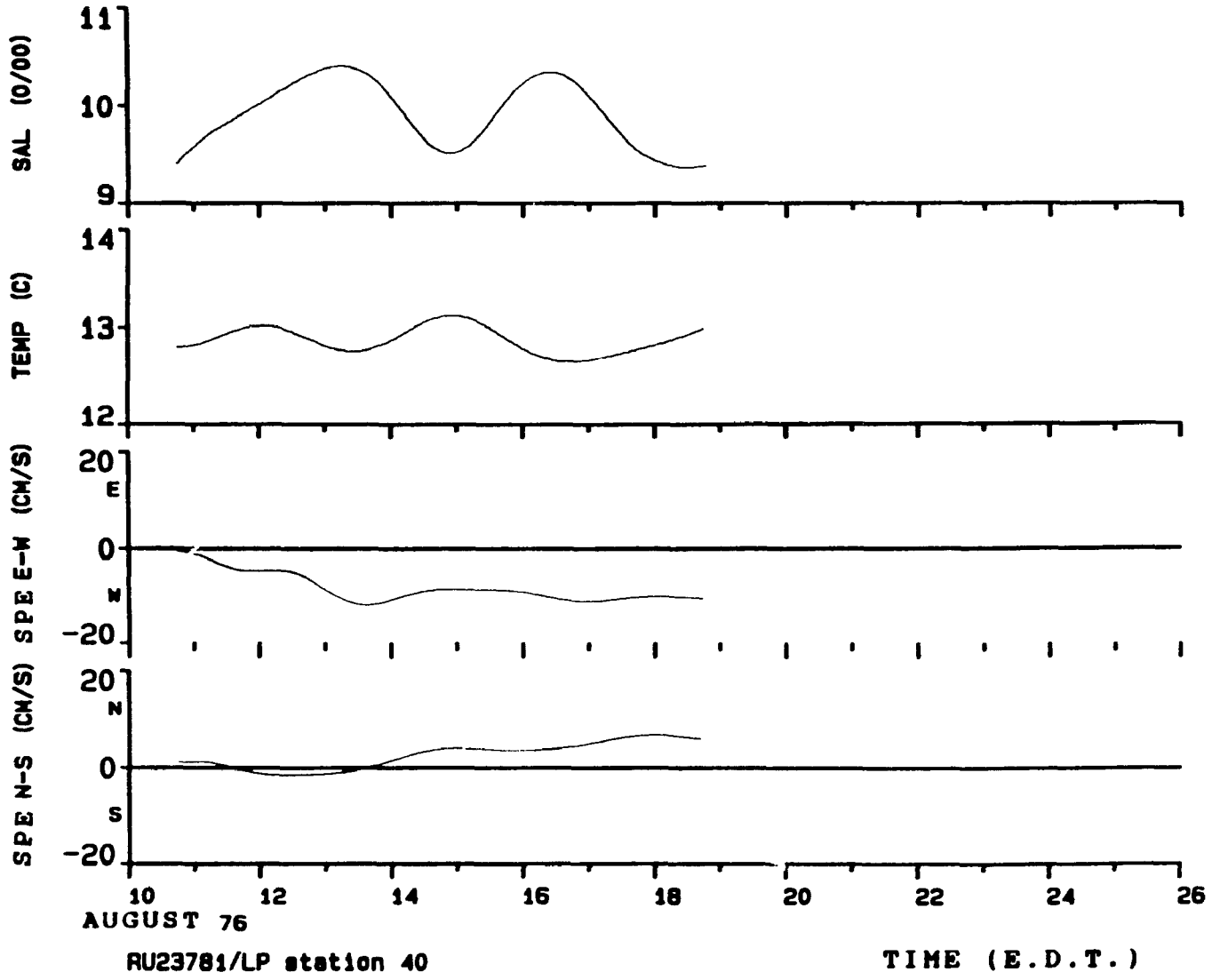
SAL (0/00)
11
10
9
TEMP (C)
14
13
12
SPE E-W (CM/S)
20
E
0
W
-20
SPE N-S (CM/S)
20
N
0
S
-20
10
12
14
16
18
20
22
24
26
AUGUST 76
RU23781/LP station 40
TIME (E.D.T.)

Figure A3.14

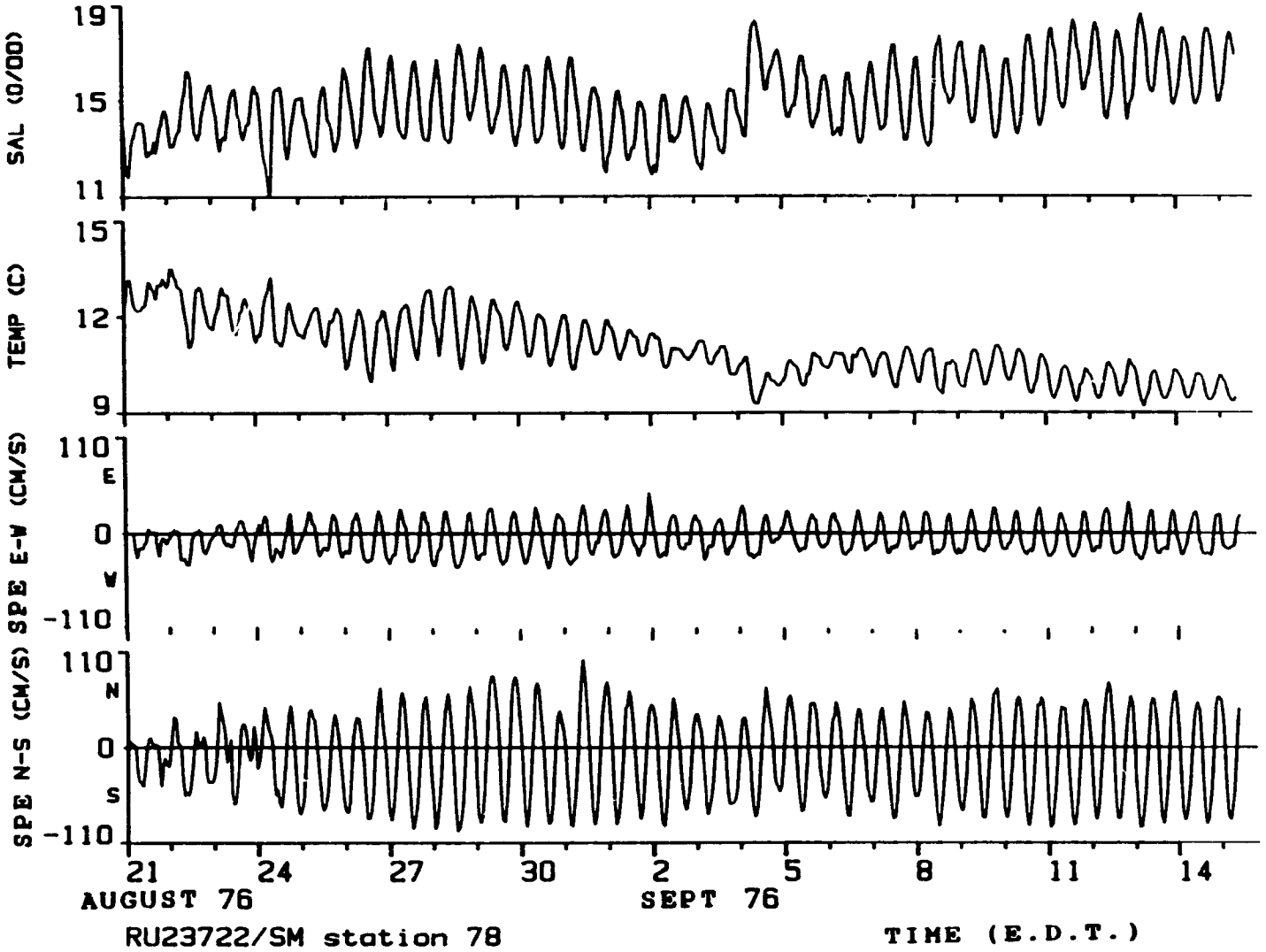
SAL (0/00)
19
15
11
TEMP (C)
15
12
9
SPE E-W (CM/S)
110
E
0
W
-110
SPE N-S (CM/S)
110
N
0
S
-110
21
24
27
30
2
5
8
11
14
AUGUST 76
SEPT 76
RU23722/SM station 78
TIME (E.D.T.)

Figure A3.15

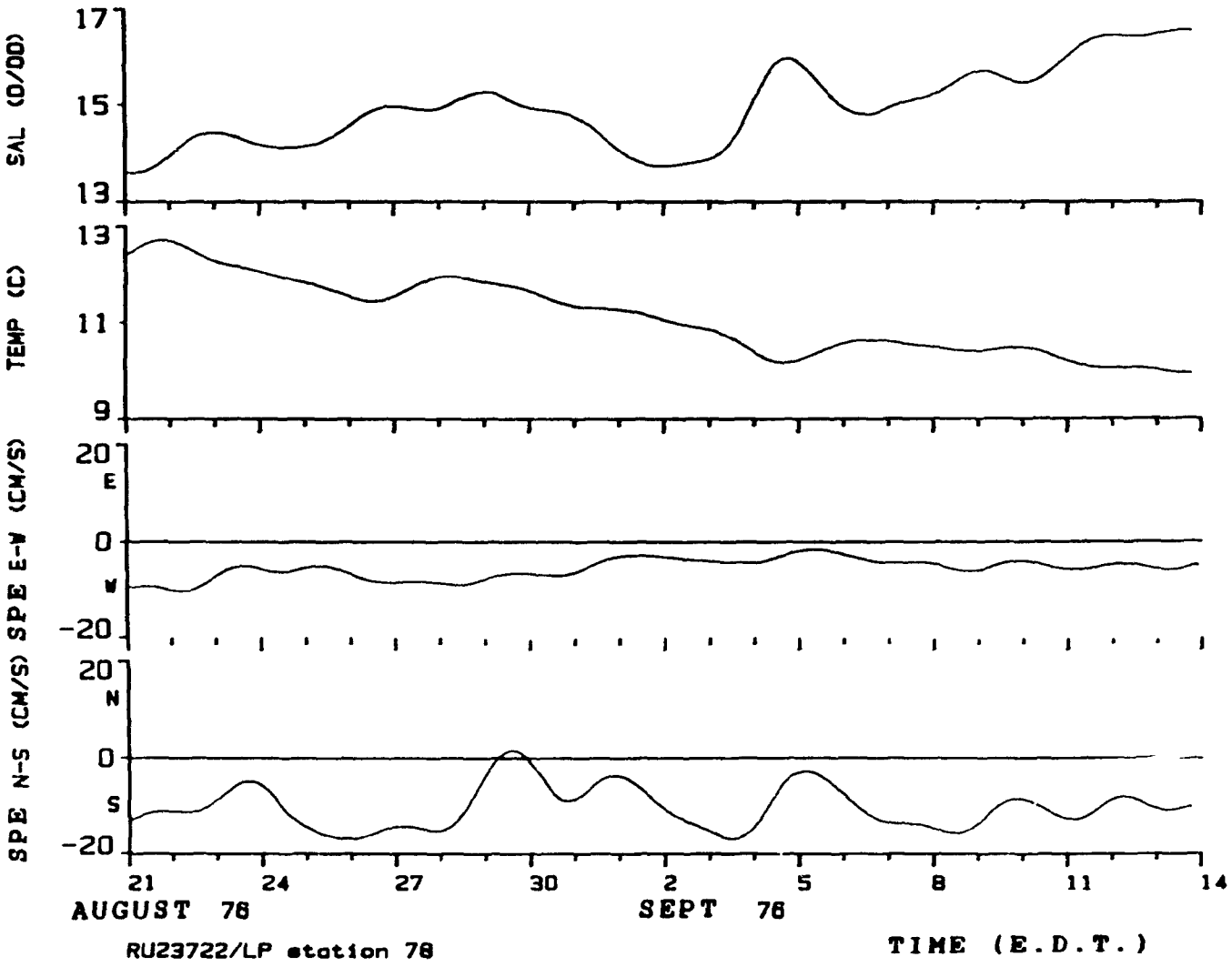
SAL (O/OO)
17
15
13
TEMP (C)
13
11
9
SPE E-W (CM/S)
20
E
0
W
-20
SPE N-S (CM/S)
20
N
0
S
-20
21
24
27
30
2
5
8
11
14
AUGUST 78
SEPT 78
RU23722/LP station 78
TIME (E.D.T.)

Figure A3.16

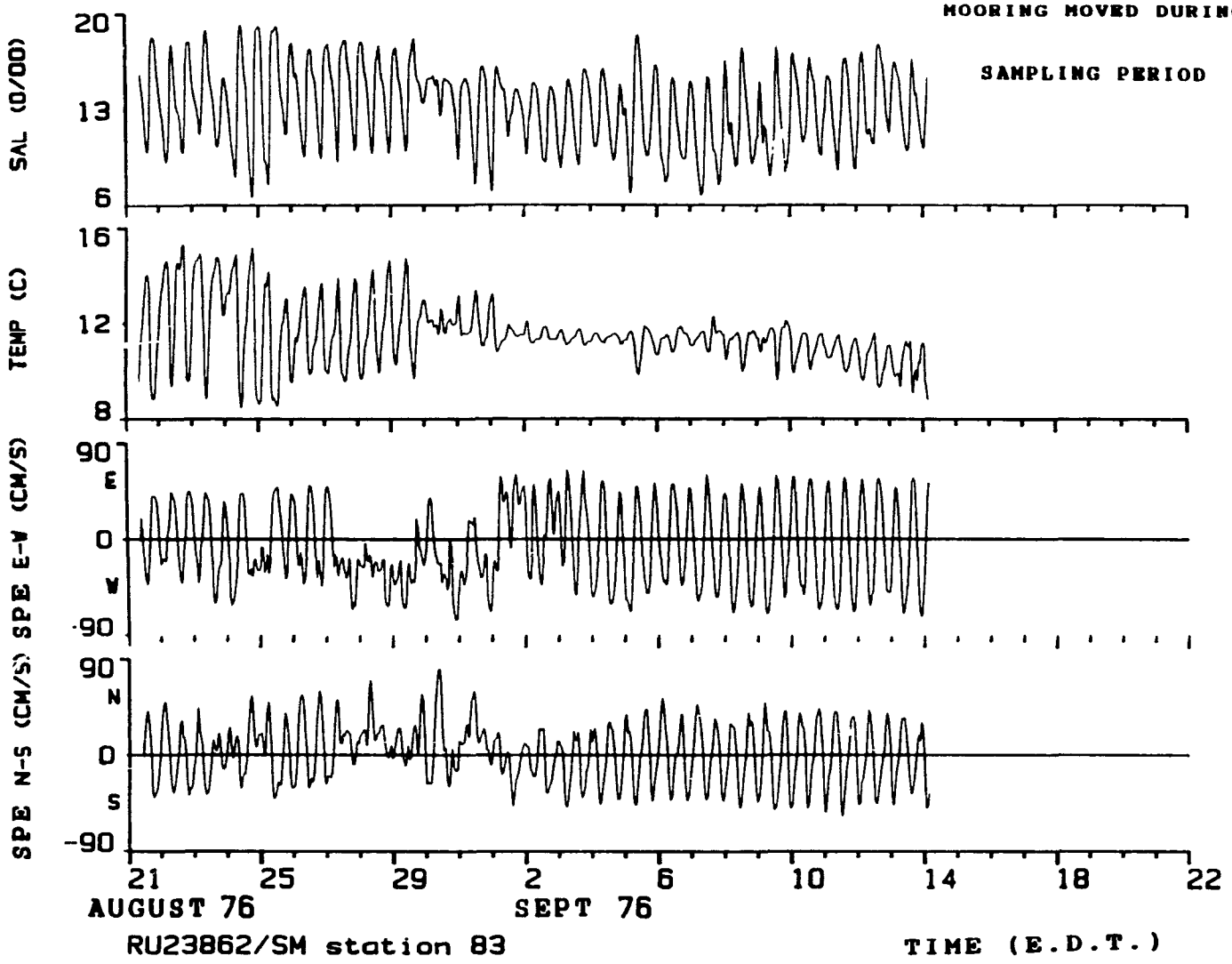
MOORING MOVED DURING
SAMPLING PERIOD
SAL (0/00)
20
13
6
TEMP (C)
16
12
8
SPE E-W (CM/S)
90
E
0
W
-90
SPE N-S (CM/S)
90
N
0
S
-90
21
25
29
2
6
10
14
18
22
AUGUST 76
SEPT 76
RU23862/SM station 83
TIME (E.D.T.)

Figure A3.17

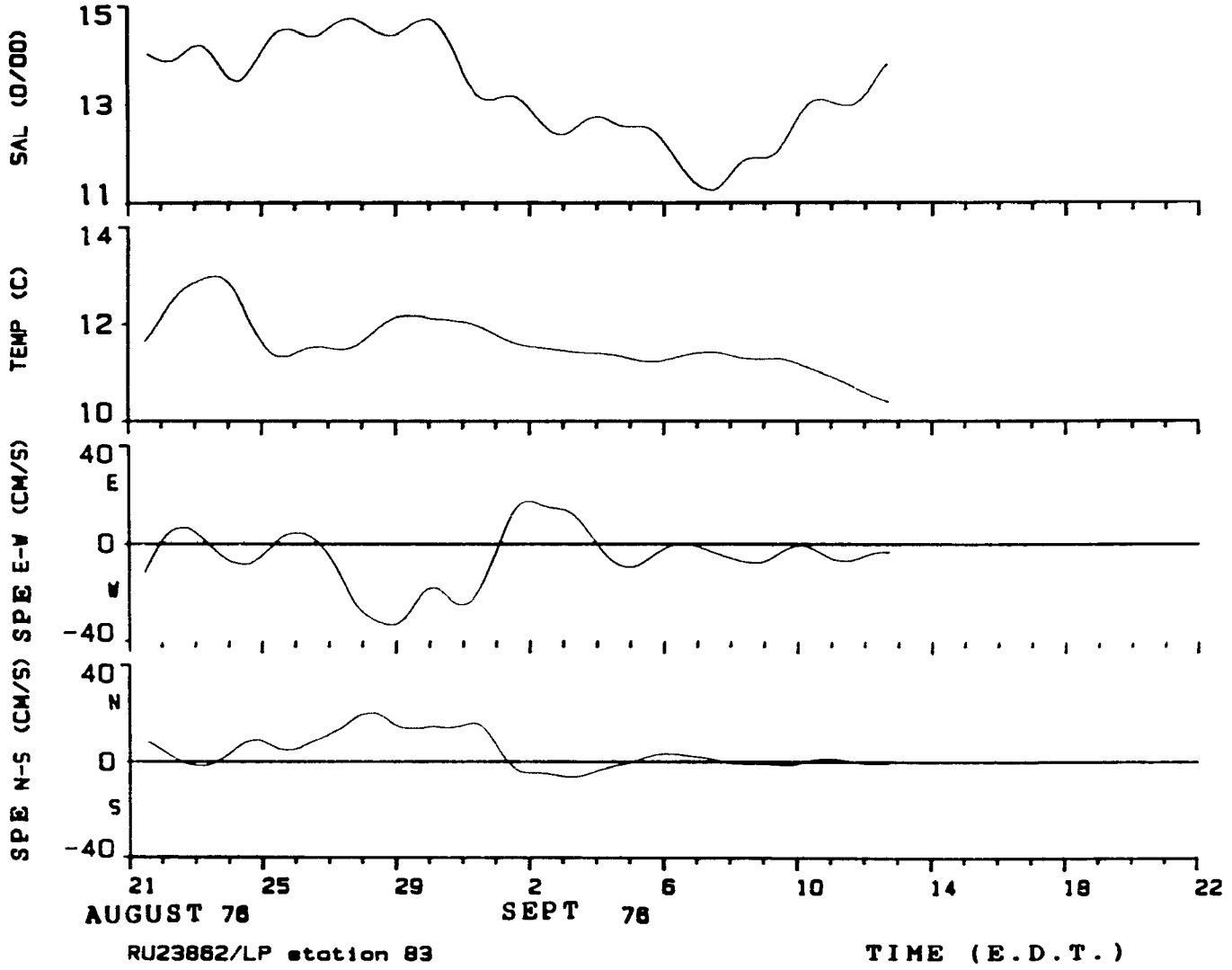
SAL (0/00)
15
13
11
TEMP (C)
14
12
10
SPE E-W (CM/S)
40
E
0
W
-40
SPE N-S (CM/S)
40
N
0
S
-40
21
25
29
2
6
10
14
18
22
AUGUST 78
SEPT 78
RU23862/LP station 83
TIME (E.D.T.)

Figure A3.18

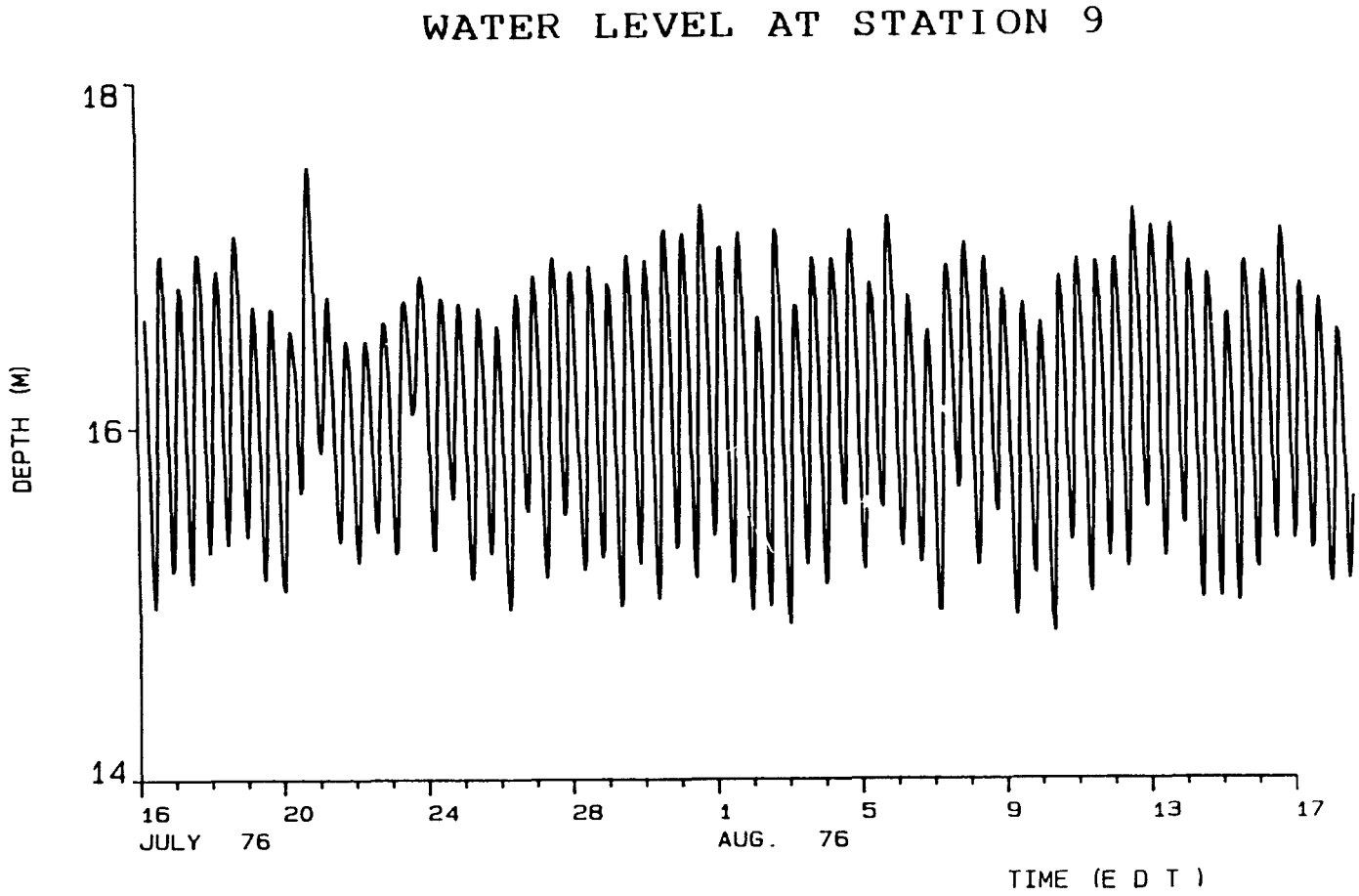
WATER LEVEL AT STATION 9
18
16
14
DEPTH (M)
16
JULY 76
20
24
28
1
AUG. 76
5
9
13
17
TIME (E D T)

Figure A3.19

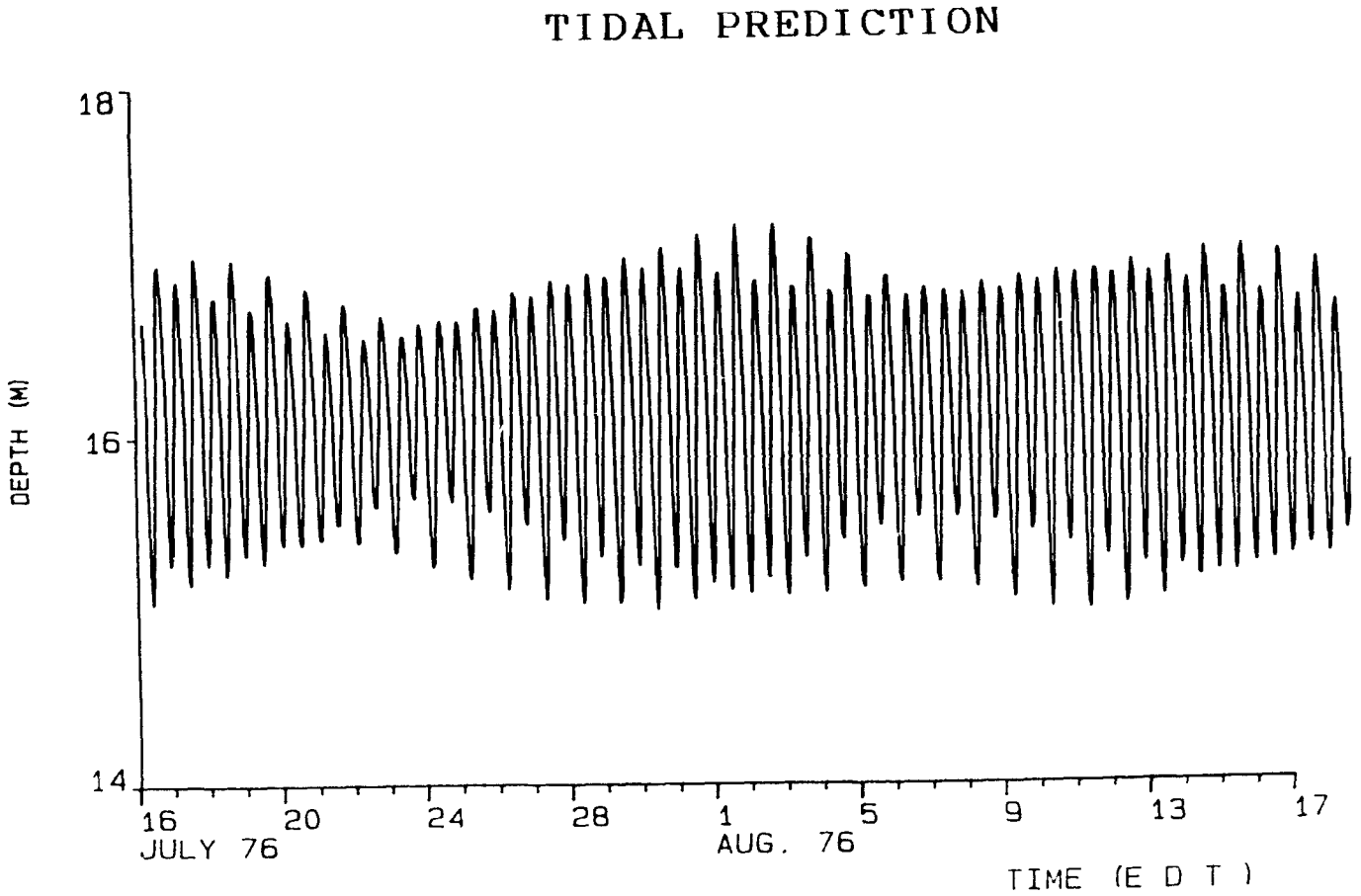
TIDAL PREDICTION
18
16
14
DEPTH (M)
16
JULY 76
20
24
28
1
AUG. 76
5
9
13
17
TIME (E D T)

Figure A3.20

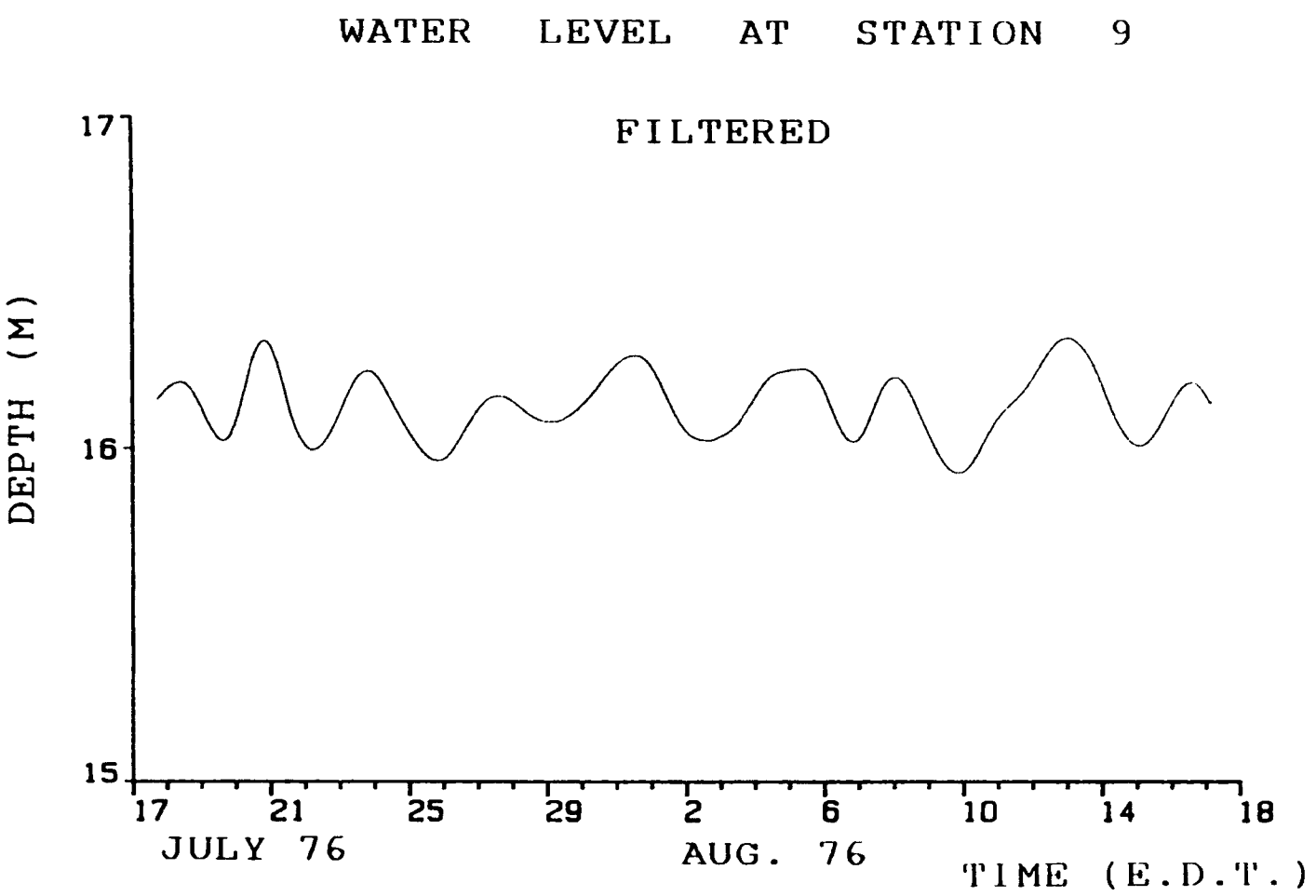
WATER LEVEL AT STATION 9
FILTERED
DEPTH (M)
17
16
15
17
21
25
29
2
6
10
14
18
JULY 76
AUG. 76
TIME (E.D.T.)

Figure A3.21

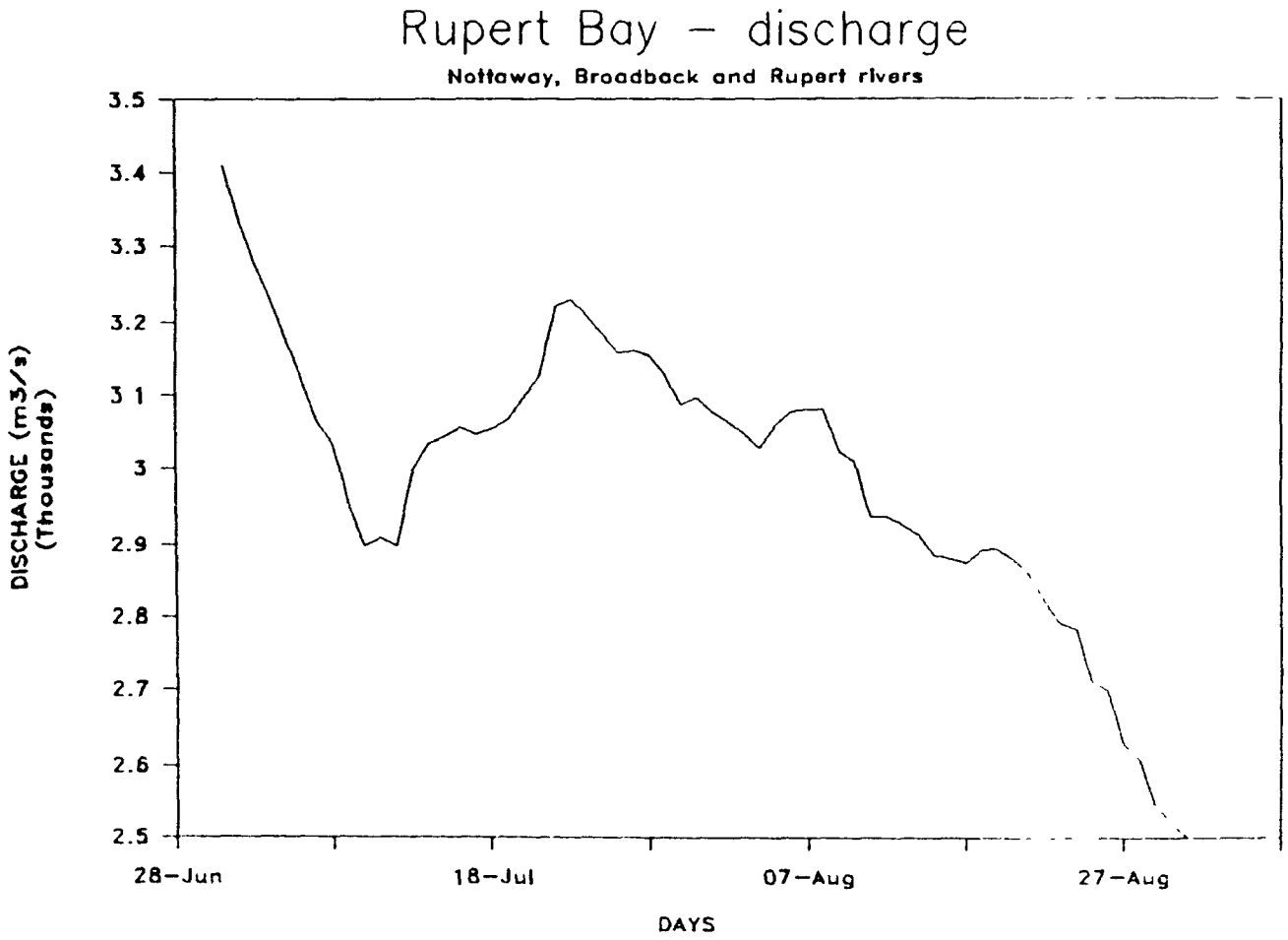
Rupert Bay – discharge
Nottaway, Broadback and Rupert rivers
DISCHARGE (m3/s)
(Thousands)
3.5
3.4
3.3
3.2
3.1
3
2.9
2.8
2.7
2.6
2.5
28–Jun
18–Jul
07–Aug
27–Aug
DAYS

Figure A3.22

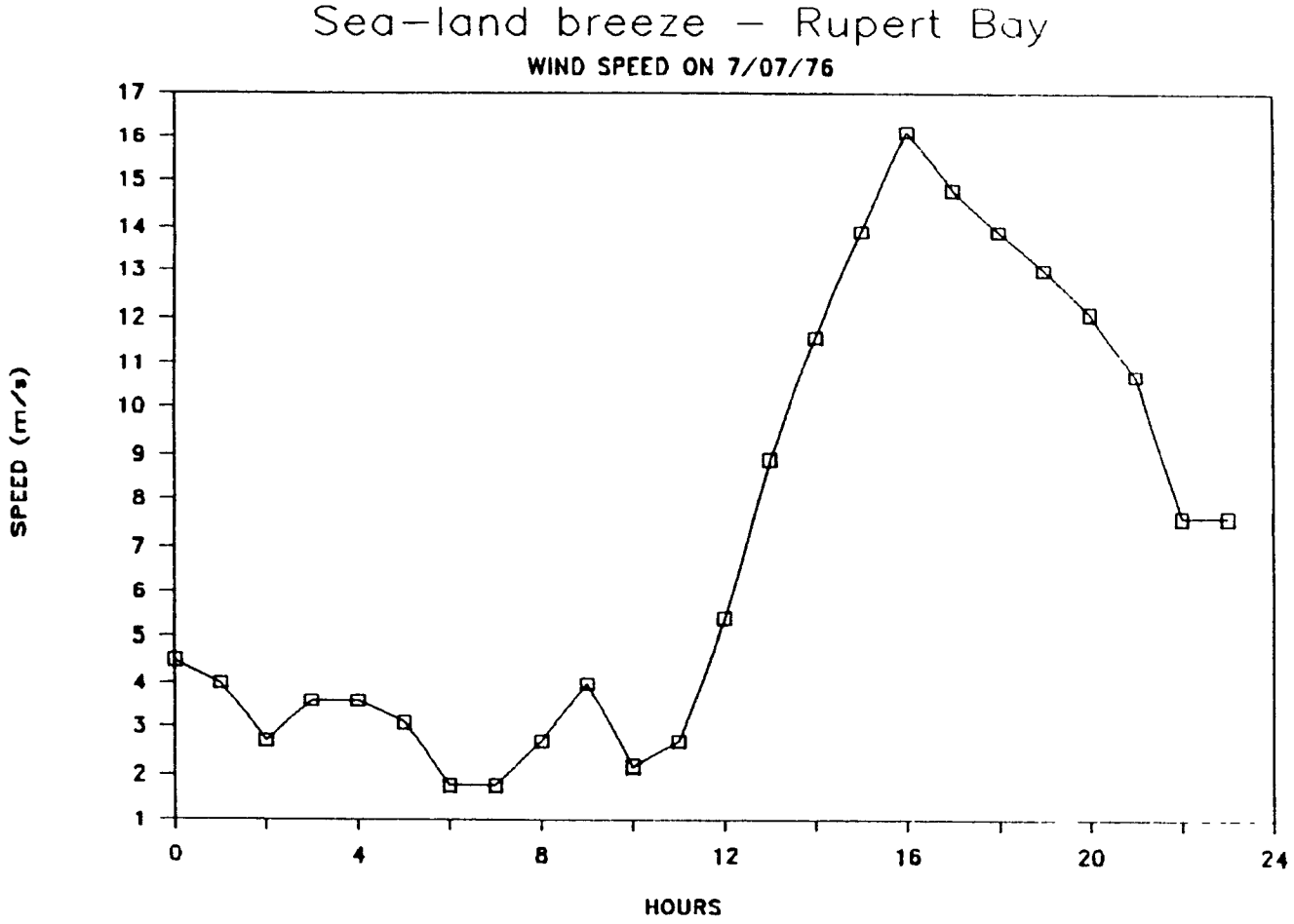
Sea–land breeze – Rupert Bay
WIND SPEED ON 7/07/76
SPEED (m/s)
17
16
15
14
13
12
11
10
9
8
7
6
5
4
3
2
1
0
4
8
12
16
20
24
HOURS

Figure A3.23

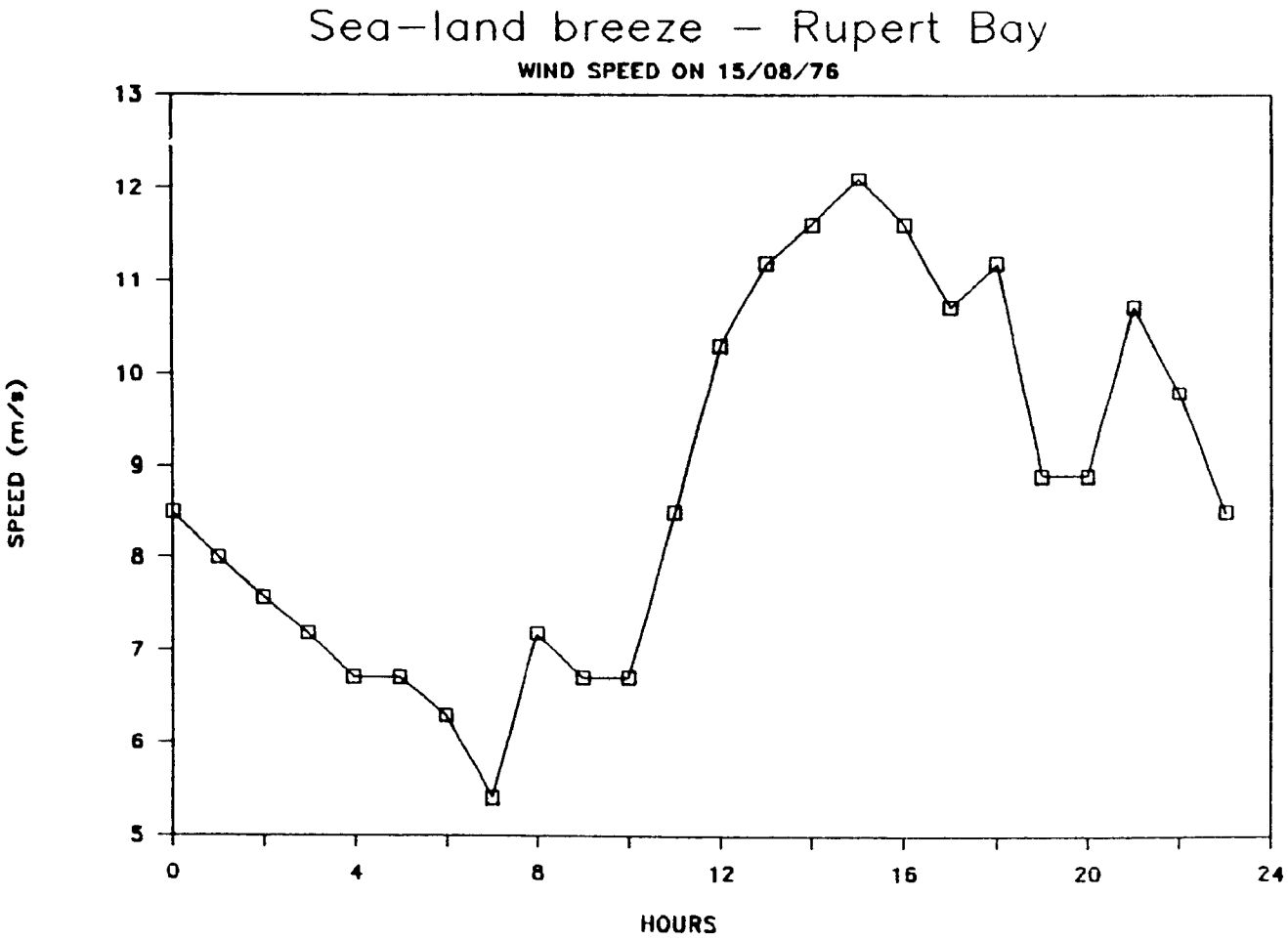
Sea–land breeze – Rupert Bay
WIND SPEED ON 15/08/76
SPEED (m/s)
13
12
11
10
9
8
7
6
5
0
4
8
12
16
20
24
HOURS

Figure A3.24

REFERENCES

Aanderaa Instruments, 1982. WLR 5/6 operating manual. Technical description No.125, Norway, 44 p.

Aanderaa Instruments, 1983. RCM 4/5 operating manual. Technical description No.119, Norway, 35 p.

Bowden, K.F., 1967. Circulation and Diffusion. in Estuaries, G.H.Lauff (editor), Publication 83, American Ass. Adv.Sci., 757 p.

Foreman, M.G.G., 1977. Manual for Tidal Heights Analysis and Prediction. Pacific Marine Science Report 77-10, Institute of Marine Sciences, Patricia Bay, Victoria, B.C., 97 p. (unpublished)

Foreman, M.G.G., 1978. Manual for Tidal Currents Analysis and Prediction. Pacific Marine Science Report 78-6, Institute of Marine Sciences, Patricia Bay, Victoria, B.C., 70 p. (unpublished)

Freeman, N.G., Roff, J.C. and Pett, R.J., 1982. Physical, Chemical, and Biological Features of River Plumes Under an Ice Cover in James and Hudson Bays. Le Naturaliste Canadien, Vol. 109, 4 : 745-764.

Gardner, W.A., 1988. Statistical Spectral Analysis : a Nonprobabilistic Theory. Prentice-Hall, Englewood Cliffs, NJ (USA), 566 p.

Godin, G.G., 1972. The Analysis of Tides. University of Toronto Press, Toronto, Canada, 264 p.

Jenkins, G.M. and Watts, D.G. 1968. Spectral Analysis and its applications. Holden-Day, San Francisco, 525 p.

Pond, S. and Pickard, G.L., 1986. Introductory Dynamical Oceanography, 2nd edition. Pergamon Press, 329 p.

Prinsenberg, S.J., 1984. Freshwater Contents and Heat Budgets of James Bay and Hudson Bay. Continental Shelf Research, Vol. 3, 2 : 191-200.

Prinsenberg, S.J., 1986. Salinity and Temperature Distributions of Hudson Bay and James Bay. in Inland Coastal Seas : 163-186 , I.P. Martini (editor), Elsevier Press, New York (USA), 494 p.

Rouse, W.R. and Bello, R.L., 1985. Impact of Hudson Bay on the Energy Balance in the Hudson Bay Lowlands and the Potential for Climatic Modification. Atmosphere-Ocean, Vol. 23, 4 : 375-392.